EUROPEAN COMMISSION

Community Research

SEVENTH FRAMEWORK PROGRAMME

ARCHER

Collaborative Project (CP)

Co-funded by the European Commission under the Euratom Research and Training Programme on Nuclear Energy within the Seventh Framework Programme

Grant Agreement Number : 269892

Start date : 01/02/2011 Duration : 48 Months

www.archer-project.eu

Archer

Advanced Reactor for Cogeneration of Heat & Electricity-R&D

Improvement of models and methods for hot spots/hot areas analysis

Authors : Dustin Sancristobal, Janis Lapins, Michael Buck, Johannes Bader

ARCHER - Contract Number: 269892
Advanced High-Temperature Reactors for Cogeneration of Heat and Electricity R&D
EC Scientific Officer: Dr. Panagiotis Manolatos

Document title	Improvement of models and methods for hot spots/hot areas analysis
Author(s)	Janis Lapins, Michael Buck, Johannes Bader, Dustin Sancristobal
Number of pages	70
Document type	Deliverable
Work Package	WP 24
Document number	D24.23
Issued by	USTUTT
Date of completion	12/03/2015
Dissemination level	Confidential, only for members of the consortium (including the Commission Services).

Summary

This document contains a detailed description of the used programmes, i.e. ZIRKUS, ATTICA3D, TORT-TD, the reference plant HTR-PM and also the methodology to produce results for a densified cluster of fuel pebbles within the pebble bed. The modification of nuclear cross sections for that case is explained. Also, results for the hot spot analysis are presented. Here, a depressurisation accident with densifications on the centreline is simulated for both a densification in the power maximum and the temperature maximum location of the nominal operation. The volume with a densified cluster of fuel pebbles does not display significantly higher temperatures. Furthermore, control rod ejection and withdrawal cases are presented for a three-rod ejection/withdrawal scenario. For these transients the densifications are even placed at outer positions. At last, a total control rod ejection case is shown. Even though temperatures are higher in comparison of partly ejection, they stay well below design limits. Additionally, the fuel temperature model was modified such that global (if available also local) power factors can be entered for different numbers of core passes (15 for the HTR-PM). This modification accounts for the different power production fractions. While fresh fuel elements have the highest fissile material content, they also have the lowest burn-up and hence the decay heat production is the least. That means that in nominal operation fresh fuel elements are the hottest. With this new model coupled calculations were performed. It could be shown that the temperature spread between the first and the last core pass was around 130 K at the location of the power maximum. The newly implemented core-pass fuel temperature model reveals significantly higher temperatures than a modelling with an average pebble ensemble. Also the power factors of the fuel element per core-pass were extracted from a steady state neutronic/thermal fluid dynamic calculation with ZIRKUS/...

Approval

Date	By
12/03/2015	Michael BUCK
12/03/2015	Norbert KOHTZ
12/03/2015	Steven KNOL

Distribution list

Name	Organisation	Comments
P. Manolatos	EC DG RTD	Through the EC participant portal
All beneficiaries	ARCHER	Through the private online workspace

subsequent analysis, the highest possible spread of power factors (at the top outer core) as “conservative” and the “realistic” ones at the very location investigated, i. e. at the power maximum and at the temperature maximum above the bottom reflector.

The new model is applied to a steady-state analysis for a reduced mass flow due to assumed core by-pass by the cooling gas, the total control rod ejection scenario and a total rod withdrawal scenario.

For the steady state analysis with reduced mass flow through the core it was found that temperatures in the centre with a densification of the pebble bed at the power maximum remained high from this location on several meters downwards. However, they did not exceed the axial maximum temperatures which occur at the bottom of the core. A densification at the bottom of the core has no sensible influence on the fuel temperatures at that point.

The total control rod ejection scenarios presented showed that with the new model, considering the different passes of the fuel spheres through the core, significantly higher fuel temperatures occur in fuel spheres of the first passes. For all cases, a fast ejection (0.1 s) from the nominal rod position and a slower ejection (100cm/s) with both “conservative” and “realistic” power factors, the limiting maximum temperature of 1620 °C is exceeded by different degrees. However, the temperatures quickly drop below that limit after less than 10 seconds. Appropriate design measures have therefore to be taken to make fast ejection of all control rods a hypothetical scenario.

For the total control rod withdrawal scenario with operational speed of the control rods, the increase of reactivity is much smaller since the reactor has time to adapt to the (in comparison to the ejection scenario) relatively slowly changing conditions. Here, no inadmissibly high temperatures could be detected.

Approval

Rev.	Short description	First author	WP Leader	SP leader	Coordinator
4	First issue	Janis Lapins (IKE-USTUTT) 01/03/2015	Michael Buck (IKE-USTUTT)	Norbert Kohtz (TÜV)	Steven Knol (NRG) ../../..

Distribution list

Name	Organisation	Comments
P. Manolatos	EC DG RTD	
All technical participants	ARCHER	
Steering Committee members	ARCHER	

Table of contents

Introduction

The aim of this task is to assess the potential for hot spots or hot areas in HTGR cores, especially pebble bed cores, which may not have been covered with standard steady state thermal analysis of HTGR cores in the past.

IKE is developing the system TORT-TD/ATTICA^{3D} as a tool for safety analyses based on three-dimensional coupled simulation of neutronics and thermal behaviour HTGRs with pebble and block fuel elements. Special emphasis is on temperature heterogeneity effects (and related reactivity effects) to identify possible thermal issues. Larger area variations of pebble bed porosity can be modelled to investigate their interdependent influence on coolant temperatures, fuel temperatures and power distribution.

The following work steps will be performed:

- Tool and method development to identify possible hot spots/hot areas by coupled neutronic/thermal hydraulic analyses (TORT-TD and ATTICA^{3D}), consideration of porosity and load variations on cross sections and spectra, feedback with thermal hydraulics.
- Application calculations for reference plants under operational conditions as well as for reactivity transients and loss of cooling accidents (reference plant with pebble or block fuel element as well as scenarios to be jointly defined in the project).

Coupled thermal hydraulic/neutronic analyses are required to identify potentially critical areas/hot spots and will be presented in this deliverable.

1 Calculation Methods

1.1 Pre-processing Codes ZIRKUS and MCNP

The code system ZIRKUS/THERMIX [1] used to calculate the cross sections of the reference case. ZIRKUS is a 2D modular code system, including microscopic and macroscopic cross sections calculations that account for the doubly heterogeneous nature of the fuel element, a pebble flow module with spectral calculations, neutron diffusion module and burn-up module. Thermal Hydraulic feedback is provided by THERMIX/KONVEK that was coupled [1]. Group cross sections are achieved by the coupled spectral code MICROX2 from the PSI [2]. The ZIRKUS cross sections are also used for the coupled ATTICA3D/TORT-TD calculations.

MICROX2 explicitly considers the double heterogonous nature of the fuel (fuel particles in a graphite shell, see Figure 6) and its effect on spectral calculations. The simulation chain of cross sections generation, flux and burn-up calculation is necessary to achieve the in situ cross sections.

The Monte-Carlo N-Particle Code (MCNP) is a well-known general code for transport problems [3].

The Code allows detailed analysis of various geometries. The geometry of the fuel pebbles, including the fuel particles, can be explicitly modelled in MCNP, as well as different possibilities for their arrangement in the pebble bed. Point wise cross sections and different material compositions of the fuel particles allow the evaluation of different burn-up states.

1.2 Transport and Diffusion Code TORT-TD

For other neutronic calculations of this task, especially 3D evaluations, the time-dependent 3-D fine-mesh few-group discrete ordinates (S_N) neutron transport code TORT-TD is used.

The neutron transport code TORT-TD is being developed at GRS [5]. It is based on the DOORS steady-state neutron transport code TORT [4] and solves the steady-state and time-dependent few-group transport equation with an arbitrary number of prompt and delayed neutron precursor groups in both Cartesian and cylindrical (r-ϑ-z) geometry. Unconditional numerical stability in transient calculations is achieved using a fully implicit time discretization scheme. Scattering anisotropy is treated in terms of a Legendre scattering cross section expansion. Computing time can be saved by extrapolating the angular fluxes to the next time step using the space-energy resolved inverse reactor period. The features of TORT-TD further include:

- 64 bit encoding to meet imposed tight convergence criteria and to enable TORT-TD to be applied to large realistic problems exceeding 32 bit RAM limitations;
- Movements of single control rods or control rod banks;
- Processing of parameterized tabulated cross section libraries for up to 5 state parameters; interpolation either linear or with cubic spline polynomials, thus allowing to study the impact of different interpolation schemes on cross section evaluation;
- Generalized Equivalence Theory (GET) at pin cell level to reduce homogenization errors in LWR applications;
- Time-dependent anisotropic distributed external source;
- Leakage and buckling calculation over larger spatial regions (e.g. spectral zones) using the neutron current density in discrete ordinates representation;
- Calculation of Xenon/Iodine equilibrium and transient distribution as a prerequisite for operational transients;
- Fully integrated 3-D fine-mesh few-group diffusion solver (steady state and time-dependent) in both Cartesian and cylindrical geometry.

TORT-TD has been extended by a 3-D fine-mesh few-group solver for the steady state and time dependent diffusion equation in few energy groups for both Cartesian and cylindrical (r-ϑ-z) geometry. The diffusion solver is fully integrated in TORT-TD and can be invoked by a single parameter in the input data set. Since it operates on the same spatial discretization and the same cross section data, the diffusion solver allows studying the impact of the diffusion approximation by directly comparing with the S_N solution. It can also be applied to fast running scoping calculations, especially for transients, or as a preconditioner to accelerate subsequent discrete-ordinates calculations.

1.3 Thermal Hydraulics Code ATTICA^{3D}

The ATTICA^{3D} Advanced Thermal Hydraulics Tool for In-vessel and Core Analysis in 3 Dimensions, developed at IKE of Stuttgart University, applies the porous medium approach in both cylindrical and Cartesian geometry [6]. Subdivision between solid and fluid fraction in a considered control volume is done via the porosity parameter ε assuming thermal non-equilibrium. Multiple gas phases are implemented in ATTICA^{3D}.

For the solid structures, the transient energy equation is

$$(1-\varepsilon)\frac{\partial}{\partial t}(\rho_s h_s) = (1-\varepsilon)\nabla\left[\cdot\, \lambda_{s,eff} \cdot \nabla T_s\right] - \dot{q}_{conv} + \dot{q}_{nu}$$

where the index s indicates the solid state, ε, ρ, h, λ_{eff}, Ts, $\dot{q}_{conv}$ and $\dot{q}_{nu}$ denote porosity, density, enthalpy, effective heat conductivity, temperature, convective heat transferred from hot solids to gases, and the amount of generated nuclear power, respectively.

The time-dependent energy equation for the gas phases is

$$\varepsilon\frac{\partial \rho_g h_g}{\partial t} + \varepsilon\, div\,(\rho_g \vec{u} h_g) = \varepsilon\, div\,(\lambda_{g,eff}\, grad\,(T_{g,i})) + \dot{q}_{conv}$$

where the index $_{g,i}$ indicates gas phase of the gas type $_i$ (e.g. Helium, Oxygen), h is the specific gas enthalpy, $\vec{u}$ denotes the velocity vector, $\lambda_{g,i,eff}$ the effective heat conductivity of the gas and Tg,i the gas temperature. The latter is calculated by

$$\dot{q}_{conv} = \alpha(T_s - T_g)$$

where α is the heat transfer coefficient. Heat transfer within the pebble bed is determined according to KTA standards [7] using the Zehner-Schlünder and, for elevated temperature levels, the Robold correlation.

The mass conservation is only solved for the fluid region. The implemented mass conservation equation comes as

$$\varepsilon\,\frac{\partial \rho_i}{\partial t} + \varepsilon\, div\,(\rho_i \vec{u}_i) = 0$$

with the same declarations as stated above.

The momentum equation has the form of a simplified equation of Ergun type for porous medium. Since the porous medium approach is strongly dominated by pressure loss, fluid-solid friction and body force, the unsteady and convection term on the left hand side, and on the right hand side diffusion of momentum, additional viscous term are neglected, yielding

$$\varepsilon\, grad\ p = -\vec{R} - \varepsilon\rho_i\,\vec{g}$$

with $\vec{R}$ denoting the friction force, and $\vec{g}$ denoting gravitational acceleration.

To capture the feedback of thermal hydraulics on neutronics a quasi-steady-state heterogeneous temperature model (HTM) for the fuel pebble (see Figure 1) is implemented. This consideration is necessary, since fission heat is mainly generated in the uranium kernel and not in the surrounding graphite. In fast transients, the temperature difference between the fuel kernel and graphite can be substantial. This pronounces strong feedback effects from the fuel Doppler temperature.

In the HTM, the fuel is subdivided into an arbitrary number n of spherical shells, see Figure 1, in our example n = 6.

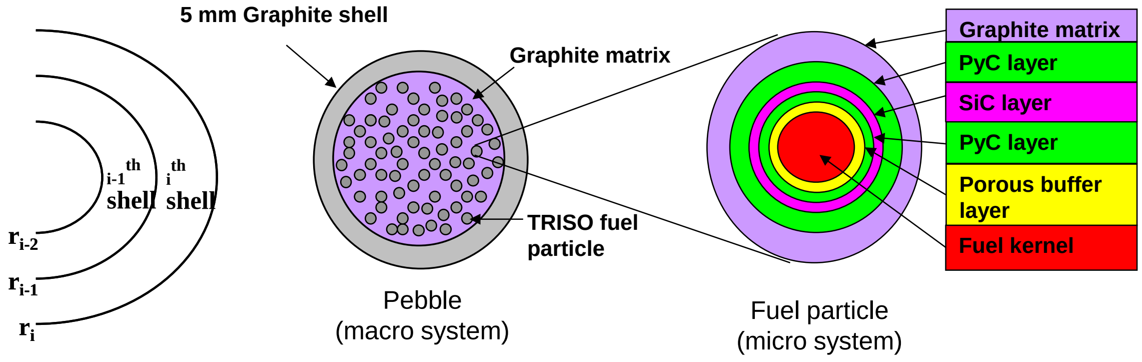

Figure 1 : Subdivision of a fuel element when applying the heterogeneous temperature model

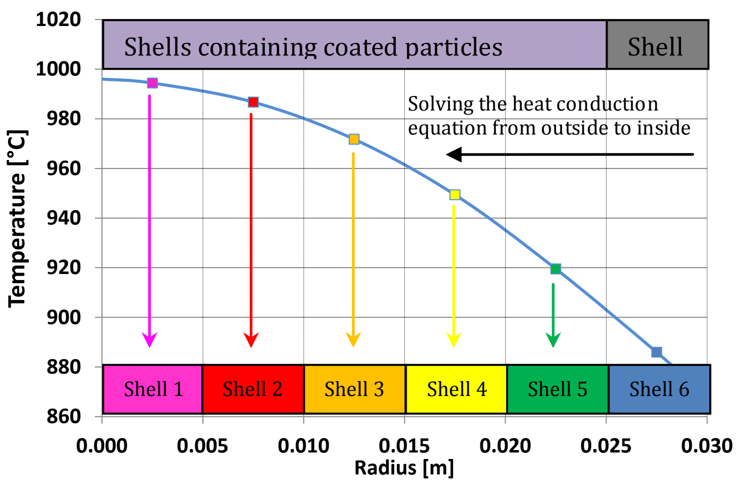

Figure 2 : Temperature distribution after solving the heat conduction equation for the fuel pebble (macro system), delivering boundary conditions for the micro system

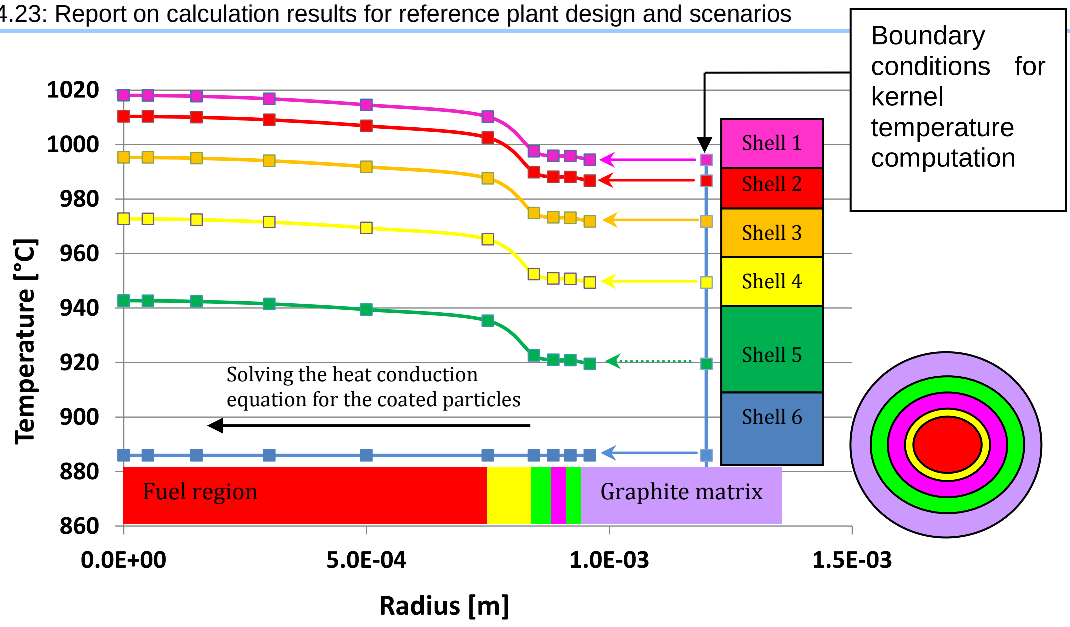

Figure 3 : Temperature distribution for the representative kernels per shell (micro system). The blue bar on the right side visualises the boundary condition after solving the heat conduction equation and is coloured as in the macro system. The colouring at the bottom display the different coatings according to Figure 2

Starting from the surface of the fuel element (kth shell or graphite matrix, here k = 6), the steady-state heat conduction equation for each shell is solved towards the fuel element centre (k-1th shell, then k-2th shell and so on). The surface temperature of the fuel element is taken as the boundary condition. Proceeding like this, one shell after another gets appointed a mean temperature until the innermost shell is reached. These temperatures, however, only apply to the graphite shells (macro system), not the fuel kernels (micro system).

For the average temperature of the fuel particles contained in a considered shell, a representative particle is determined that gets appointed the mean temperature for all the fuel kernels contained within. In order to determine the representative particle temperature, the respective shell temperature of the surrounding graphite serves as boundary condition.

Here, the heat conduction equation is solved for the micro system once more, taking into account the different heat conductivities of the coatings of the particles. After fuel and moderator temperatures are determined, the temperature values are averaged and one fuel temperature and moderator temperature per thermal hydraulic mesh is obtained to process nuclear cross section. Thus, fuel temperature feedback is much more pronounced than it is without HTM.

In order to correctly account for variation of material properties, ATTICA^{3D} comes with a large material properties library. For the description of other phenomena like heat transfer outside the pebble bed, pressure losses due to changing diameters in the flow path, thermal radiation and so on, a set of constitutive equations are provided within ATTICA^{3D}.

Technically, the coupled code system TORT-TD/ATTICA^{3D} is represented by a single executable in which ATTICA^{3D} acts as the main program and calls TORT-TD in terms of a subroutine whenever an update calculation of the power distribution is requested. For the data exchange between TORT-TD and ATTICA^{3D}, already existing TORT-TD interface routines have been utilized in combination with the ATTICA^{3D} mesh overlay feature that transfers 3-D distributions from its thermal-hydraulic mesh to a superimposed neutron-kinetics mesh and vice versa. This allows for efficient data transfer via direct memory access of array elements.

A TORT-TD/ATTICA^{3D} transient simulation consists of a three-step procedure. First, a coupled steady state calculation is performed. ATTICA^{3D} and TORT-TD are called repeatedly, followed by exchange of thermal-hydraulic and neutron kinetics data, until convergence of the 3-D temperature and power distributions are achieved. At the beginning of the iteration process, TORT-TD calculates for a given thermal-hydraulic initial distribution the corresponding power distribution that is transferred to ATTICA^{3D} as first estimate. Second, a zero transient follows based on the converged steady state with no changes being imposed on the system. A few seconds zero transient may help verify the stability of TORT-TD and ATTICA^{3D} when both codes switch to their respective time-dependent mode of operation. In the last step, the actual transient is being initiated and subsequently calculated.

2 Description of Reference Plant

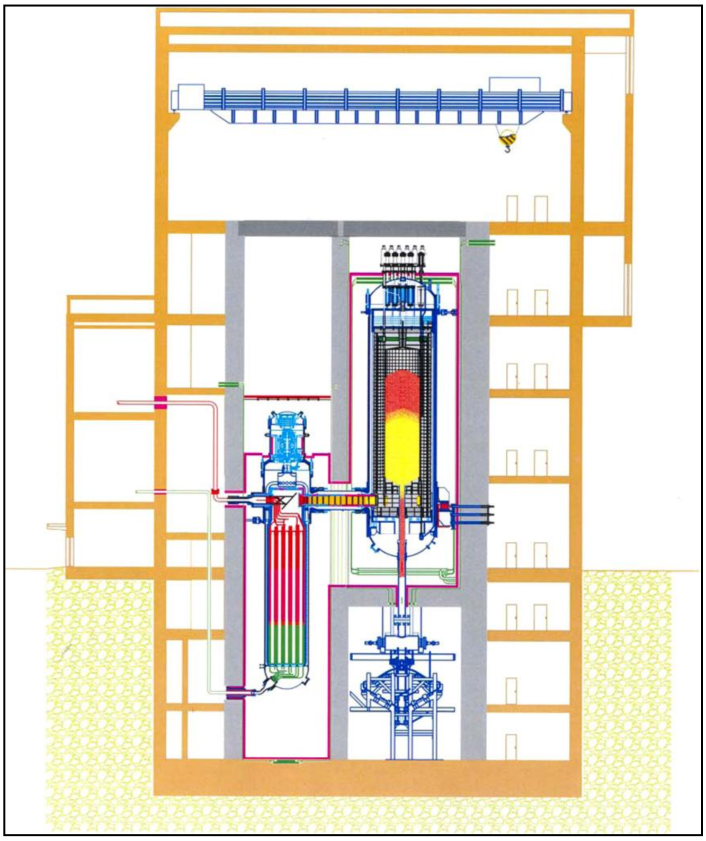

Figure 4 : Cross section of HTR-PM building [9]

The only HTR concept at the brink of finalization at the moment is the Chinese HTR-PM [9] [10], which stands for High Temperature Reactor – Pebble Bed Modular. It was developed after the successful test with the HTR-10 test reactor and is based on HTR-Modul designed in Germany by Siemens-Interatom in the 1980s [8]. It was decided that a pebble bed reactor based on the HTR-PM will be selected as a reference case for further calculations.

The layout of the HTR-PM is therefore a one zone cylindrical annular core consisting of a pebble bed (Figure 4, Figure 5). To compete economically with current Light Water Reactor (LWR) designs, two or more reactor cores should be coupled to one power conversion unit (turbine). To benefit from existing equipment, the power conversion is a Rankine Process (steam turbine) which includes a steam generator at the reactor.

A centre graphite structure consisting of a fixed structure or moderator pebbles is not foreseen. The core has the same diameter 3m which is the same as the HTR-Modul and HTR-PM (Table 1). The height of the flattened core is 11m. With an estimated average porosity of 0.39 of the pebble bed there are approximately 420,000 pebbles in the reactor. The Helium pressure in the primary loop is 7 MPa. The Helium in the primary loop flows from the steam generator with a temperature of 250°C and a rate of 96.3 kg/s through a coaxial pipe, through the helium risers to the top of the core, through the pebble bed and the porous bottom reflector with a temperature of 750°C back to the steam generator. The control rods (CRs) consist of multiple B_4C rings (Figure 7). Each CR can be driven independently. In case of station blackout, the control rods fall into their shut-down position by gravity. As secondary and additional shut-down system, small absorber spheres with a diameter of 1cm can fall by gravity (withheld by electrical valves) into long holes in the side reflector (Figure 8). The side reflector has a thickness of 75cm (this includes borated carbon bricks with a thickness of 5cm to protect the outer components of the reactor). The side reflector is divided into 30 azimuthal sections, each with either a CR-hole or two long holes for the SAS (hole circle diameter of 162.5cm).

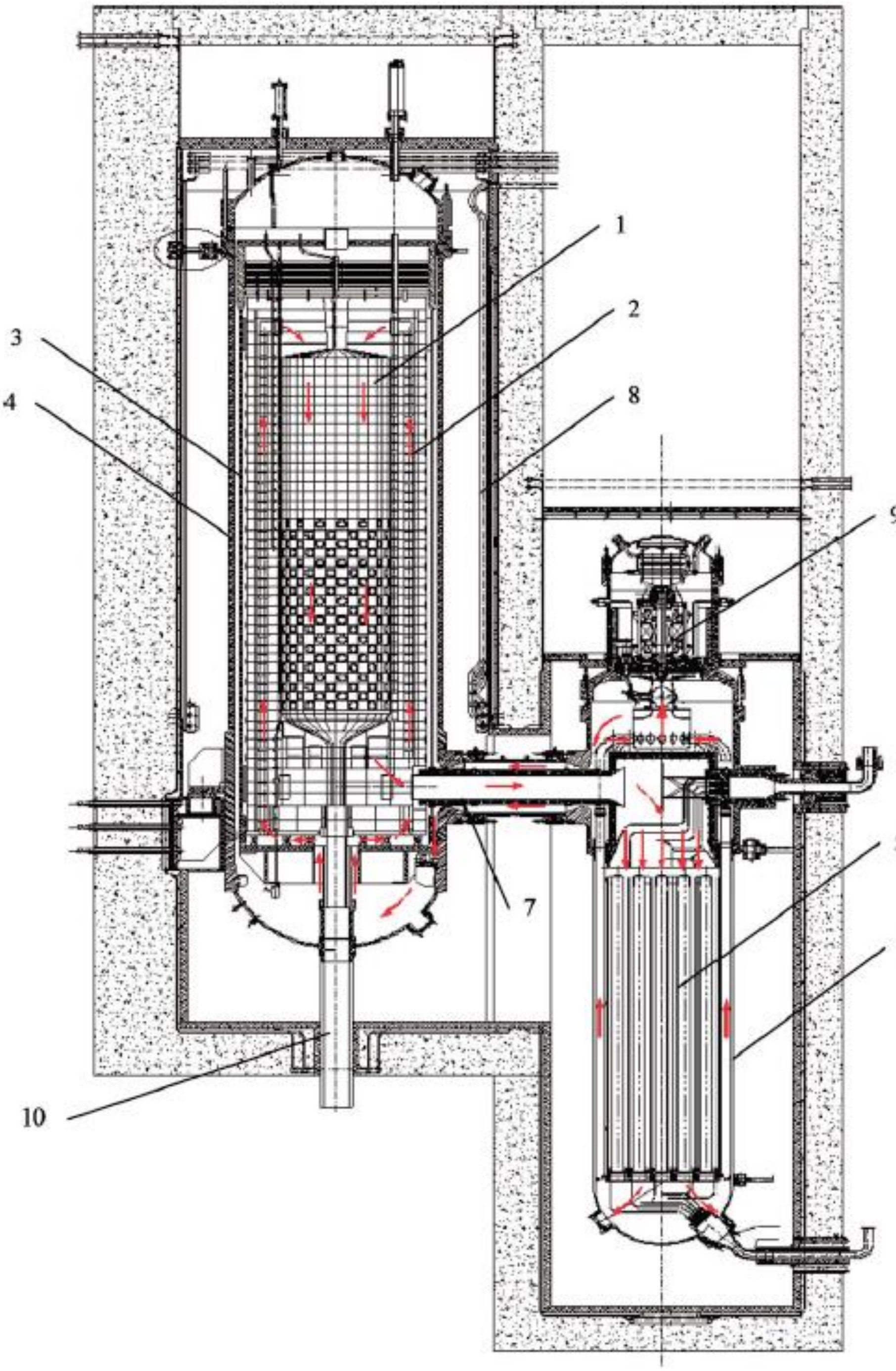

Cross-section of the HTR-PM reactor: (1) reactor core, (2) side reflector and carbon thermal shield, (3) core barrel, (4) reactor pressure vessel, (5) steam generator, (6) steam generator vessel, (7) coaxial gas duct, (8) water-cooling panel, (9) blower, (10) fuel discharging tube, (11) control rod driving system, and (12) small absorber sphere unit

Figure 5 : Cross section of HTR-PM [10]

The graphite components are kept in shape by a core barrel, which is then followed by a gaseous gap to thermally de-couple the RPV from the core barrel. The whole setup is located inside a Reactor Pressure

Vessel (RPV) made of steel. At the outside of the RPV the Reactor Cavity Cooling System (RCCS) is installed, which protects the reactor structures from temperature induced damage during accidents by transporting the expected excessive heating power to a low pressure RCCS.

The fuel of the reactor consists of fuel pebbles made of graphite, which include fuel particles with a diameter of 500µm (Figure 6). The particles have different coatings, namely a buffer graphite coating to absorb gaseous fission products, a pyrolytic carbon coating, a Silicon-Carbide coating and another pyrolytic carbon layer (TRISO). The Silicon carbide coating forms a strong barrier for diffusion of fission products and forms itself a pressure tight containment for fission products. The main fuel parameters can be found in

Table 2.

Table 1 : Main design parameters [9]

Parameter	Unit	Value
Rated electrical power	MW	110
ReactorThermal Power	MW	250
Average core power density	MW/m^3	3.22
Eletrical Efficency	%	42
Primary helium pressure	MPa	7
Helium temperature at reactor inlet/outlet	°C	250/750
Helium flow rate	kg/s	96.3
Numer of Helium riser channels	-	30
Active core diameter	m	3
Equivalent core height	m	11
Height upper void	m	0.57
Number of control rods	-	8
Diameter of control rod holes	cm	65
Number of SAS	-	2x22
Type of steam generator	-	Once through helical coil
Main steam pressure	MPa	13.24
Main steam temperature	°C	566
Main feed-water temperature	°C	205
Main steam flow rate at the inlet of turbine	t/h	673

Table 2 : Main fuel element parameters [9]

Parameter	Unit	Value
Fuel Type	-	TRISO
Heavy Metal (HM)	-	UO2
Radius of U- Kernel	µm	250
Thickness of the 4 Kernel Layers	µm	95 / 40 / 35 / 35
Density of HM-Oxide	g/cm3	10.4

Density of the 4 Coatings	g/cm3	1.05 / 1.9 / 3.18 / 1.9
Radius of Fuel Matrix	cm	2.5
Radius of Fuel Element	cm	3.0
Graphite Density of Matrix	g/cm^3	1.74
HM per fuel element	g	7
Enrichment of fresh fuel	%	8.9
Thermal absorption cross section of Graphite [Fuel and Reflector]	mbarn	4
Number of fuel elements in reactor core	-	420,000
Average burn-up	GWd/tU	90
Pebble-bed porosity	-	0.39
Fueling mode	Multipass	15

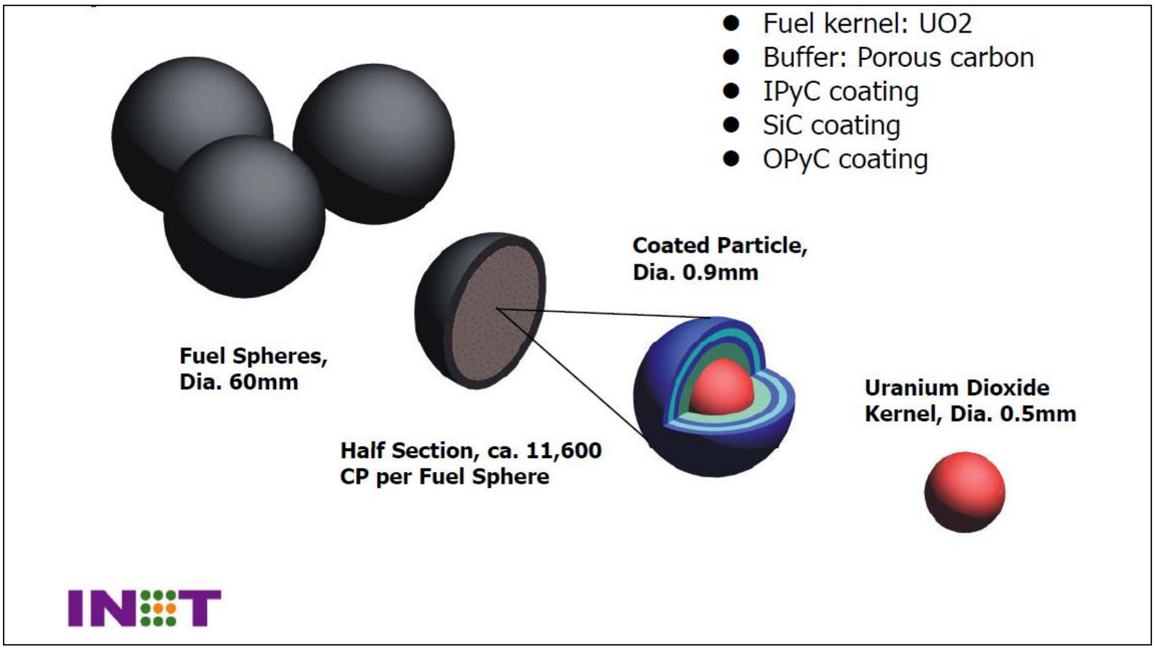

Figure 6 : Layout of fuel Elements (Source: INET)

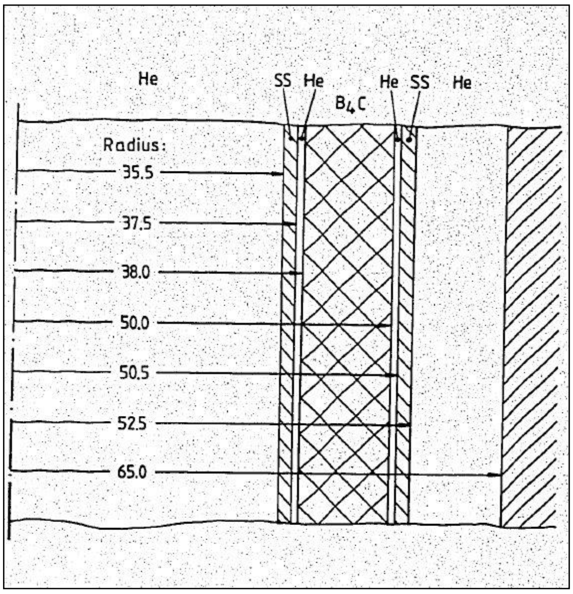

Figure 7 : Control Rod layout (SS : Stainless Steel)

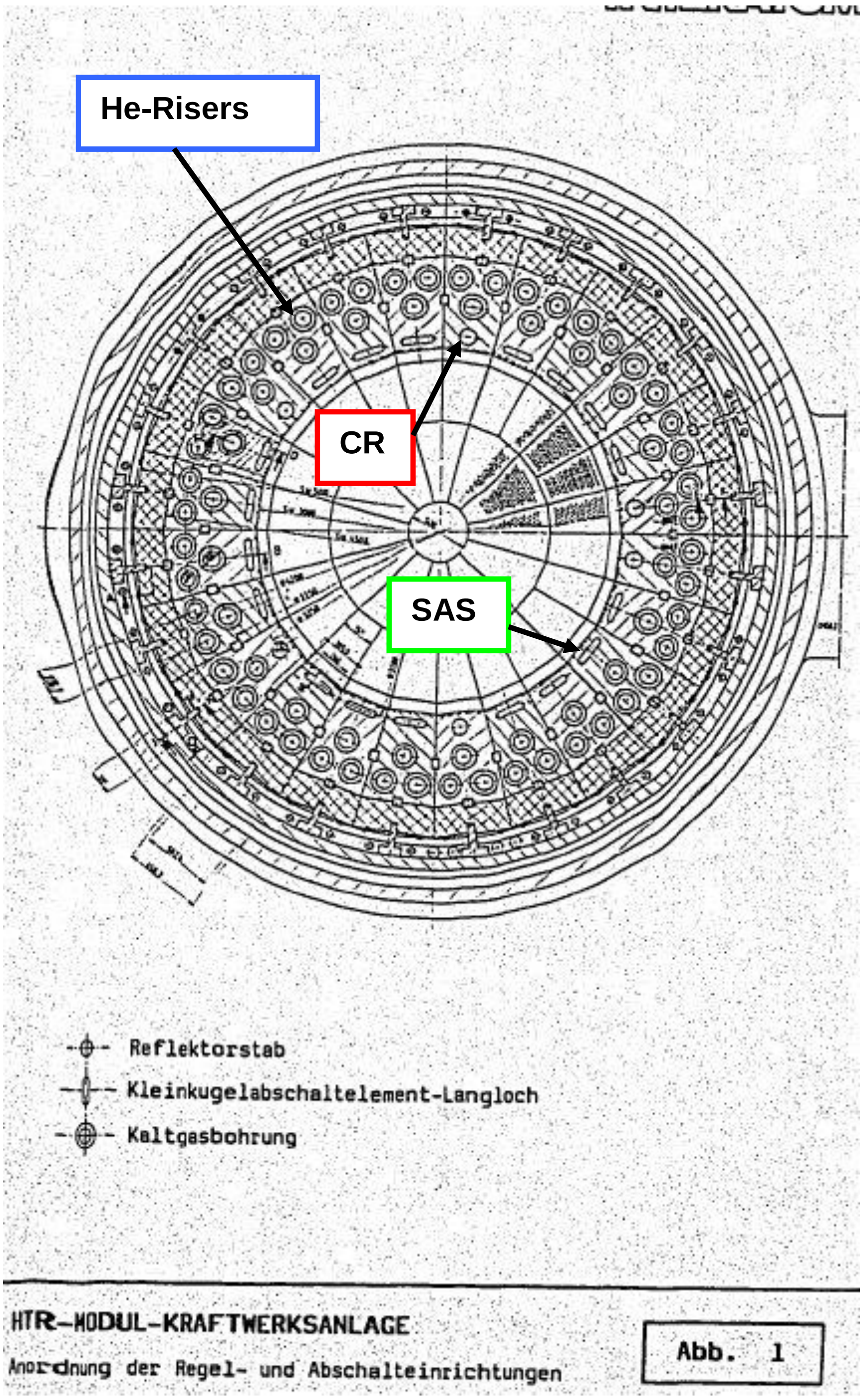

Figure 8 : Horizontal cross section of HTR-Module

3 Coupled hot spot analysis for one average fuel element

3.1 Definition and Configuration of Hot Spots and Areas

Hot spots and areas in pebble bed cores can occur as a consequence of more densified pebble clusters or of unexpected fuel loading patterns and fuel handling inside the reactor.

A variation of the flow velocity of one of the pebble flow channels mentioned above might lead to a higher or smaller burn-up of the specific zones and therefore to a more imbalanced power distribution. The highest effect is expected at the radially innermost flow channel since the highest pebble flow velocity occurs here.

Hot spots in Pebble Beds might be triggered through a densification of the fuel pebbles [11] [12]. This will lead to a reduction of coolability of the densification. A higher density of the fuel pebbles also leads to a local increase of the moderator density.

If the densification migrates through the core as part of the normal fuel cycle, the change in moderator to fuel ratio may lead to spectral changes and as a consequence, to burn-up and power density changes which could be determined.

The densification might also occur spontaneous during normal operations, which leads to a cluster of pebbles with an unaffected nuclide vector of previous burn-up.

The consequences of these considerations during accident conditions have also to be determined.

The effects described above can also occur for a cluster of fresh fuel pebbles.

3.2 Definition of Evaluation Cases

One working point would be the modification of the flow channel velocity. A variation of +-20% of the velocity during normal steady state will be accomplished and compared to the previous steady state.

Another study will be the influence of a wrong fuel loading pattern. It will be assumed that, after the run-in phase to the equilibrium core, only fresh fuel pebbles will be loaded to a pebble flow channel. The effect is expected to be greatest at the innermost flow channel resulting from the highest neutron flux. A test case loading fresh fuel in the innermost zone will be investigated and compared to the previous steady state results.

For the following considerations for the TORT-TD/ATTICA^{3D}, it is assumed that the densification occurs after the run-in phase of the core.

A small zone with a modified cross section set is to be defined with the following modifications:

The densification forms an area with a smaller porosity, additional influence may be the fuel loading pattern where a series of fresh fuel is introduced into the core and forms a densification.

Stationary results are to be achieved for the following different cases:

- Densification in the maximum of neutron flux
- Densification in the maximum of neutron flux with a bulk of fresh loaded fuel elements
- Densification at the temperature maximum (near the lower end of the core)
- Densification at the temperature maximum (near the lower end of the core) flux with a bulk of fresh loaded fuel elements

To gather reference information about local densifications, MCNP calculations will investigate the influence of the lower porosity of the pebble bed as a reference for the following simulations. The MCNP calculations will be done without consideration of burn-up. The results will be compared to the normal pebble bed results.

Transient calculations are intended for the following cases:

- Control rod ejection: The ejection of one control rod leads to a power excursion. The influence on temperature and power distribution will be investigated.
- PLOFCA (pressurized loss of forced cooling accident): The influence on temperature will be investigated.

- DLOFCA (depressurized loss of forced cooling accident): The influence on temperature will be investigated.

With the transport code MCNP, it is possible to simulate every single fuel particle inside the pebble. In this example, the distribution of the fuel particles are achieved by using a regular lattice of cubes, each consisting of the fuel particle with a diameter of 500 µm and a surrounding mixture of fuel matrix graphite with the coating materials (Figure 9). The MCNP built-in uranium card can provide additional information by randomly distributing the fuel particles inside the graphite matrix.

It is foreseen to do MCNP calculations with some fuel pebbles in different configurations, thereby simulating different porosities of the pebble bed. Fuel compositions of the equilibrium core will be will be used as starting point. The calculations results are intended to be used as reference for the influence on neutron flux of the densification for the following TORT-TD/ATTICA^{3D} calculations.

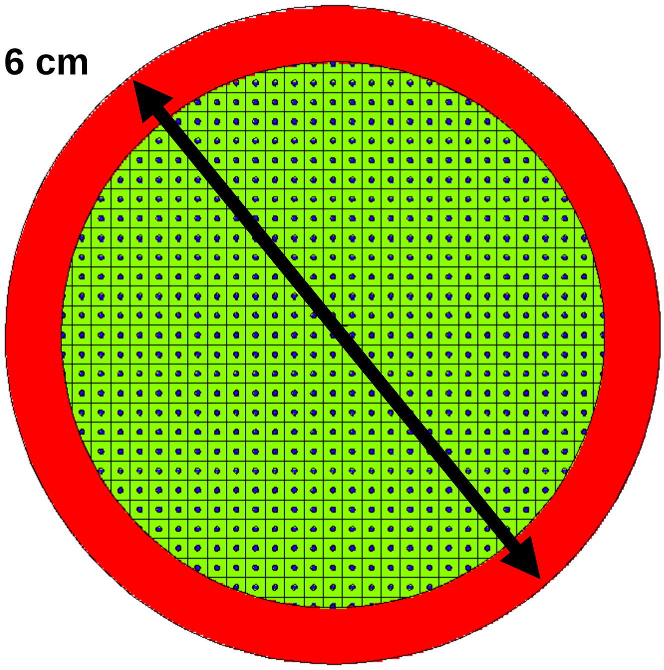

Figure 9 : Representation of a fuel pebble in MCNP

For pre-processing, a ZIRKUS calculation of the HTR-PM layout is performed to achieve the nuclide densities and cross sections of the equilibrium state. For this purpose, the core is divided into 8 flow zones of equal area (and therefore volume) to model the pebble flow adequately, see Figure 10 For every reload interval the fuel shuffling and re-loading module of ZIRKUS takes the determined nuclide densities and transfers them to the next lower core zone. Due to the different number of axial subdivision, real pebble flow behaviour can be accounted for, i.e. pebbles flow like sand in an hour-glass. From earlier experiments for pebble flow it was concluded that the innermost channels are 1.5 times faster than the outermost flow channel. This explains the number of subdivisions to be 16 for the innermost and 24 for the outermost channel. When preparing the macroscopic parameterised cross sections for the coupled transient calculation (especially for a rod ejection), the geometry necessary for pebble refuelling and shuffling can be simplified and the number of compositions within the geometry is reduced. For the starting point of the equilibrium core, the HTR-PM was simulated with 13 neutron groups and 399 material compositions. With the adequate condensation and averaging tools of ZIRKUS, the 13 neutron groups were condensated to 7 neutron groups. Also the 399 material zones including flow lines are averaged volumetrically to a 234 material zone map, see Figure 11.

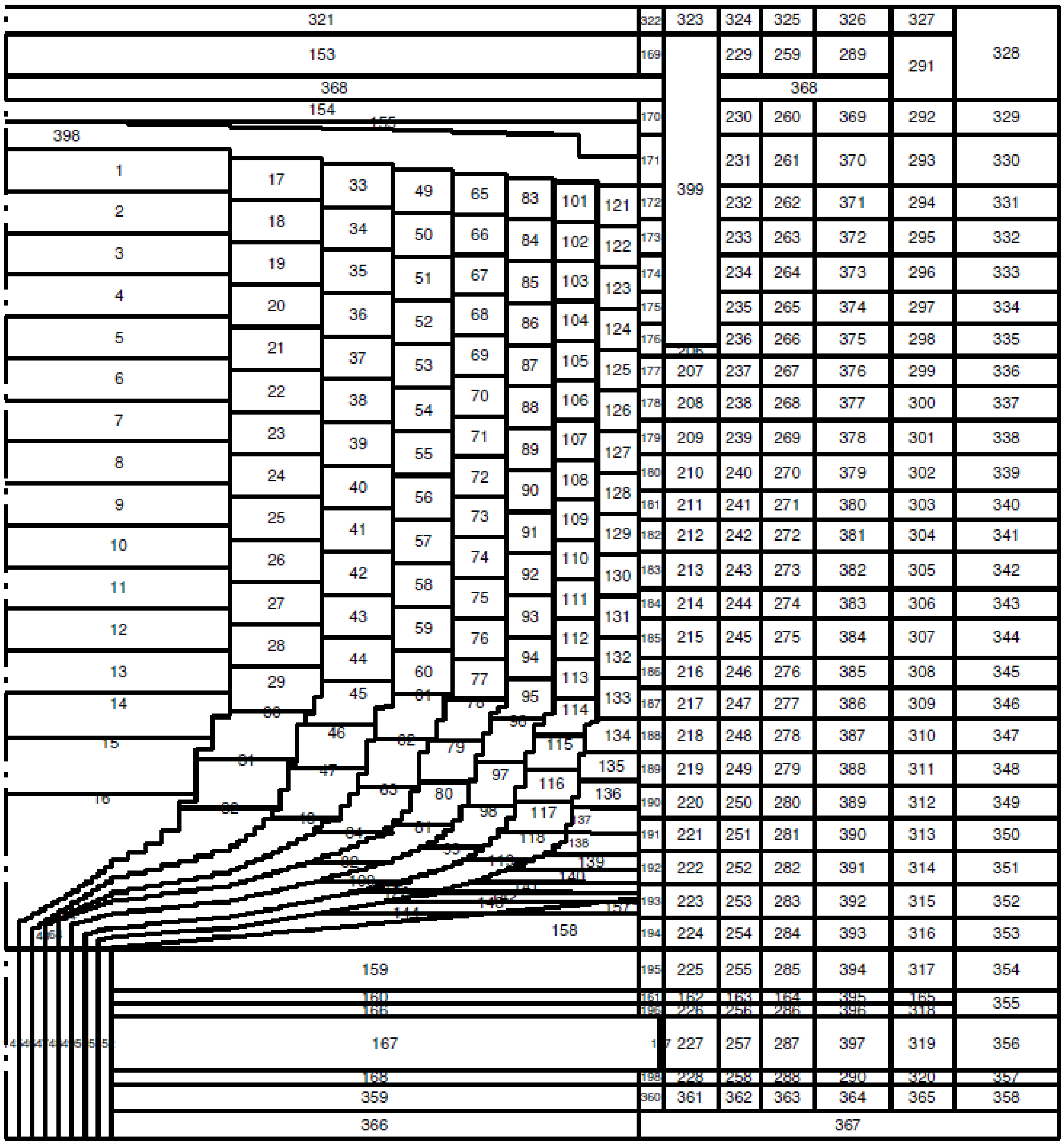

Figure 10 : HTR-PM geometry with pebble flow channels modelled according to experimental findings of pebble flow

The control rods are modelled as a grey curtain to achieve a critical reactor (Figure 11, zone 199). The reflectors and other core structures are divided into different zones to provide detailed consideration of thermal and material for the cross sections. Different pebble flow velocities and their influence can be investigated with analysis of ZIRKUS results. It will be assumed that the densification occurs after the formation of the equilibrium state of the core.

Since ZIRKUS is a 2D-code, the cross sections represent a 2D reactor model. Therefore, only densifications on the symmetry axis can be correctly simulated by ZIRKUS. The densification leads also to a decrease of pebbles in the surrounding channel areas. Since it is assumed that the pebbles move in flow channels, the decrease is only expected to occur in the flow channel cells above or below the densification. The unintended loading of fresh fuel can also be simulated.

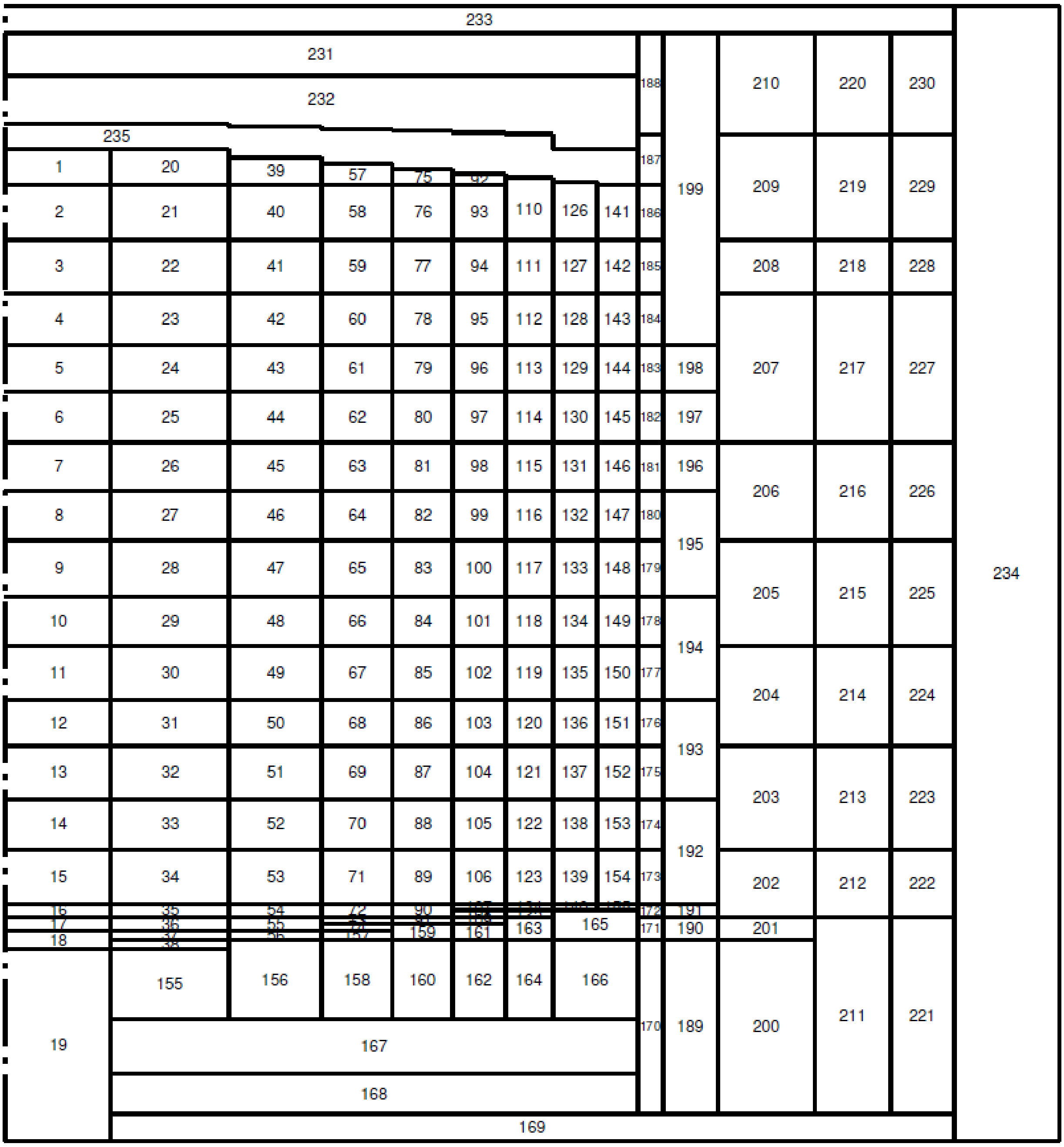

Figure 11 : Representation of neutronic zones in ZIRKUS after condensation from 13 to 7 neutron groups. TORT-TD uses this material composition map

For the calculation in TORT-TD/ATTICA^{3D}, the generated cross sections from ZIRKUS are used. Figure 12 and Figure 13 show a 180° representation of the HTR-PM in ATTICA^{3D}.

The neutronics discretisation model of TOR-TD is similar with the ZIRKUS model, but expanded azimuthally to 180° into 13 zones, also representing the control rods. The ATTICA^{3D}-model is divided into similar azimuthal zones. The control rods can be driven individually by TORT-TD input options. The flux and spectra are calculated by TORT-TD model. The zonal structure in the densification is more resolved than adjacent regions to gather the desired information.

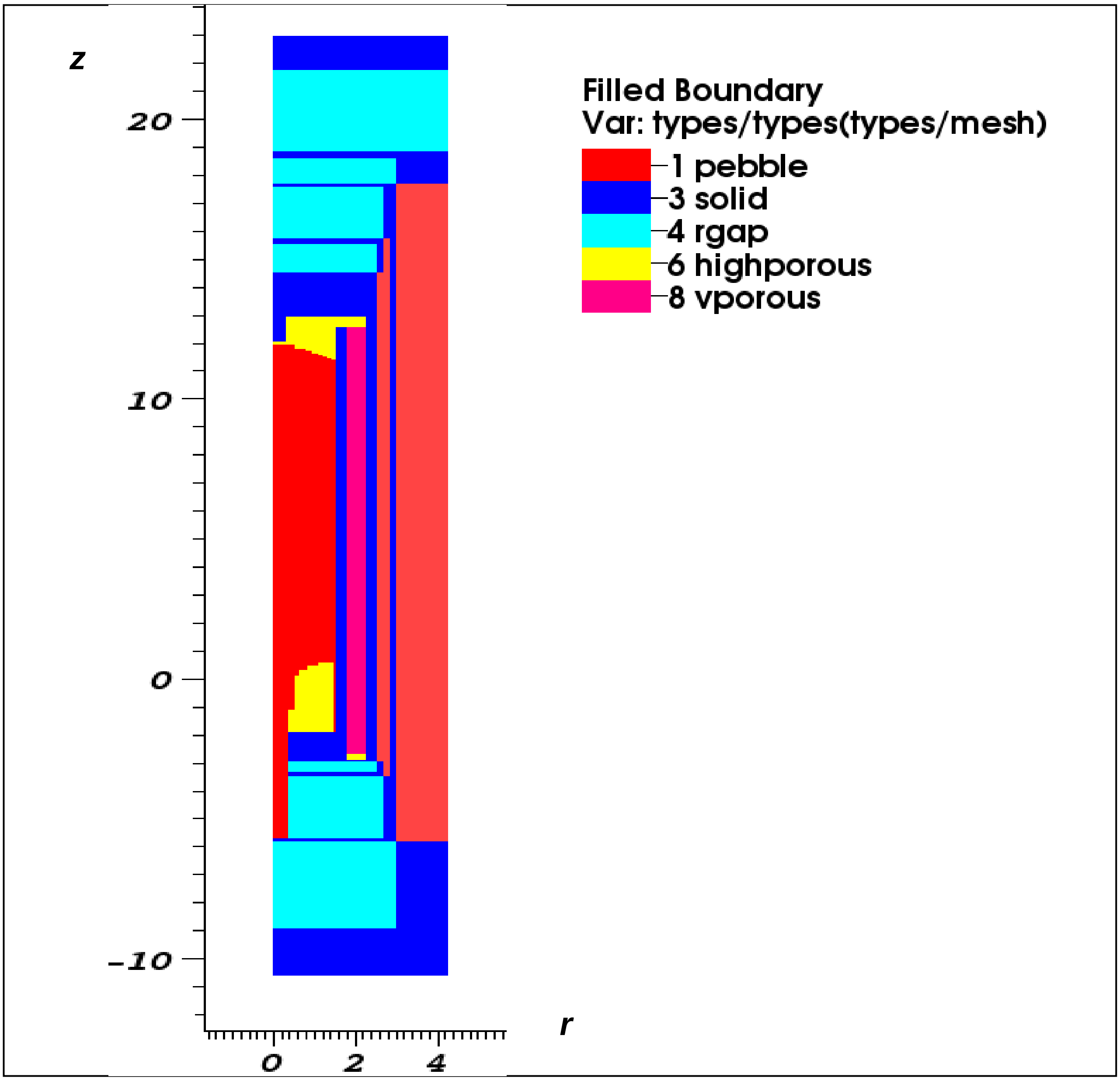

Figure 12 : Cross section of representation of thermal hydraulic zones in ATTICA^{3D}

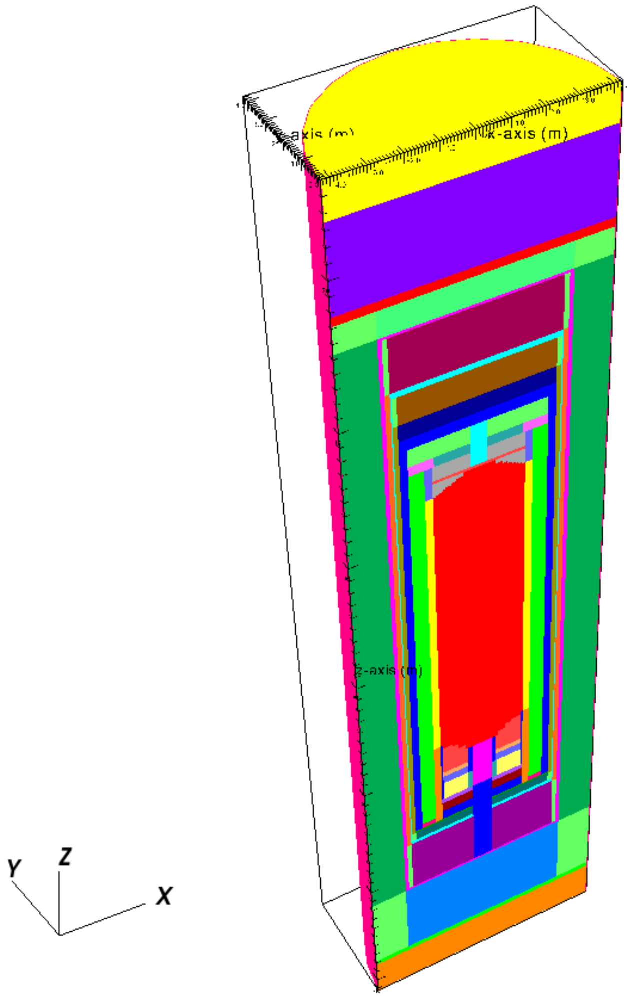

Figure 13 : 180° ATTICA^{3D} model with components

3.2.1 Modeling of densifications

The densification in the pebble bed is modelled according to the results of Auwerda [13]. Auwerda specifies a number of around 45 pebbles for the size of one densification cluster. The radius is determined by the cubic root of 45, resulting in around 3.5 pebbles per cube. This results in a diameter for a certain cylindrical densification of almost 20 cm. For the densification cluster, the cross sections must be modified, because in ZIRKUS only the global porosity of the densification cluster can be determined. As the cross section must be specified for each zone in the model, a zone with a height of 70 cm is produced for the densification cluster. Figure 14 shows the porosity over the radius.

Under the assumption that the pebble loading of the reactor operates correctly, meaning that the pebble flow is not interrupted, a more porous region above the densified zone is assumed. Furthermore it is assumed that the densification is formed during normal operation. Therefore there is no influence of the depletion to be expected within the pebbles and their nuclide compositions. So the corresponding cross sections are modified according to the change of porosities.

As a filling factor for the densification, a maximum 0.71 was estimated by Auwerda; for the less densified zone above the densification, a filling factor of 0.58 is assumed.

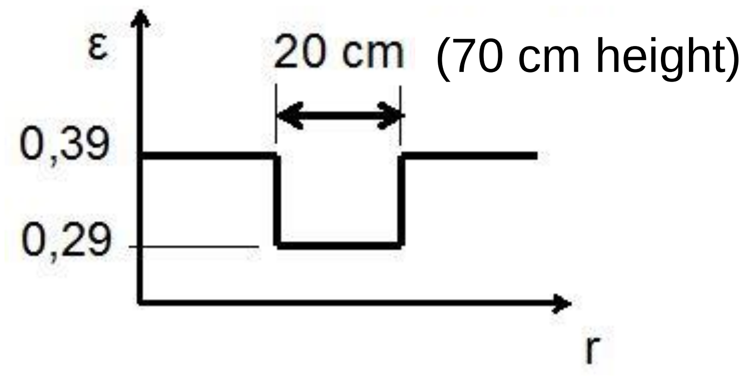

Figure 14 : schematics of the porosity change

The modification of the cross section can be derived from the following equation:

$$N_T = \frac{A}{M}\rho \tag{1}$$

The effective density in a mesh, as well as in the pebble bed, depends on the porosity:

$$\rho_{eff} = \varepsilon\rho \tag{2}$$

Here M denotes the molar mass and A mass number. The macroscopic cross section Σ is proportional to nuclide density. The ratio of A/M is constant. It can be concluded:

$$\Sigma = \frac{A}{M}\cdot\rho_{eff}\cdot\sigma \tag{3}$$

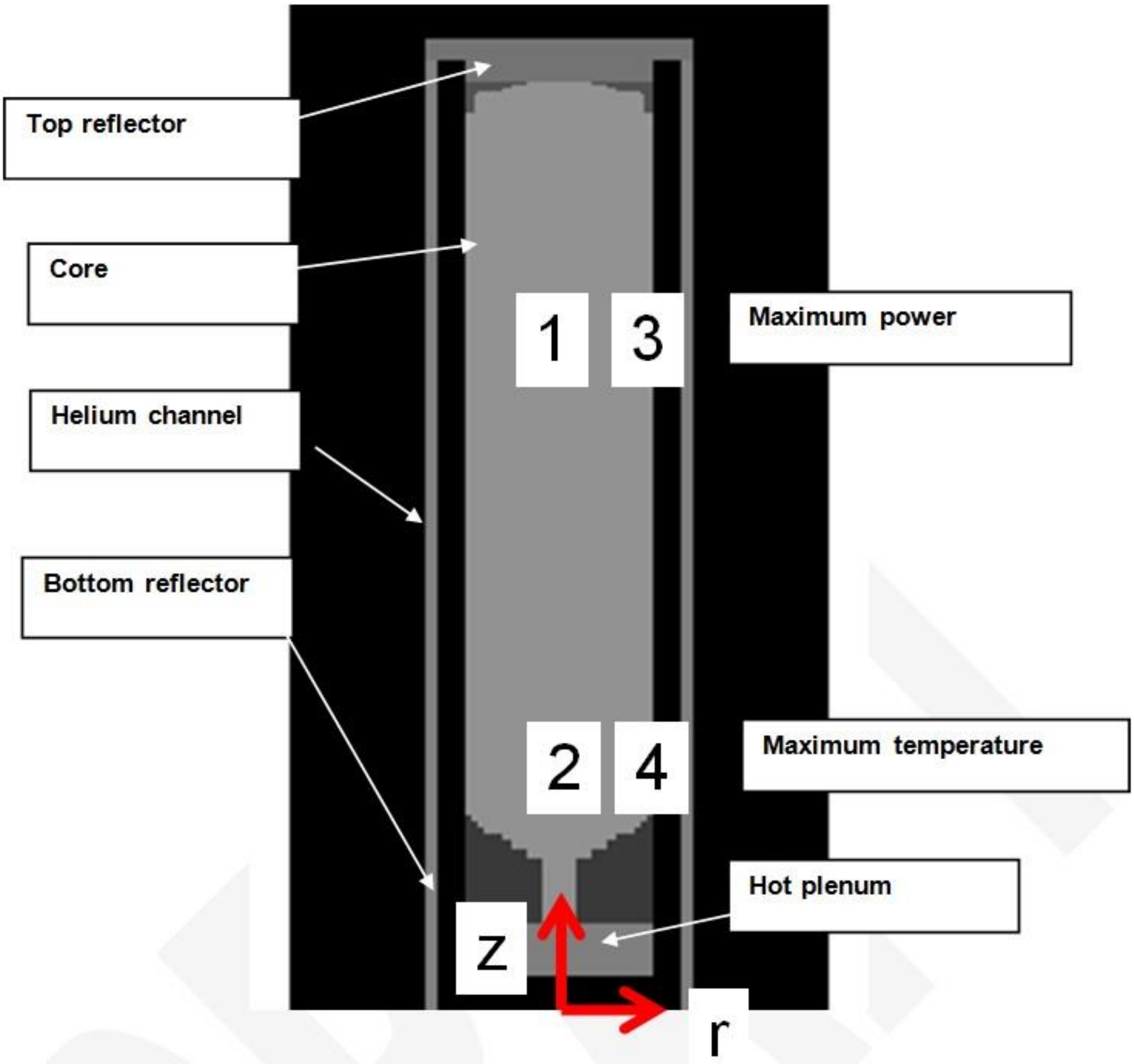

Figure 15 : Location of the densifications

By decreasing the porosity, the nuclide density increases to the same extent and, hence, also the cross sections will change. The moderation ratio, the ratio of the nuclide density of moderator over fuel, remains the same. Under the assumption that the influence of the neutron spectrum in the densification cluster is of minor importance, the corresponding cross section can be modified according to the porosity. A densification with a porosity of 0.29 - in comparison to the normal 0.39 - produces a power factor of 1.168 for the densified region; and 0.951for the less dense region (porosity 0.42). This factor will be used to modify the cross sections for the regions of interest.

For this investigation, the porosity change is carried out in different selected positions in the pebble bed: one in the region with the maximum power, at the symmetry axis and at the edge of the pebble bed, another in the region with the maximum gas temperature at the bottom of the pebble bed, also at the symmetry axis and the edge of the pebble bed.

Table 3 : Location of densifications

	Symmetry axis	Outer channel
Power maximum	1	3
Lower core	2	4
Geometry	Cylinder on centreline	Annular segment

Table 4 : Position of densifications

Case	Height [cm]	Radius [cm]	Angle [°]
1	1034,1 - 1100,1	0 - 10,94	0 - 180
2	1034,1 - 1100,1	129,90 bis 140,31	0 - 7,66
3	351,1 - 431,1	0 - 10,94	0 - 180
4	351,1 - 431,1	129,90 - 140,31	0 - 7,66

The positions of the densification clusters are represented in Figure 15. The densified regions in the symmetric axis are of cylindrical shape, the densification at the edge change is a fraction of an annulus. Therefore the angle is calculated as consequence of the volume unit with cylindrical form. As inner and outer radius the radii of the TORT-TD geometry will be used (Table 3, Table 4). The angle of the outer densification is calculated as 15.31, for a 180°. For symmetry reasons, the densification of the simulation is only half the angle.

The ATTICA^{3D}-model consists of 17 angles with 5 control rods. With 75 z-meshes and 33 radial meshes, there are 42,705 meshes for the ATTICA-model (Figure 16). The whole height of the model is 30.957 m with a 4.26 m radius. As boundary condition a constant heat transfer over the edge of the cylinder is modeled. The cooling gas flows enters with an initial temperature of 523 K and a flow of 96 kg s^{-1}. The heterogeneous temperature model is used with an outer free-fuel zone and 5 subdivisions for the fuel zone.

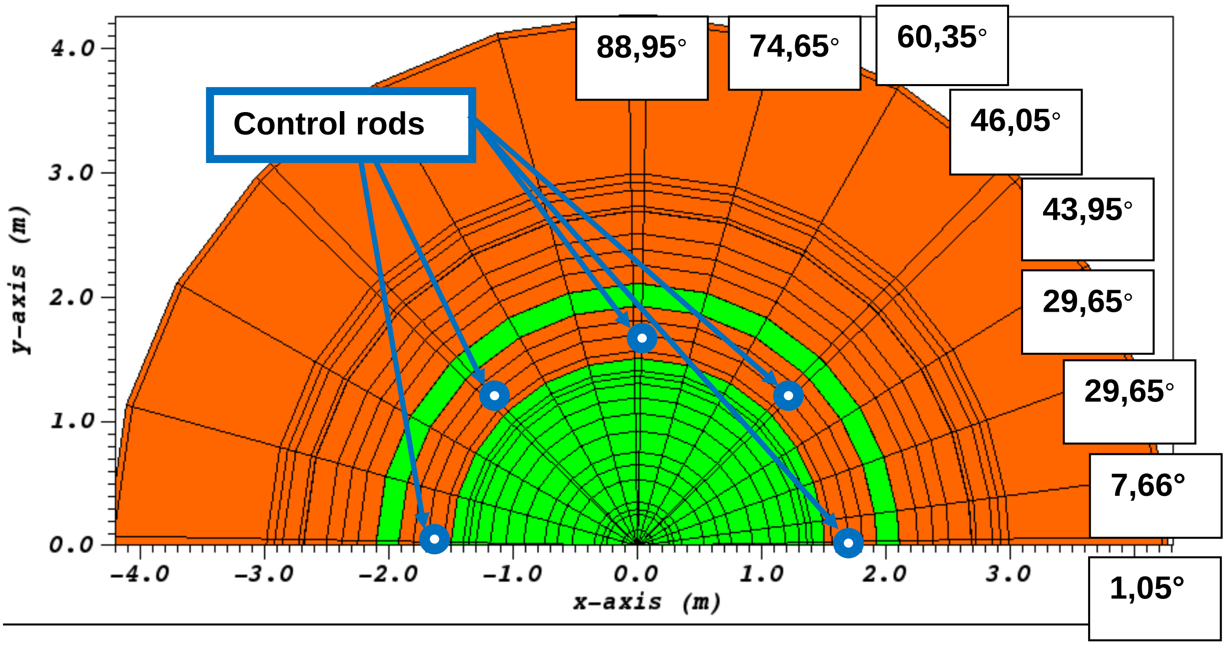

Figure 16 : Horizontal section with 180 ATTICA-model HTR-PM (orange: no flow, green: flow path)

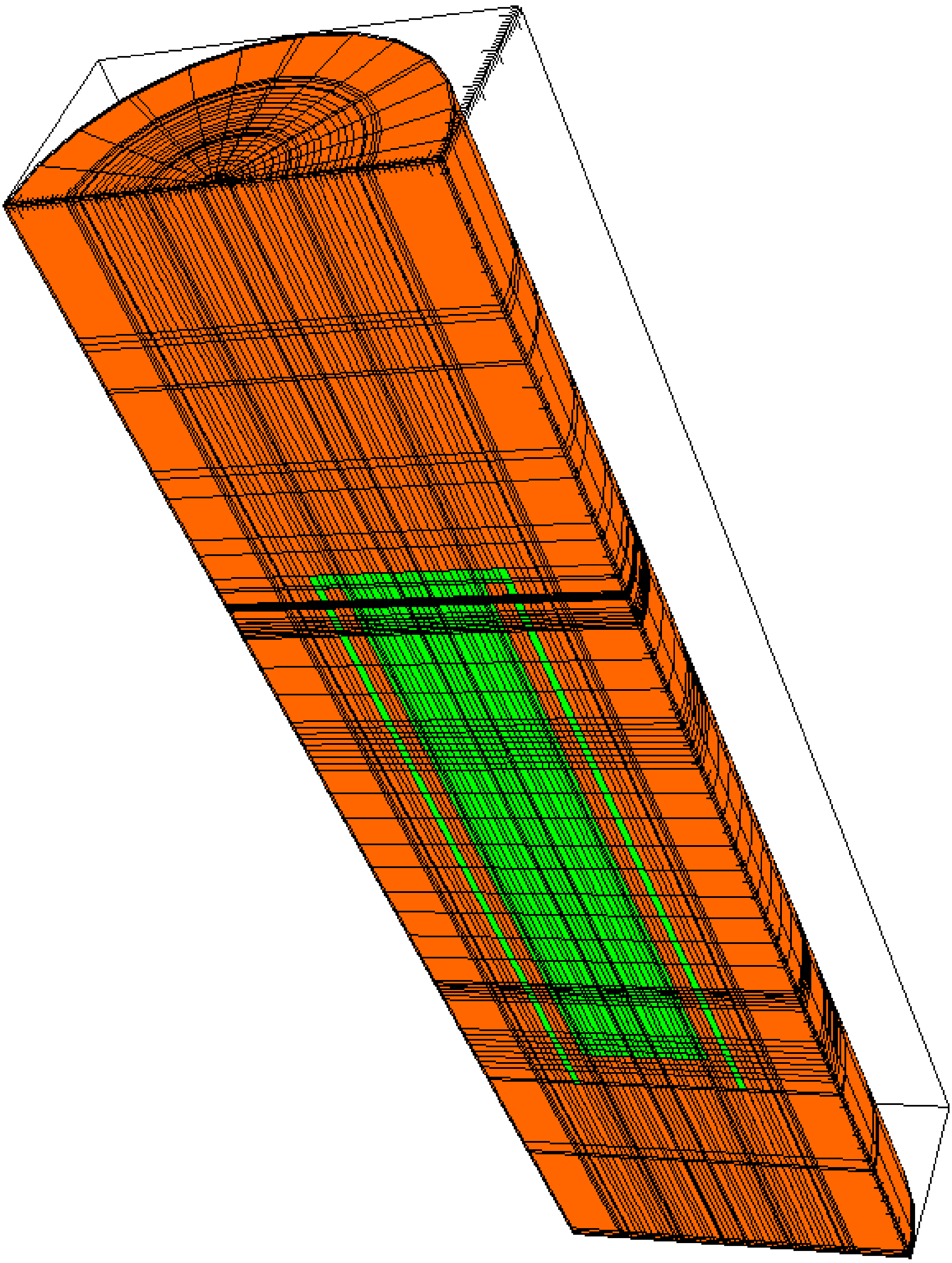

Figure 17 : 180° ATTICA^{3D}-model (orange:no flow, green: flow path)

3.2.2 Depressurised loss of forced cooling accident with densifications

1)

2)

3)

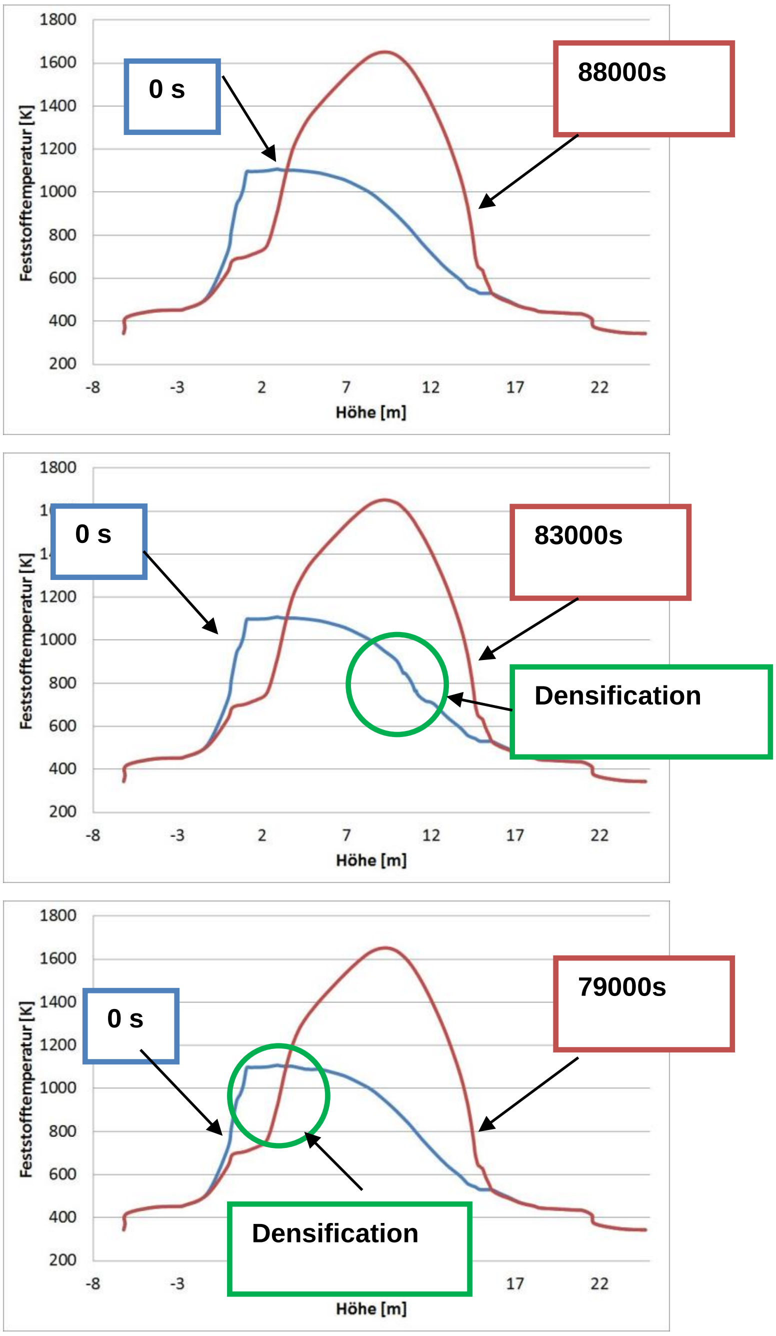

Figure 18 : DLOCA at the HTR-PM, maximum temperatures at the symmetry axis: 1) without densification, 2) with a densification at z = 10 m, 3) with a densification at z = 1m

A DLOFCA is simulated to analyse the influence of the densification. An instantaneous pressure relief to atmospheric pressure is assumed as well as a reactor shutdown, so just the remaining decay heat must be carried out of the system.

To simulate this case faster, an implemented ATTICA^{3D} function was used. For the DLOFCA approach, it is assumed that the coolant has no significant impact in the heat transport at atmospheric pressure and therefore the coolant's impact is not calculated which can be regarded conservative. For the simulation, the decay heat is computed according to DIN 25485. The power distribution is taken from the previous ZIRKUS calculations, for the densification cluster and the less dense cluster the power is partially modified according to the porosity change. A coupling with neutronics is not performed.

For the densification on the symmetry axis, the problem reduces to a quasi-2D (one azimuth) 30-model of the HTR-PM.

Figure 18 shows the temperatures at the centreline of the ATTICA^{3D}-model. Small deformations can be seen at 0 s in the densification cluster, apparently it can be transported with the coolant leading to temperatures increase of only 10 K.

3.2.3 Asymmetrical ejection of rods with densification

The data for the modified cross sections of the densification cluster and the control rods were used for the control rods ejection simulation. The transient is based on the OECD/NEA-Benchmark for the PBMR [15], this means that the complete control rod ejection out of the reactor occurs in 0.1 s. resulting in a rod velocity of 46 m/s. The complete simulation time of the transient is 50 seconds. Only 3 control rods are ejected.

Figure 19 shows the flow within and around the densification cluster. The reduced flow velocity is obvious. In addition, the coolant avoids the densification cluster. With helium the heat transfer coefficient increases with increasing temperatures, also in the graphite. Hence, the effective heat transfer capacity in the zone increases such that power increase can be compensated by adjacent zones and the surrounding gas (Figure 20).

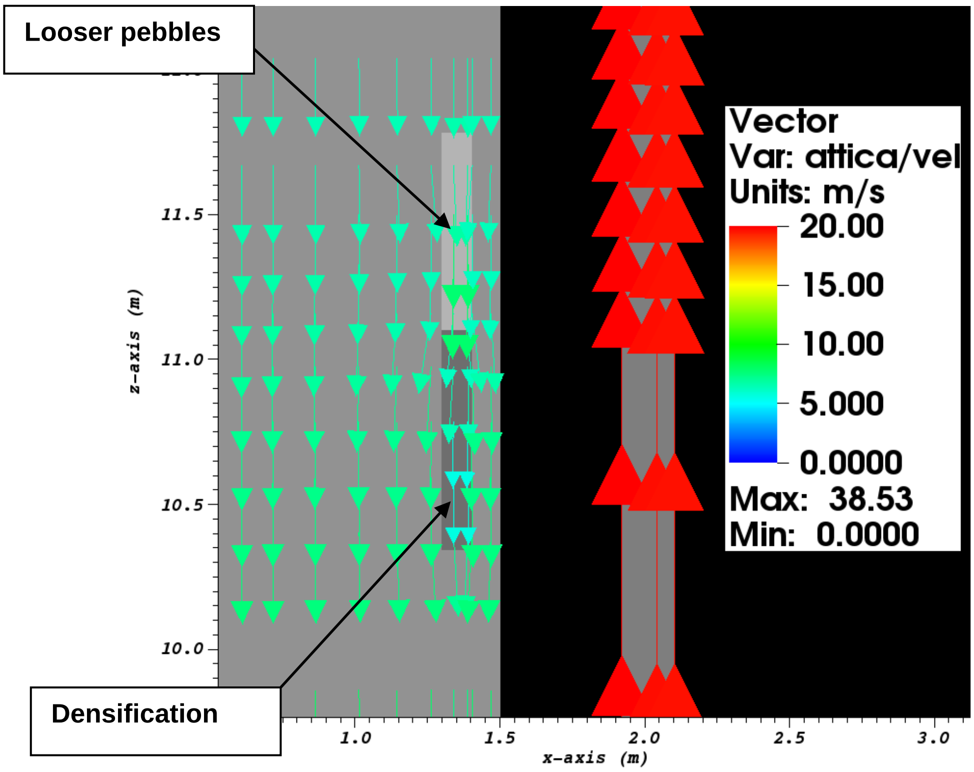

Figure 19 : Flow ratio in the densification cluster (at the maximum power height, edge region) at 0s.

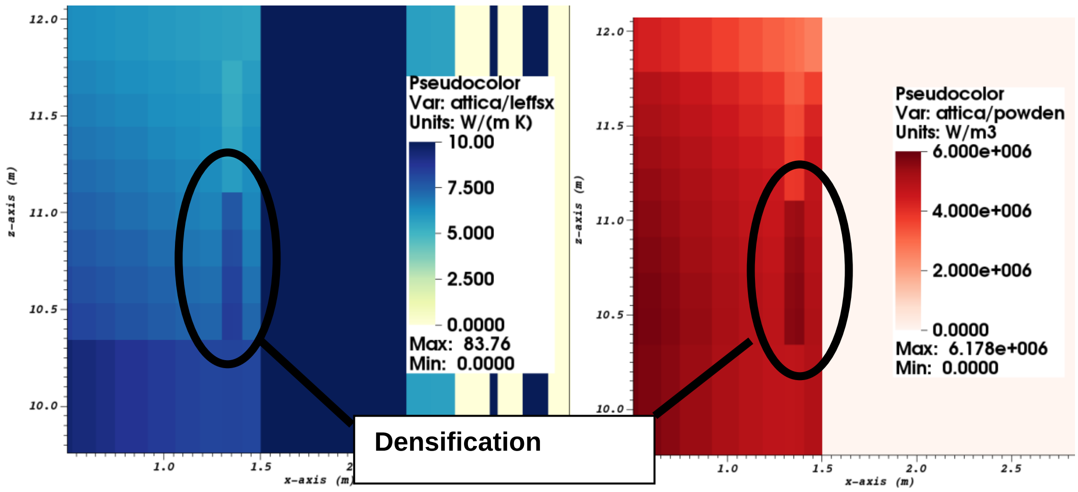

Figure 20 : effective heat transfer capacity of solid material in radial direction (left) and power density (right) in the densification cluster (at maximum power height, edge region) at 0s

The different densification scenarios are simulated for the 3-rod ejection. The power densities as well as the maximum fuel temperature are shown and discussed.

At first, the transient without densification is computed (Figure 21, Figure 22). The deformation of the power distribution as a consequence of the asymmetric control rod ejection is clearly visible, also the asymmetric temperature distribution. The maximum power is reached after 3.75 s, then, the fuel temperature coefficient counter-acts and the power reduces again. As the power is still elevated, the temperature increases and is still increasing after the final simulation time of 50 s. however the temperature increase in the fuel is in the range of 30 K.

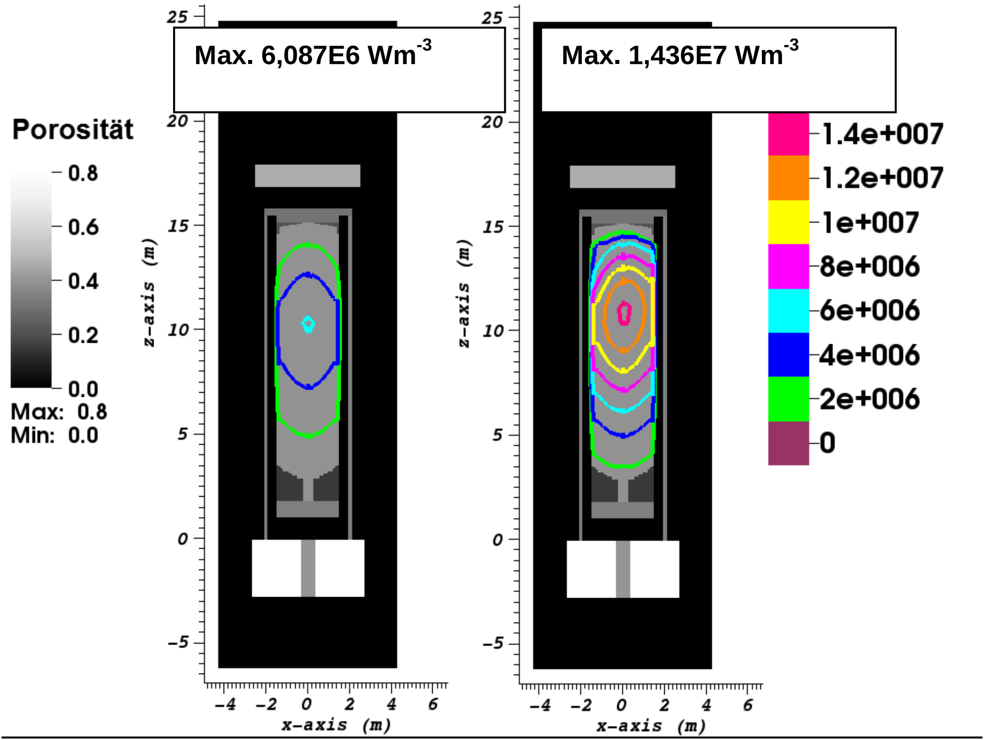

Figure 21 : Power distribution at the beginning (0s, left) and at the maximum power achieved at 3.75 s (right) for a one side control rod ejection, without densification.

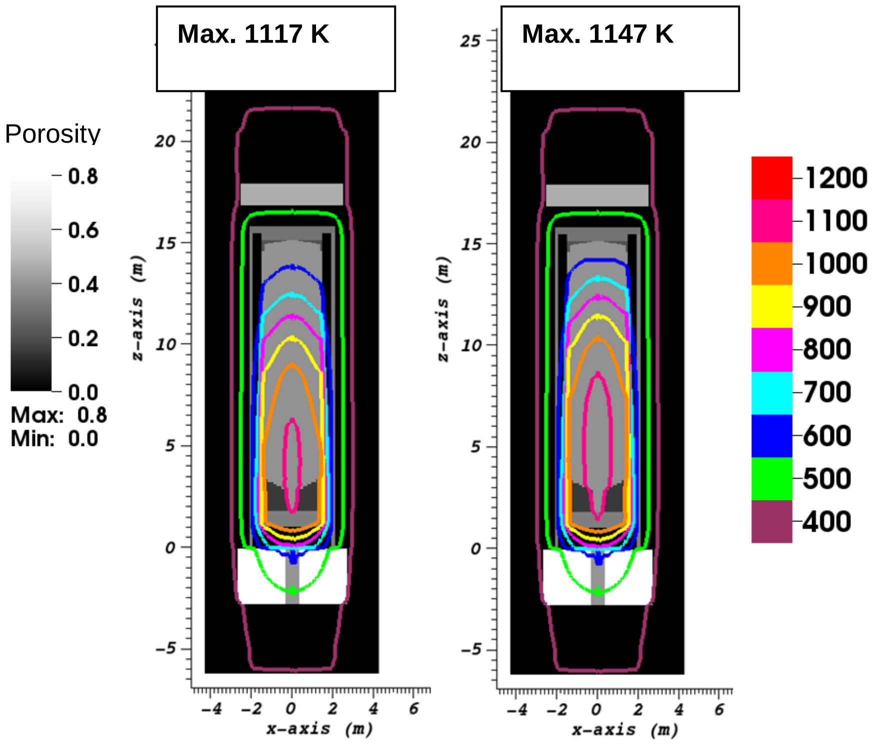

Figure 22 : Maximum fuel temperature distribution at the beginning (0 s, left) and at the end (45 s, right) of the transient for a one side control rod ejection, without densification.

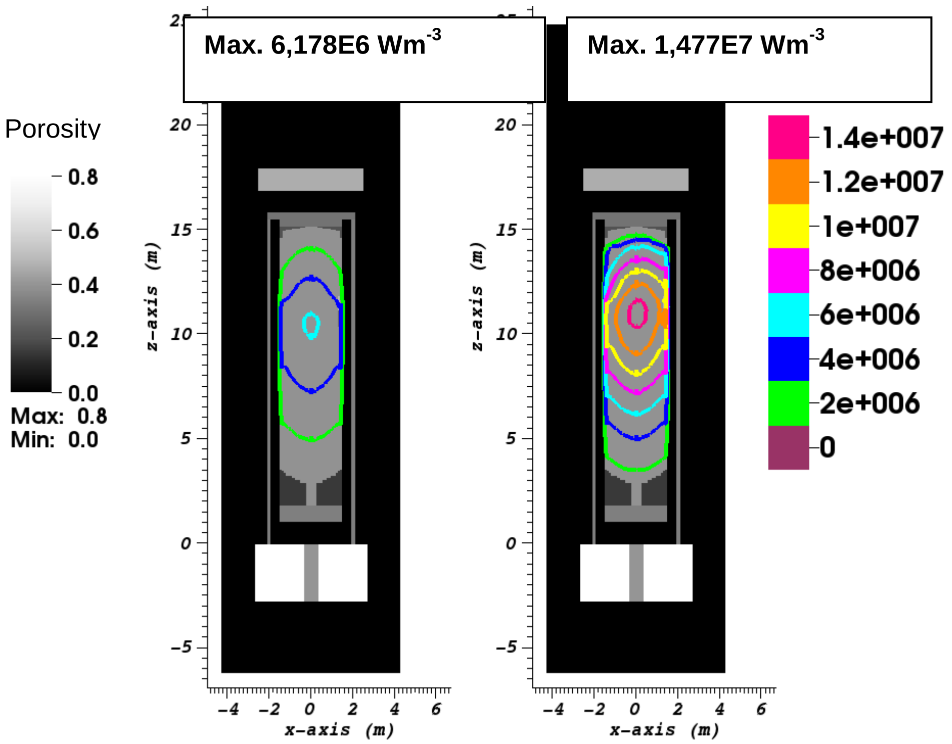

Figure 23 : Power distribution at the beginning (0s, left) and at the maximum power achieved at 3.75 s (right) for a one side control rod ejection, densification at the maximum power height, edge region

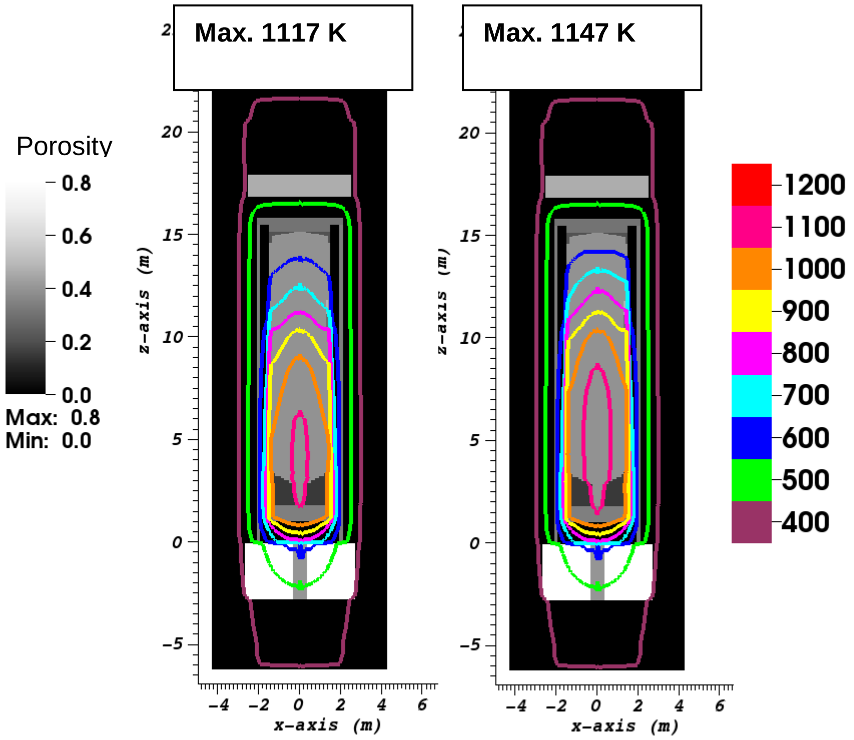

Figure 24 : Maximum fuel temperature distribution at the beginning (0 s, left) and at the end of the transient at 45 s (right) for a one side control rod ejection, densification at the maximum power height.

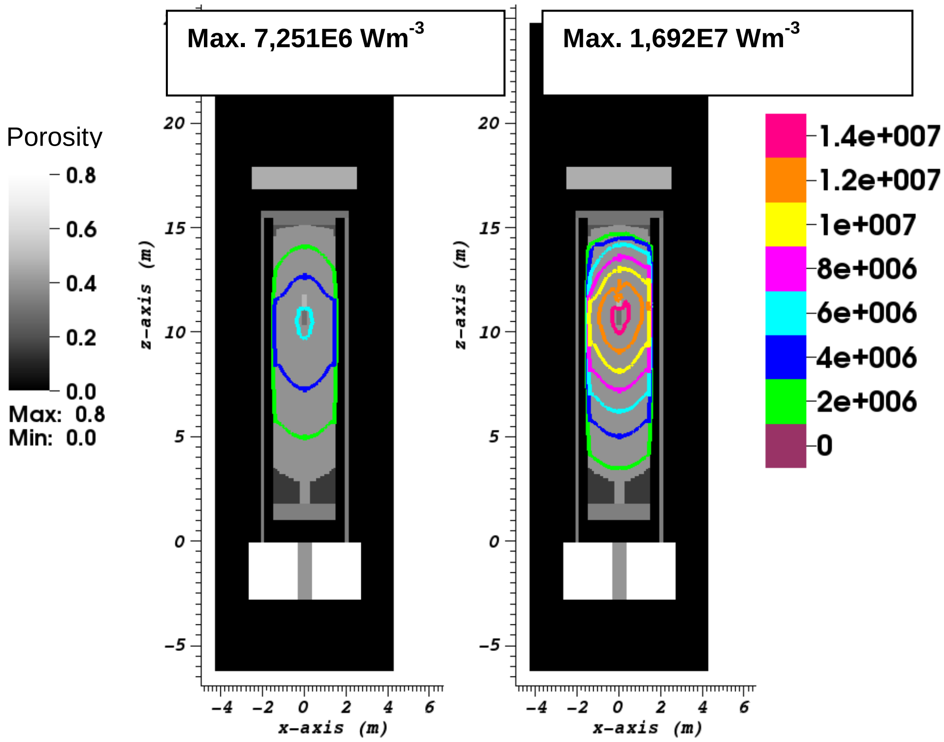

Figure 25:power distribution at the beginning (0 s, left) and at maximum power (3.75 s, right) for a one side control rod ejection, densification at the maximum power height, middle.

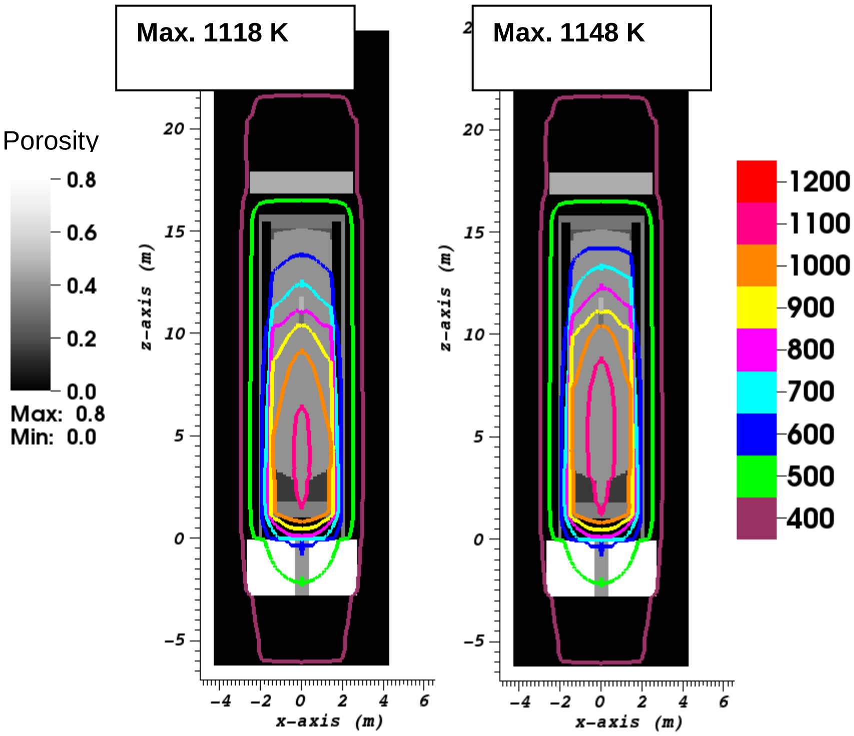

Figure 26:Maximum fuel temperature at the beginning (0 s, left) and at the end of the transient (44 s, right) for a one side control rod ejection, densification at the maximum power height, middle.

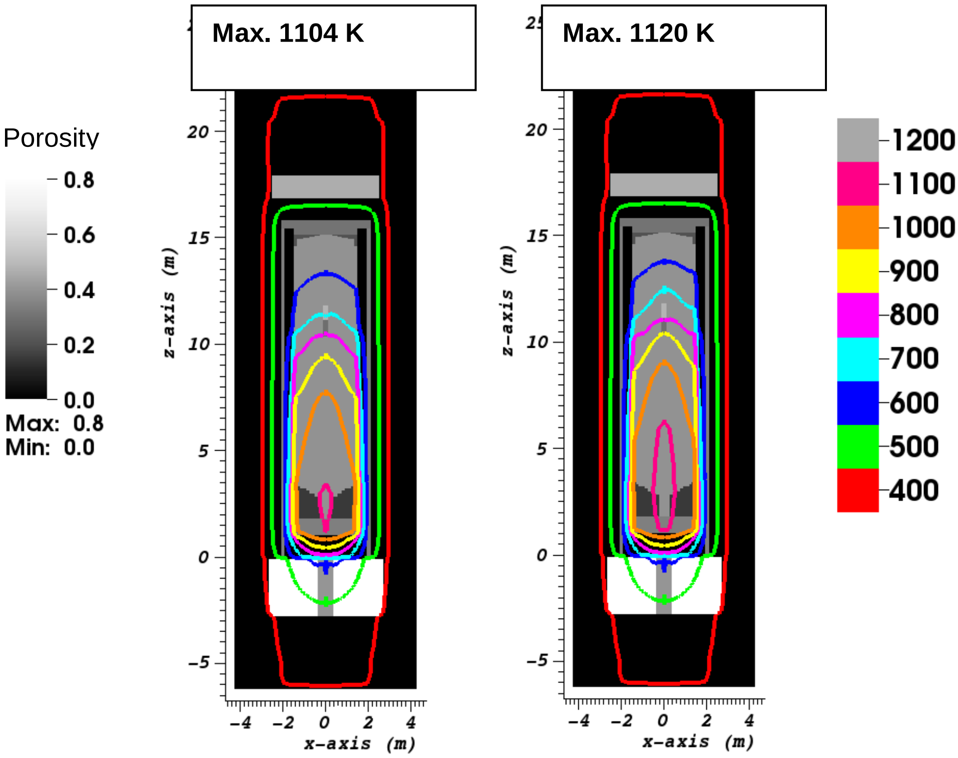

Figure 27: Gas temperature distribution at maximum power (3.75 s, left) and at the end of the transient (44 s, right) for a one side control rod ejection, densification at the maximum power height, middle.

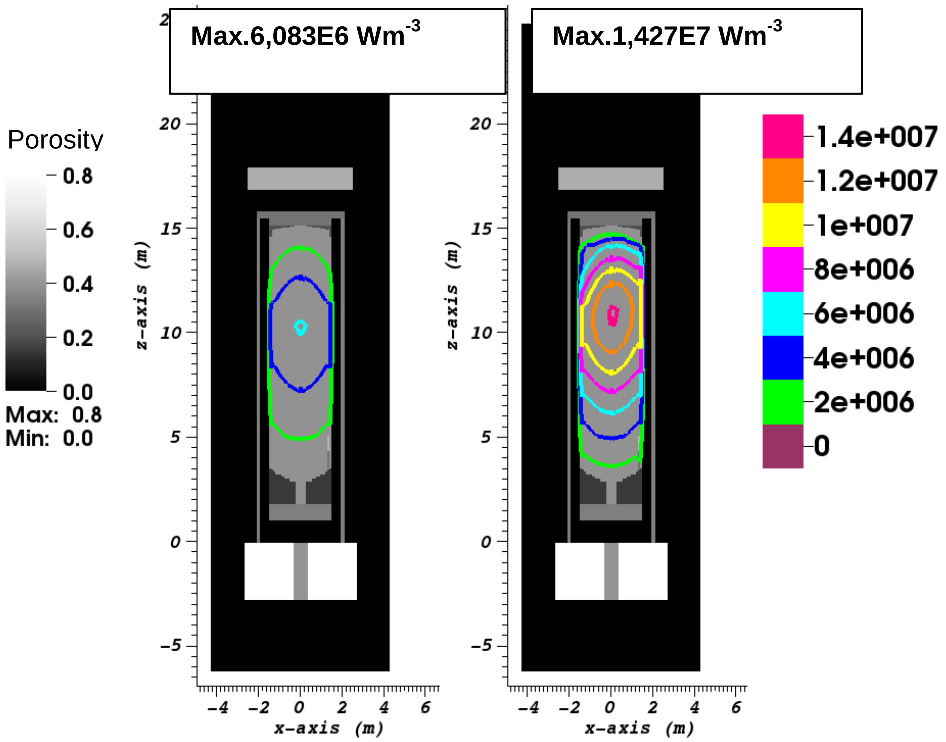

Figure 28:Power distribution at the beginning (0 s, left) and at the maximum power (3.75 s, right) for a one side control rod ejection, densification close to the bottom, edge region.

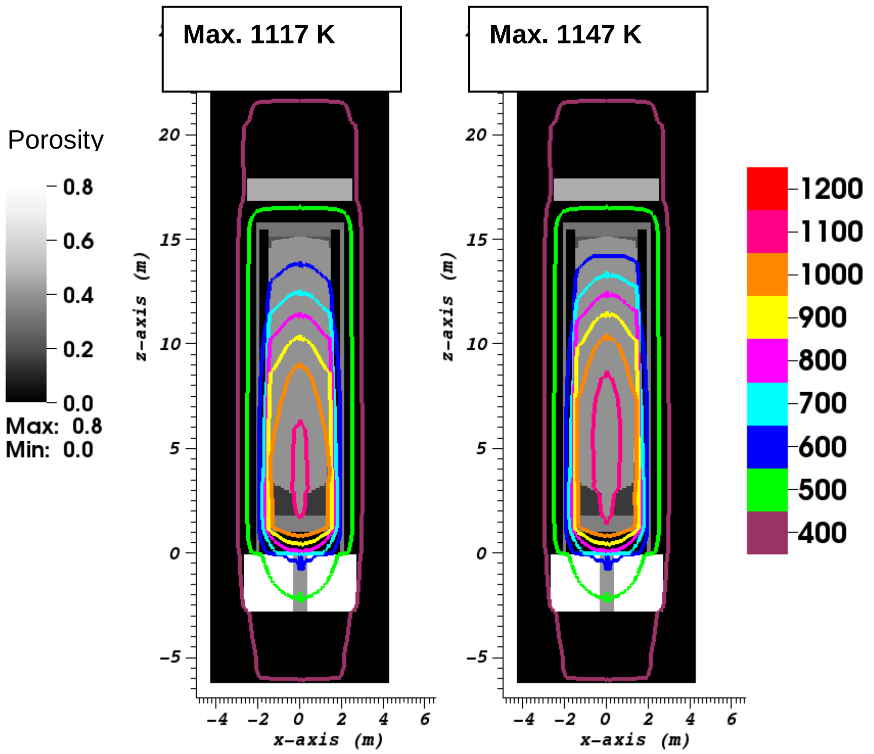

Figure 29 : Maximum fuel temperature distribution at the beginning (0 s, left) and at the end (45 s, right) of the transient for a one side control rod ejection, densification close to the bottom, edge region.

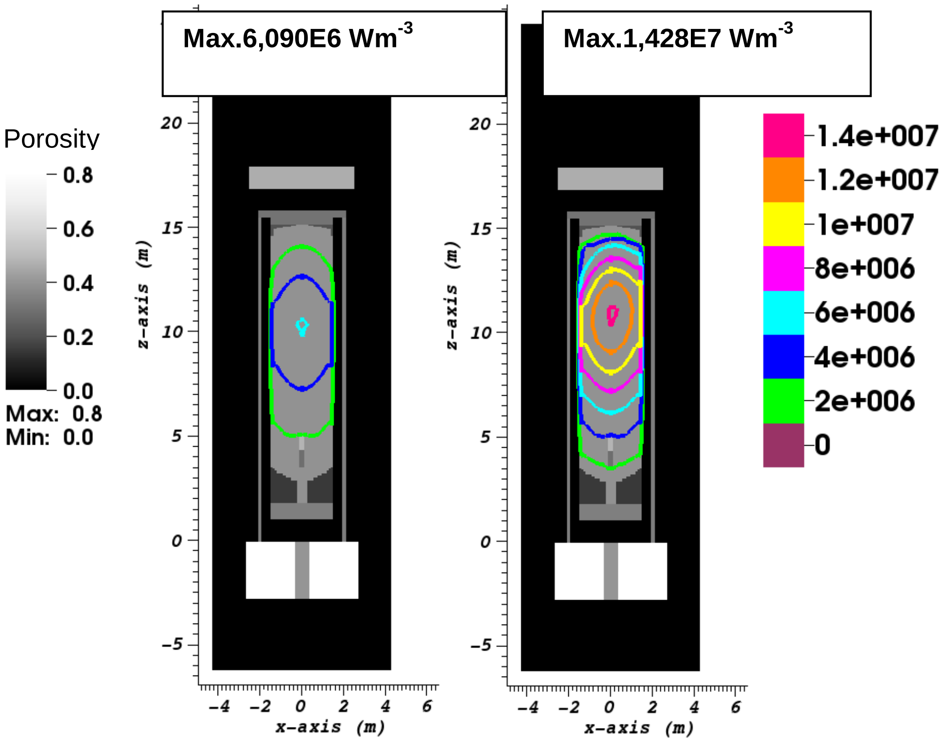

Figure 30: Power distribution at the beginning (0 s, left) and at the maximum power time (3.75 s, right) for a one side control rod ejection, densification close to the bottom, middle.

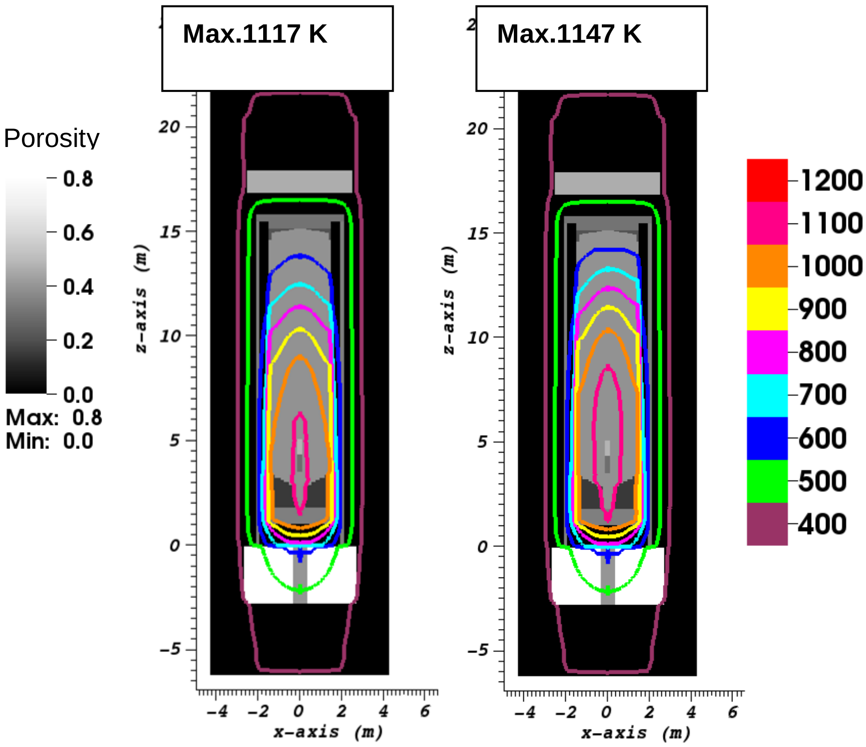

Figure 31 : Maximum fuel temperature distribution at the beginning (0 s, left) and at the end (45 s, right) of the transient for a one side control rod ejection, densification close to the bottom, middle

For the densification in case 3, the power is shifted towards the densification cluster, however the maximum power is not as big as in case 1. But the increase in the maximum fuel temperature is minimal. In case 2 and

4 the fuel temperature increases stronger as in cases 1 and 2, because here the fuel is heated by the down-coming gas from the top. The maximum power is not as high as in cases 1 and 3 and occurs also at 3.75 s.

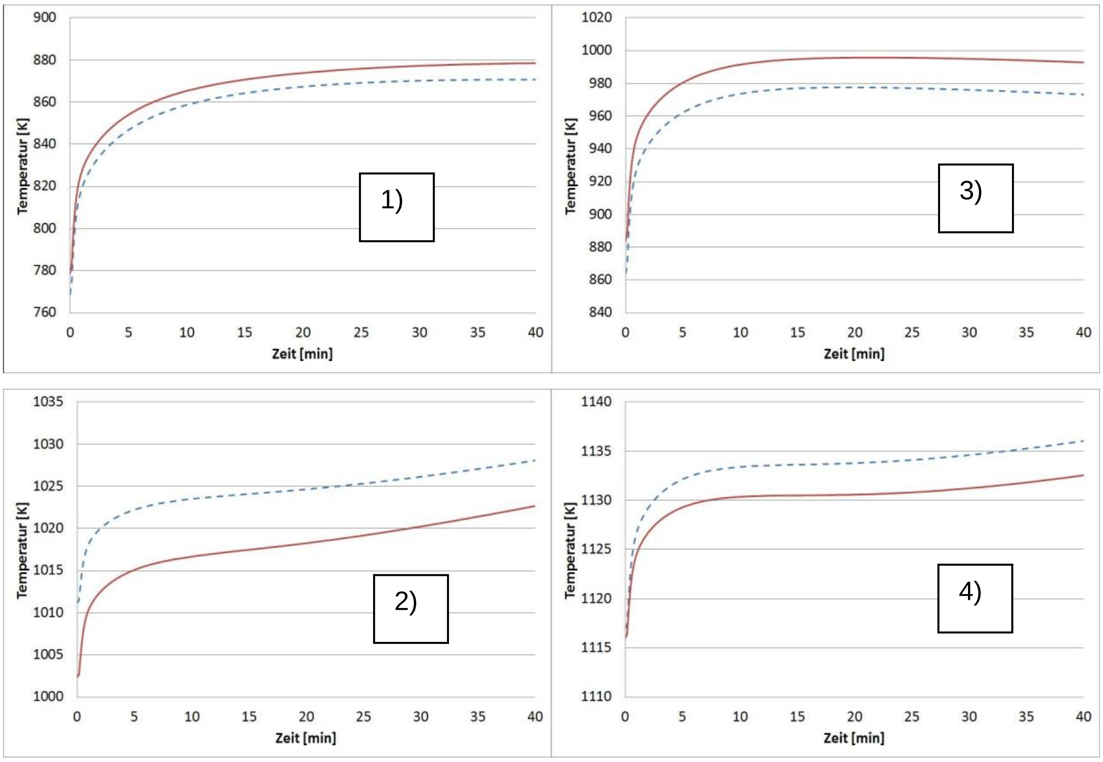

Figure 32: Maximum fuel temperature, compare to densified (red) and non densified pebble bed (blue): 1) case 1, 2) case 2, 3) case 3, 4) case 4.

For case 1 and 3, the temperature evolutions are dominated by the generated power in the zones, after a short temperature maximum in case 2 and 4 (in case 4 more pronounced), the hot spots are further heated by the hot gas coming from the pebble bed above the densification.

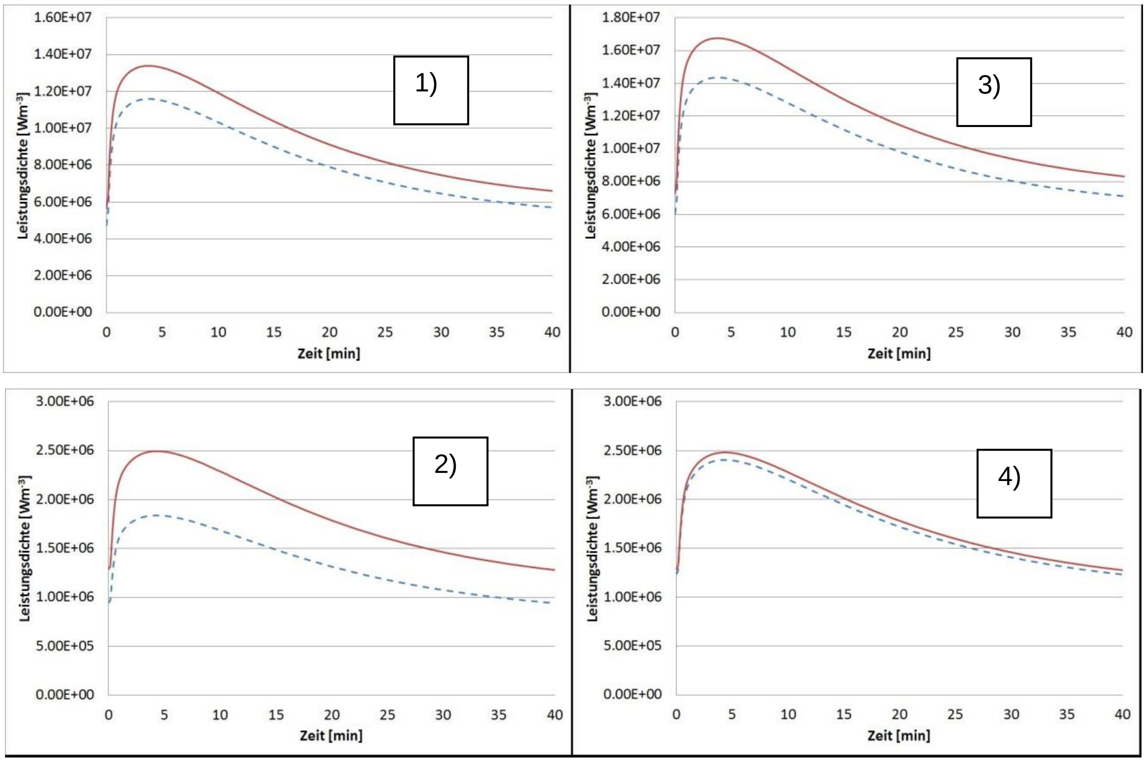

Figure 33: Power density of densified (red) and non densified pebble bed (blue): 1) case 1, 2) case 2, 3) case 3, 4) case 4.

The maximum fuel temperature in the densification cluster over time is plotted in Figure 32. In the densified regions in the middle of the core, the temperatures are slightly increased compared to the undisturbed pebble bed; in the densified regions at the bottom, it is the opposite case. This effect is produced through the moving of the hotspot with the maximum fuel temperature towards the location of the power maximum. The phenomenon is caused by the influence of the undensified pebble bed on the power density, which profiles are shifted towards the top.

Figure 33 shows the comparison of the power density over the time in the densification clusters and the maximum temperature. The influence on the power density is dominated by the feedback of the fuel temperature on the power. The effect in case 2 is the biggest, however the absolute value of the power density in case 3 is the biggest due to the maximum power and flux.

3.2.4 Asymmetric control rod withdrawal with densifications

To continue the investigation an asymmetric control rod withdrawal of 3 control rods at the same position as in a control rod ejection was executed. For that the velocity was reduced to 1 cm/s. The results with the ejection in general display the same tendency; but through the smaller inserted reactivity the maximum power and temperature are lower. The temperature increase is around 20 K. The maximum power occurs at 39 s.

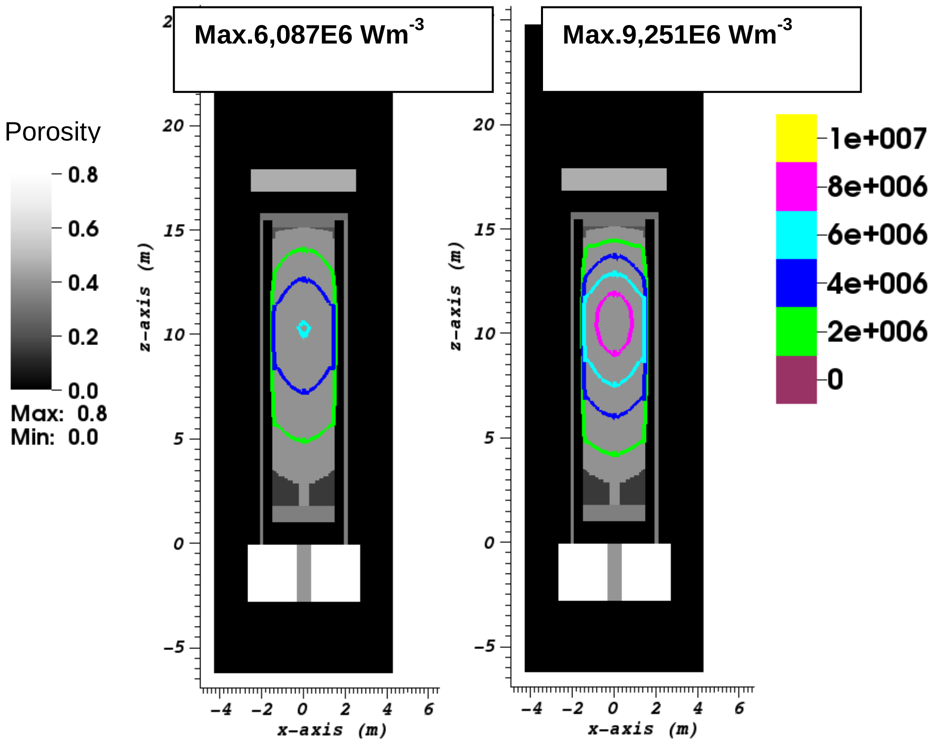

Figure 34: Power distribution at the beginning (0 s, left) and at the maximum power time (39 s ,right) for a one side control rod withdraw, without densification.

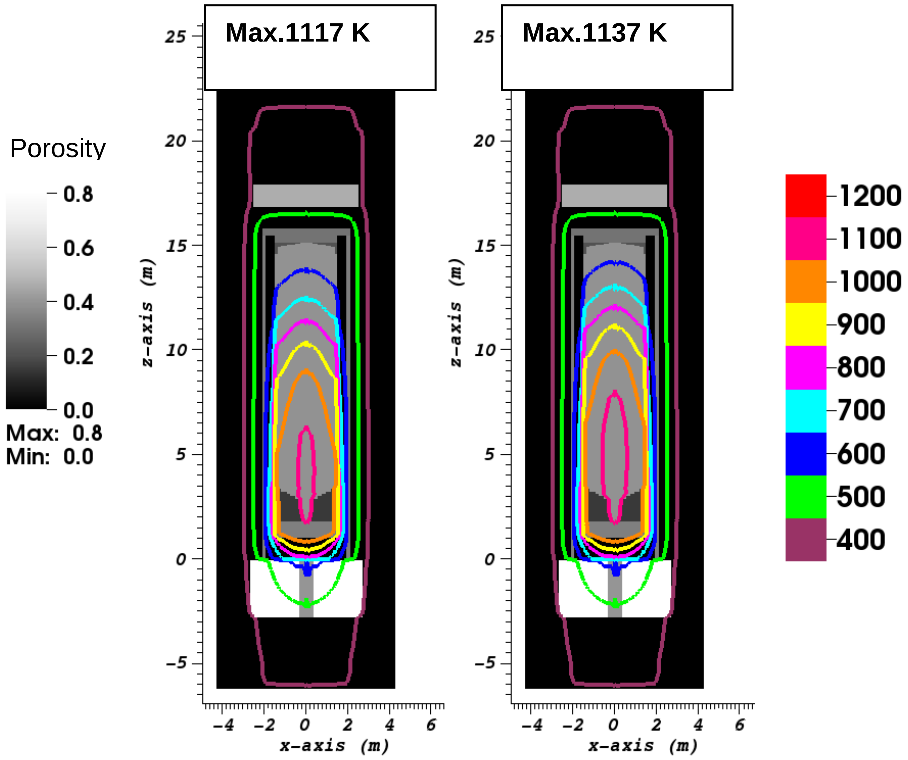

Figure 35: Maximum fuel temperature distribution at the beginning (0 s, left) and at the end (45 s, right) of the transient for a one side control rod withdrawal, without densification.

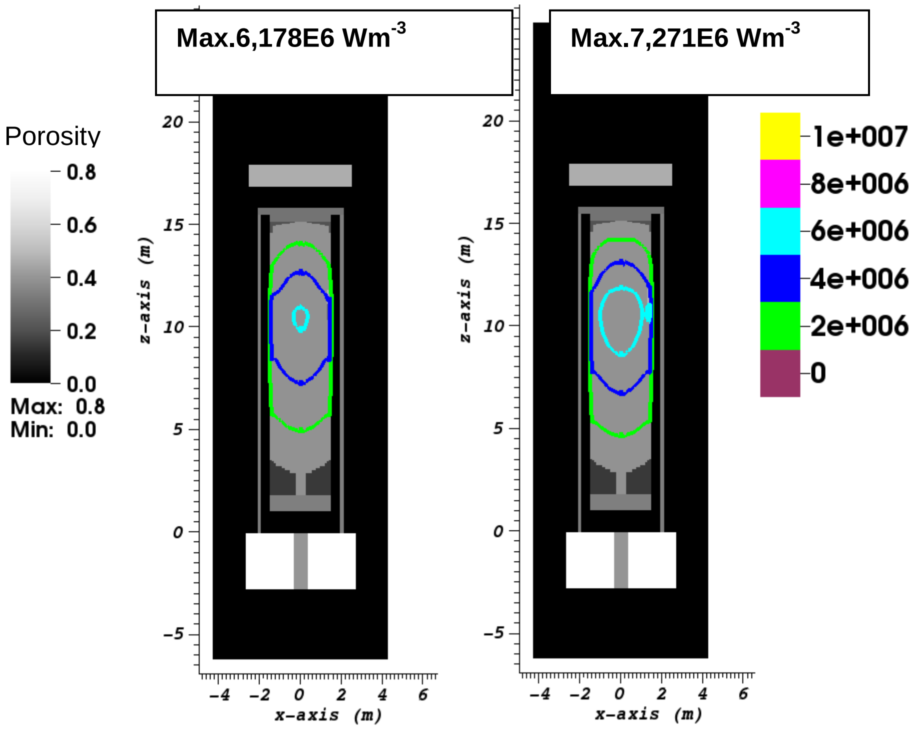

Figure 36: Power distribution at the beginning (0 s, left) and at the maximum power time (39 s, right) for a one side control rod withdraw, densification at the maximum power height, edge region.

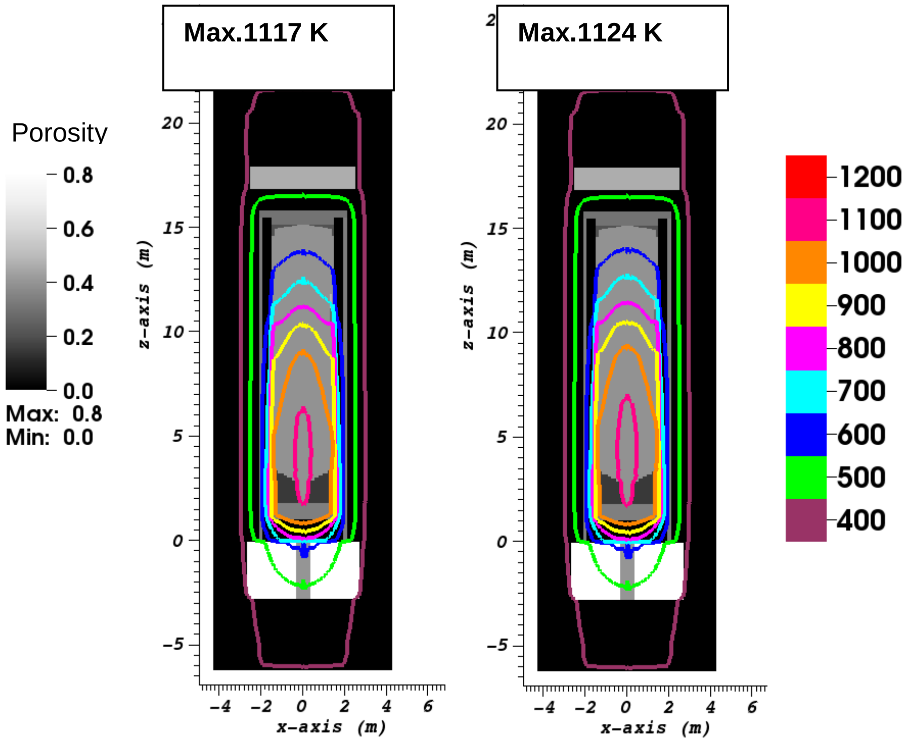

Figure 37: : Maximum fuel temperature deistribution at the beginning (0 s, left) and at the end (45 s, right) of the transient for a one side control rod withdraw, densification at the maximum power height, edge region.

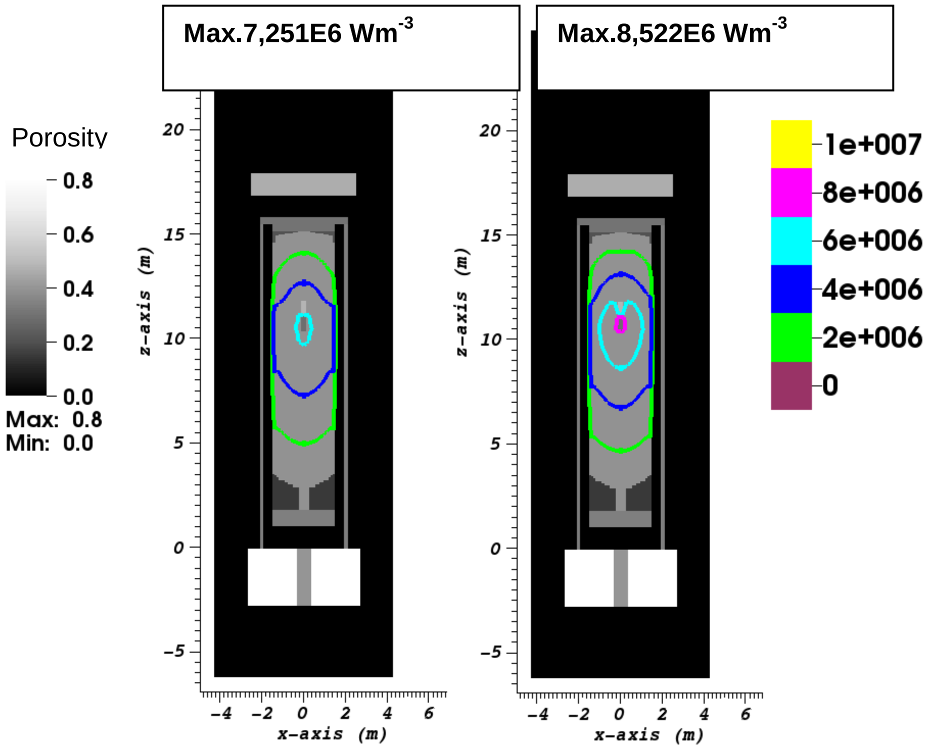

Figure 38: power distribution at the beginning (0 s, left) and the maximum power time (40 s, right) for a one side control rod withdraw, densification at the maximum power height, middle

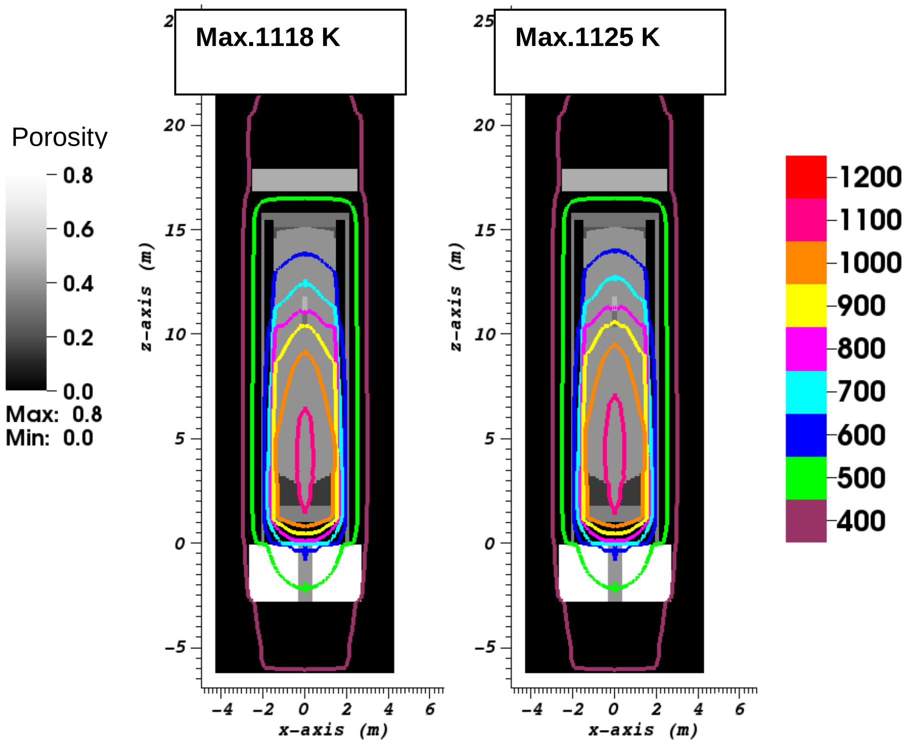

Figure 39: maximum fuel temperatureat the beginning (0 s, left) and end (40 s, right) of the transient for a one side control rod withdraw, densification at the maximum power height, middle.

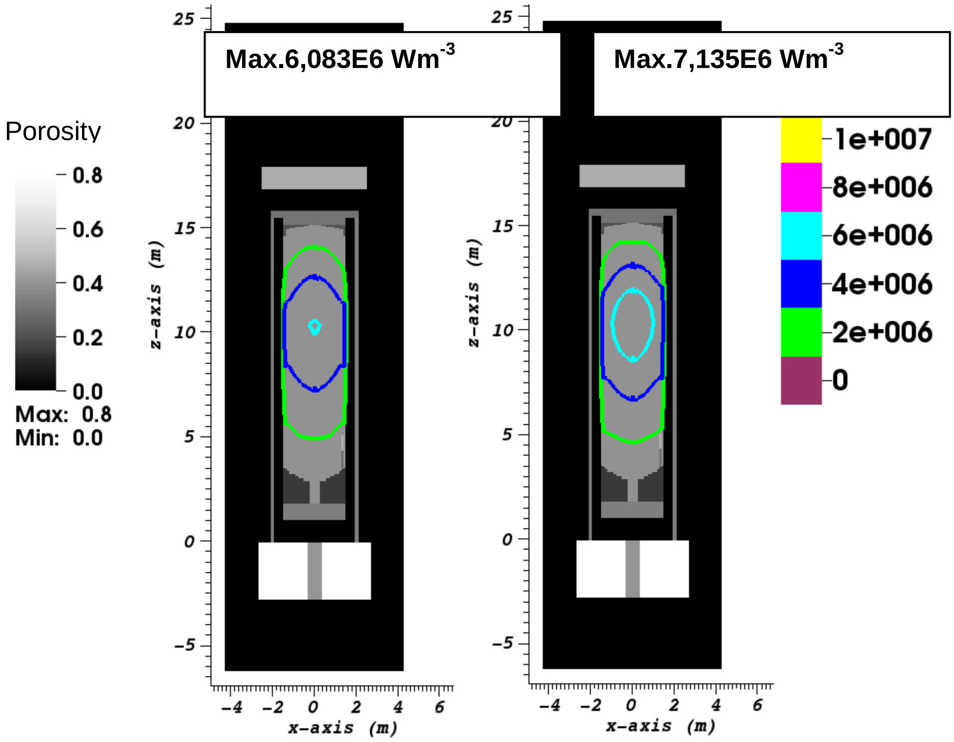

Figure 40: Power distribution at the beginning (0 s, left) and at the maximum power time (39.5 s, right) for a one side control rod withdraw, densification close to the bottom, edge region.

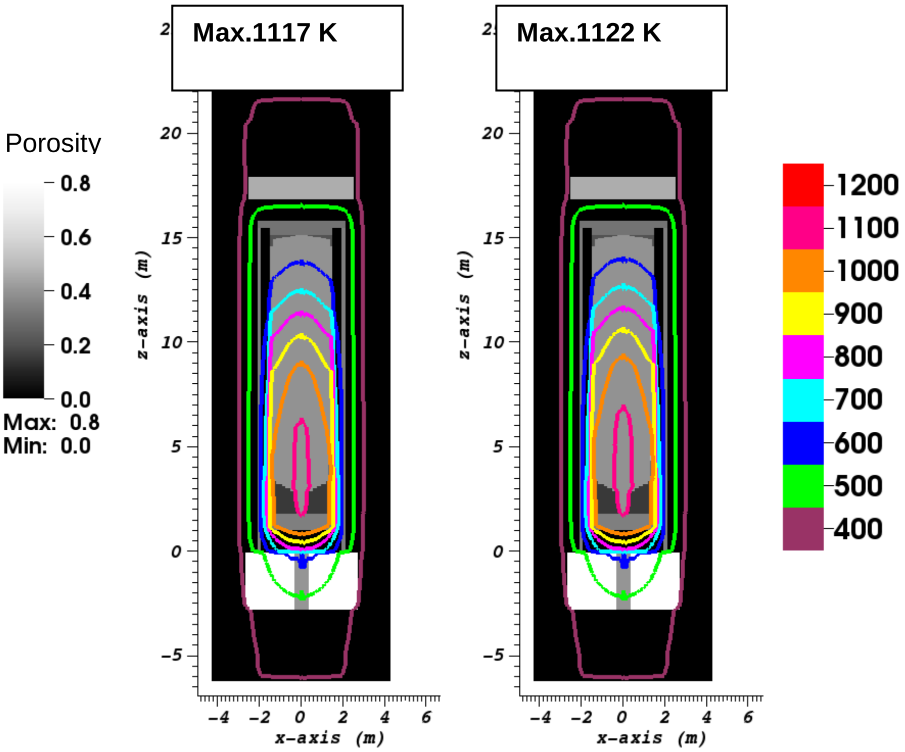

Figure 41: Maximum fuel temperature distribution at the beginning (0 s, left) and at the end (45 s, right) of the transient for a one side control rod withdraw, densification close to the bottom, edge region.

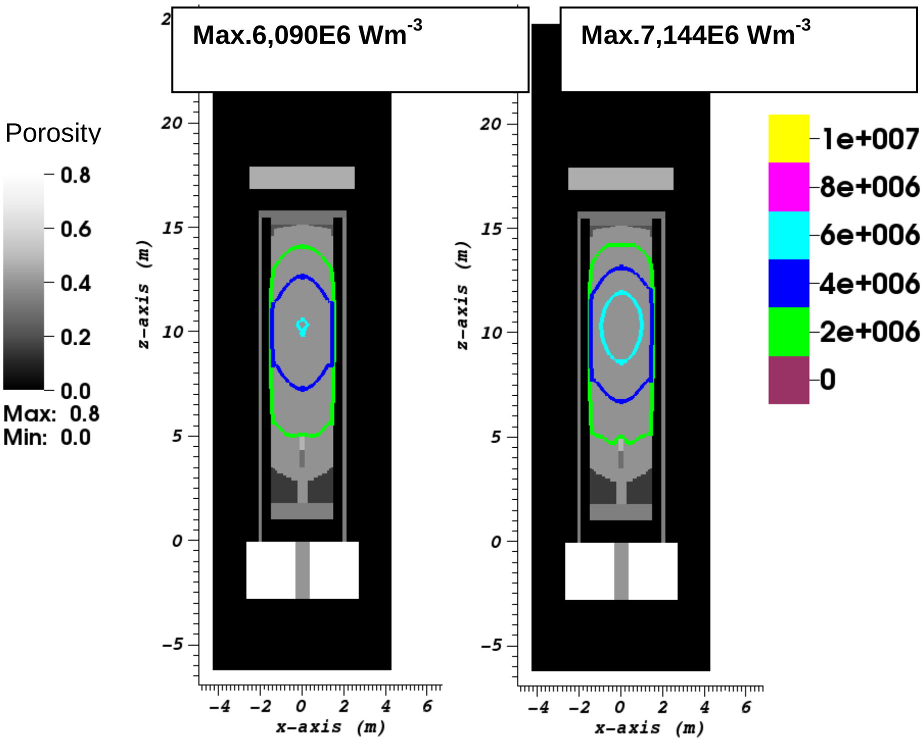

Figure 42: Power distribution at the beginning (0 s, left) and at the maximum power time (39.5 s, right) for a one side control rod withdraw, densification close to the bottom, middle.

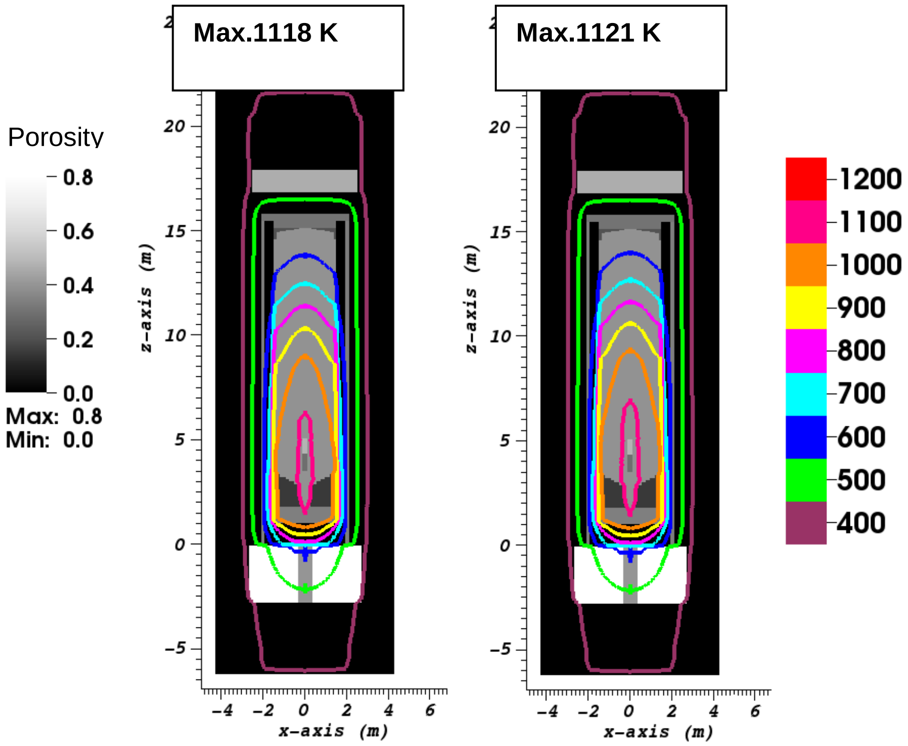

Figure 43: Maximum fuel temperature distribution at the beginning (0 s, left) and at the end (45 s, right) of the transient for a one side control rod withdraw, densification close to the bottom, middle.

3.3 The total control rod ejection scenario

The worst case of the ejection and withdrawal cases is the ejection (0.1 s) of all of the control rods at the same time. Since the rods are inserted 4.6 metres from the top reflector the ejection speed is 46 m/s. The hottest part for this case lies on the centreline of the core. This fast ejection scenario assumes a total destruction of the control rod drives where the rods are ejected from the system with 60 bars against ambient pressure.

Since the ejection time of 0.1 seconds is very small, the maximum time step size for the transient in the first second is 0.0025 seconds, before it is increased to 0.05 seconds after the first 3 seconds. Selecting a time step size this small, the ejection time is subdivided in 40 steps. This time step size should be small enough to cover the short-term processes taking place.

Previous analysis indicated that no inadmissible temperature rise to the fuel occurs. When analysing the fuel kernel temperatures assuming one average fuel type, the maximum temperature criterion of 1620°C is not exceeded. However, if the introduced modifications of distinction of the fuel pass number is used, the hottest fuel kernel will exceed this temperature (~2100°C), but only for a very short time (less than 10 seconds).

The power increases by a factor of ~10 in less than a second, as shown in Figure 44 and Figure 45. The maximum power value of 24,166 MW is reached after 0.79 seconds after start of the transient or 0.69 seconds after control rods were ejected. The corresponding maximum kernel temperatures, average fuel and moderator temperatures are shown in Figure 46.

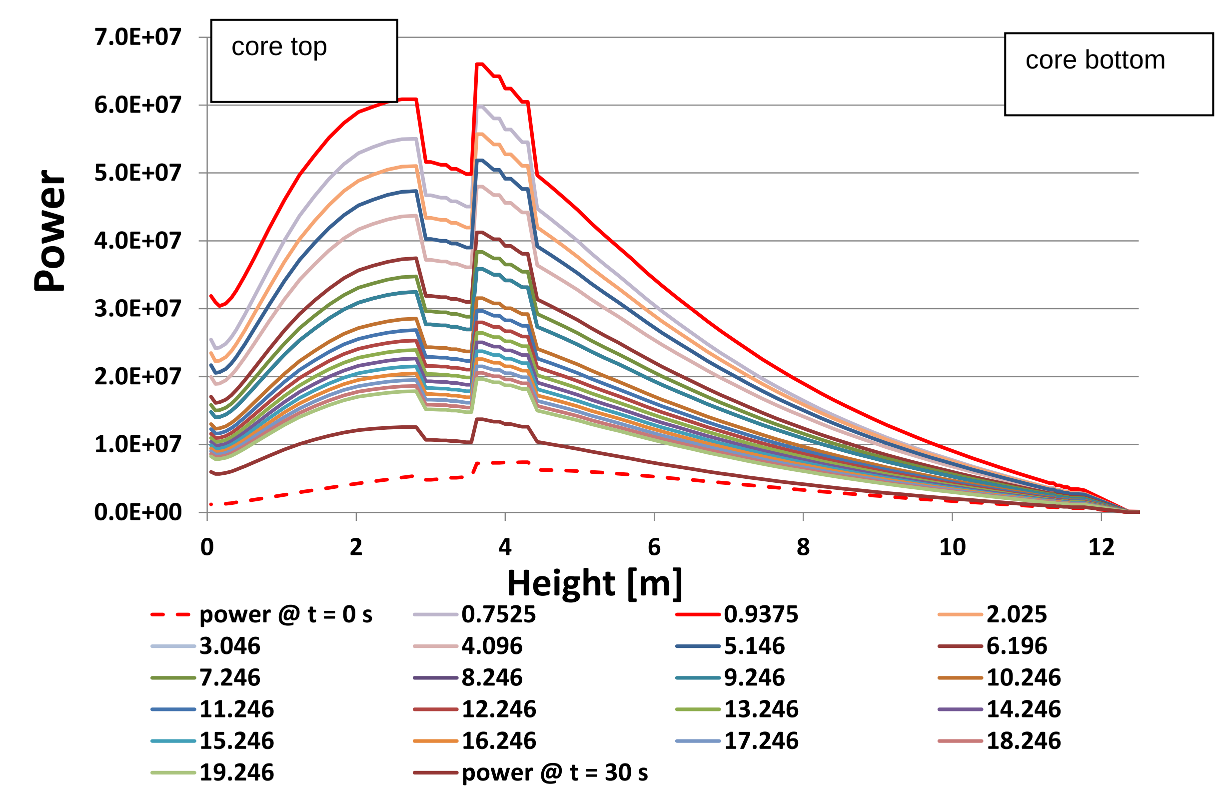

Figure 44 : Power density at the centreline for a total control rod ejection for different times

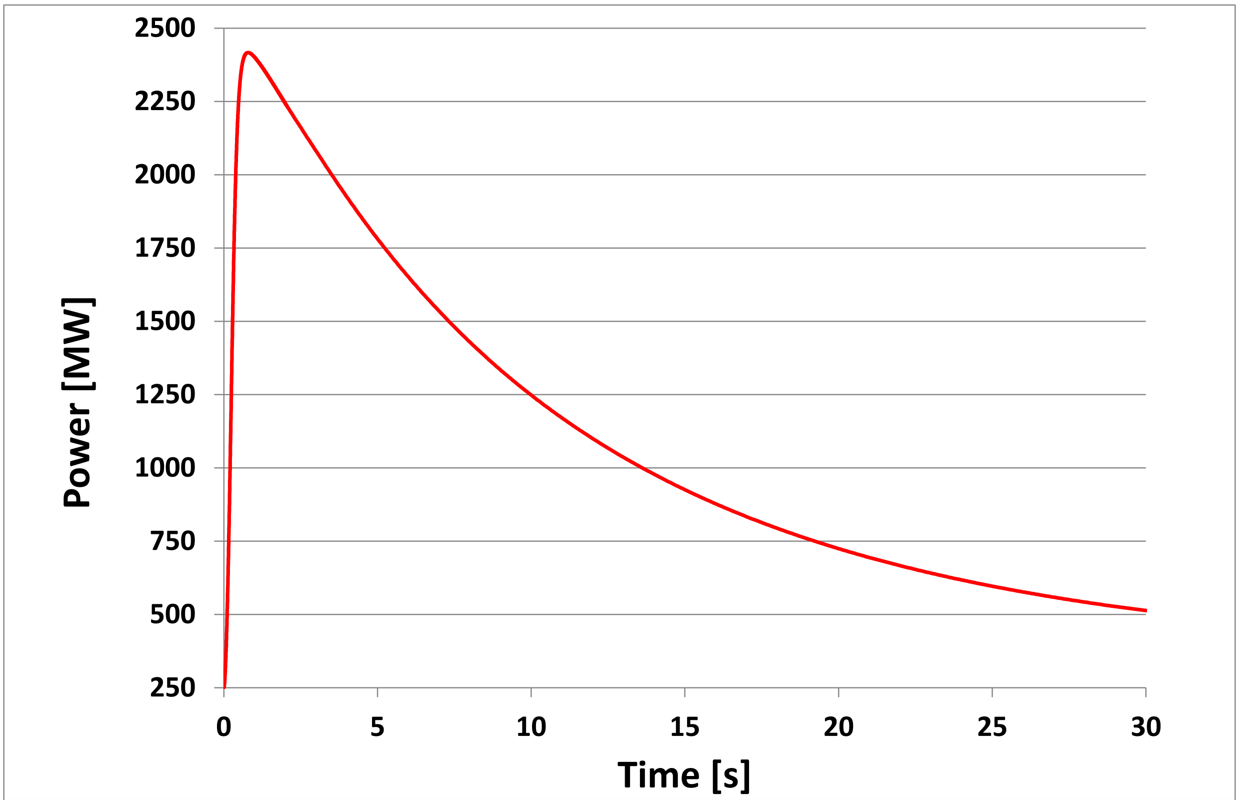

Figure 45 : Total power evolution for a total control rod ejection scenario of the HTR-PM, the maximum power is reached after 0.785 seconds after the beginning of the ejection

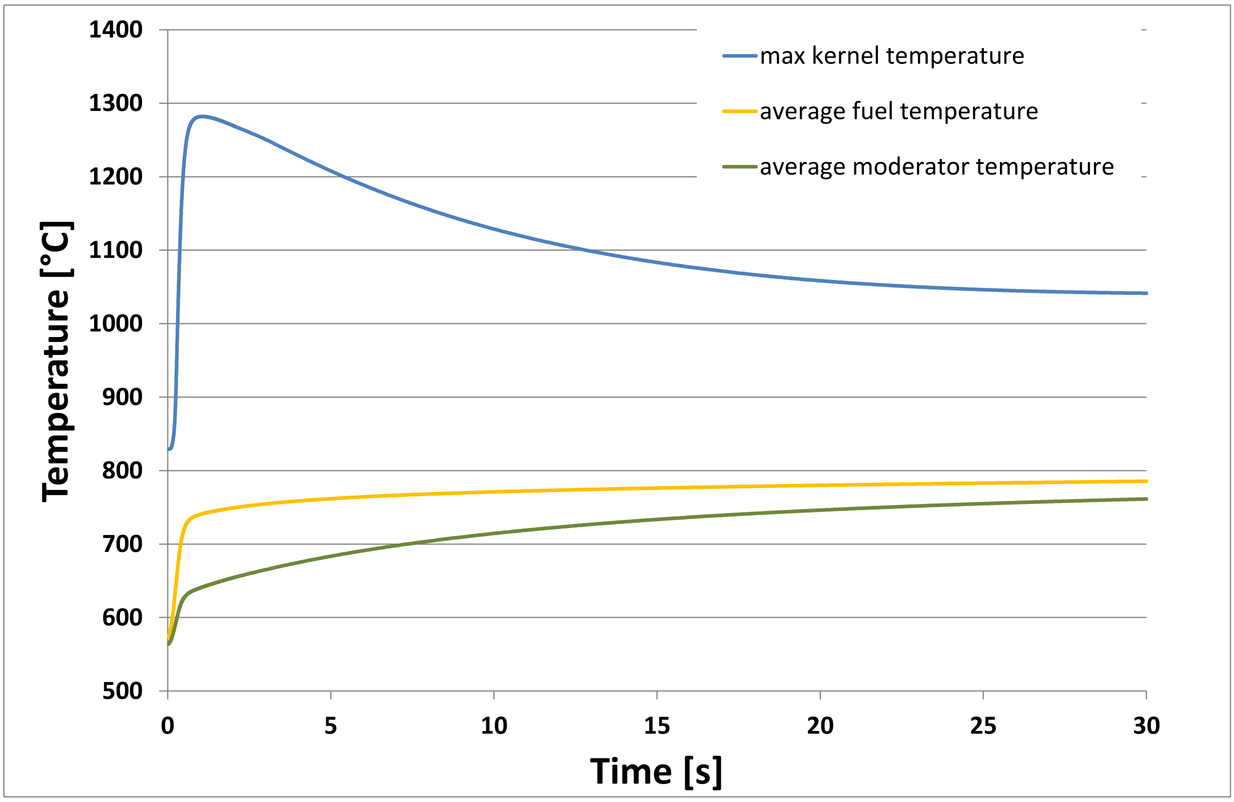

Figure 46 : Temperature evolution for a total control rod ejection case for the maximum kernel temperature, average fuel and average moderator temperatures.

4 Hot spot analysis with accounting for core pass number

4.1 Modifications in ATTICA^{3D} to account for cycle number

The HTR-PM loading pattern for fuel elements foresees fifteen core passes before the pebbles are discharged. Assuming a random uniform distribution, the pebbles in the pebble bed are arranged homogeneously such that if a random batch of pebbles would be extracted a mean number of each core pass can be expected. This was also assumed when the temperatures of the fuel elements were calculated.

Now, modifications are introduced into ATTICA^{3D} to be able to account for different heating powers of a fuel element according to its core pass number.

The reason for this modification is the fact that fresh pebbles do contain most of the fuel and has the least burn-up, i.e. fission product content and, hence, the lowest decay heat production. So in nominal operation the highest temperatures can be expected for a fresh fuel element. When decay heat comes into play, the highest temperatures will occur in the fuel pebbles that experienced the highest burn-up.

The new model in ATTICA^{3D} allows the user to provide different heating powers per fuel pass. Starting from the assumption that each computational mesh contains a fraction of fuel elements, the total volume of pebbles within the pebble bed amounting is proportional to each cycle, that is 1/15. This heating power was varied assuming the power factors presented in Table 5. These power factors have been evaluated from steady-state analysis with the ZIRKUS system and represent values averaged over the whole core. The power factors for the pebbles are given relative to the mean power production where no distinction per fuel cycle was done. Hence, these power factors were all “1”.

Table 5 : Power factors for fuel pebbles (previous included)

Fuel pass	Power factors (assumed)	Power factors (ZIRKUS) @hotspot location, "realistic"	Power factors (ZIRKUS) maximum, "conservative"	Power factors (ZIRKUS) maximum, "realistic" at core bottom
1	1.9	1.47825	1.6008	1.40744
2	1.7	1.41692	1.50422	1.35055
3	1.5	1.33424	1.39456	1.27992
4	1.3	1.24698	1.28543	1.20699
5	1.1	1.16272	1.18321	1.13691
6	1.05	1.08449	1.0901	1.07176
7	1.02	1.01322	1.00637	1.01214
8	1	0.948833	0.931486	0.95802
9	0.98	0.890912	0.864649	0.909081
10	0.95	0.838908	0.805045	0.864929
11	0.9	0.792258	0.751892	0.825152
12	0.7	0.750442	0.704491	0.789356
13	0.5	0.712979	0.662226	0.757173
14	0.25	0.679438	0.624548	0.728263
15	0.15	0.649426	0.590971	0.702312

These new power factors are global values meaning they are applied to every computational core mesh of ATTICA^{3D}, thus far, omitting possible local variations of the factors. The temperature of each distinct pebble core pass is taken and averaged together according to their mean volume in the pebble bed. This approach yields 15 different fuel temperatures. The values were estimated from previous experience where power factors have been determined for a 15 core pass fuel cycle. The maximum power value of 1.9 is not expected to be too high, but will still be verified for the HTR-PM. Also, from previous works done in the framework of the PUMA project, one of the predecessors of the ARCHER project, it was found that the mean spectrum is approximated best by an ensemble of pebbles (mixture), and, that single pebble spectrum calculations which are later weighted and mixed are much less suitable to describe the spectrum, realistically. Therefore, a modification of the interface for TORT-TD and ATTICA3D to instantaneously feed-back the fuel temperatures to the neutronics for each core pass number was considered not necessary. Therefore the power factors will also be kept constant for the duration of the transient.

4.2 Results with assumed power factors

For demonstration purposes of the new fuel temperature model, a steady-state TORT-TD/ATTICA^{3D} analysis is performed without a densification (Figure 47), with a densified region in the ATTICA^{3D} domain, omitting the densification for the TORT-TD neutronics model and with a densified region in both the TORT-TD and ATTICA^{3D} simulation model. Additionally, with the newly obtained power factors determined by the ZIRKUS/THERMIX analysis, the hotspot calculations are repeated with the most unfavourable power factors (at the top of the core), and with the power factors determined for the location of the pebble cluster of increased density. This analysis is presented in chapter 4.3.

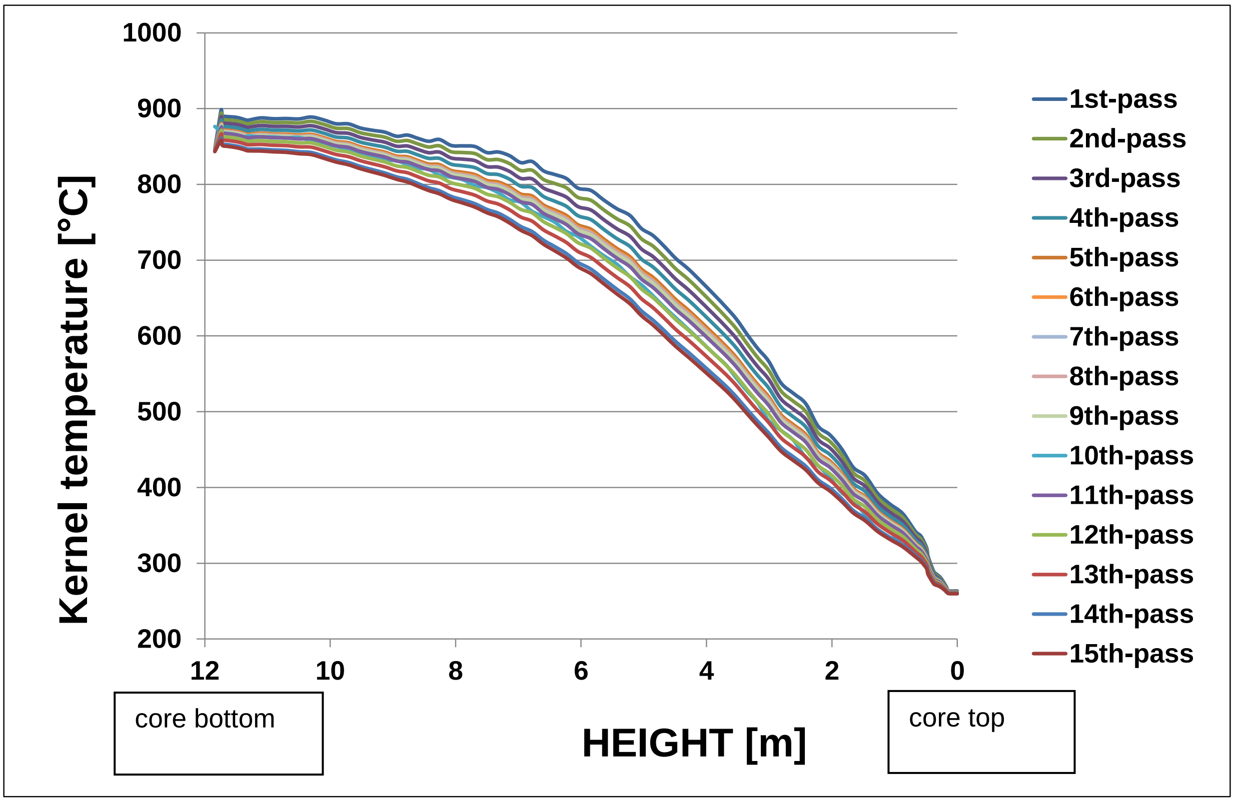

Figure 47 : Steady state fuel temperatures per core pass without densified region and with estimated power factors

The maximum temperature difference between the first and the last core pass of a pebble with the power factors from above is 118 K at about 4.5 metres from the top of the core. Including a densification in the thermal fluid dynamic part only, a more densified region (28.75 %) is located in the power maximum while a less densified region (47.6 %) is located above or below the densified cluster to preserve the pebble mass within the core cavity without increasing or decreasing the core height.

For the result with a densified cluster of ATTICA^{3D}, the maximum temperature difference of between the first and the last core pass amounts to 136 K, see Figure 48.

The results of densified clusters in both, neutronics and thermal fluid dynamics, are shown in Figure 49. The maximum fuel temperature difference between the first and the last core pass reduces to 130 K again. The centreline temperatures of the different core pass numbers are shown together with the centreline power.

All results with a densification modelled in both neutronics and thermal fluid dynamics or in thermal fluid dynamics only do not display any significantly higher temperatures for steady state. Therefore it is concluded that a densification in the power maximum will not lead to inadmissibly high fuel temperatures if the pebbles can be assumed to be mixed homogeneously.

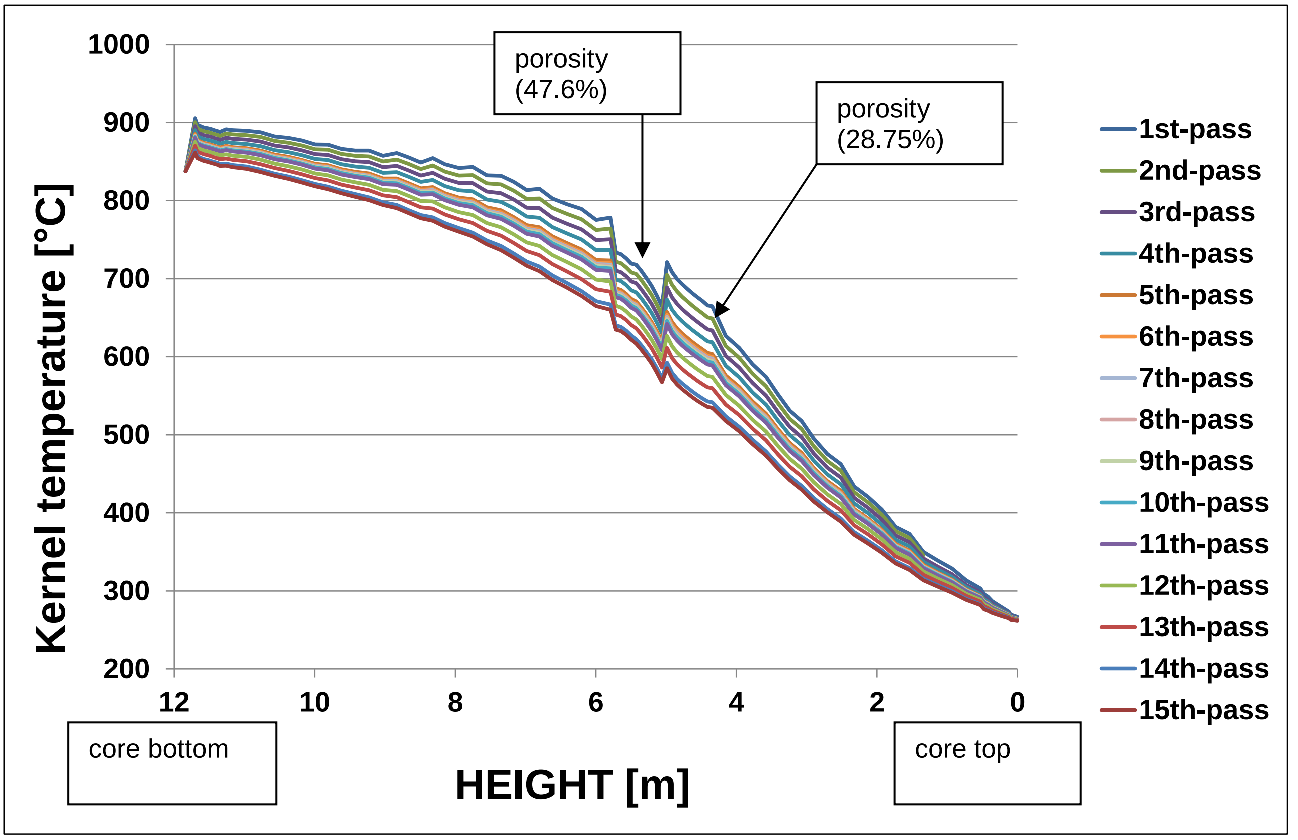

Figure 48 : Coupled TORT-TD/ATTICA^{3D} results with a densification in the thermal fluid dynamics only

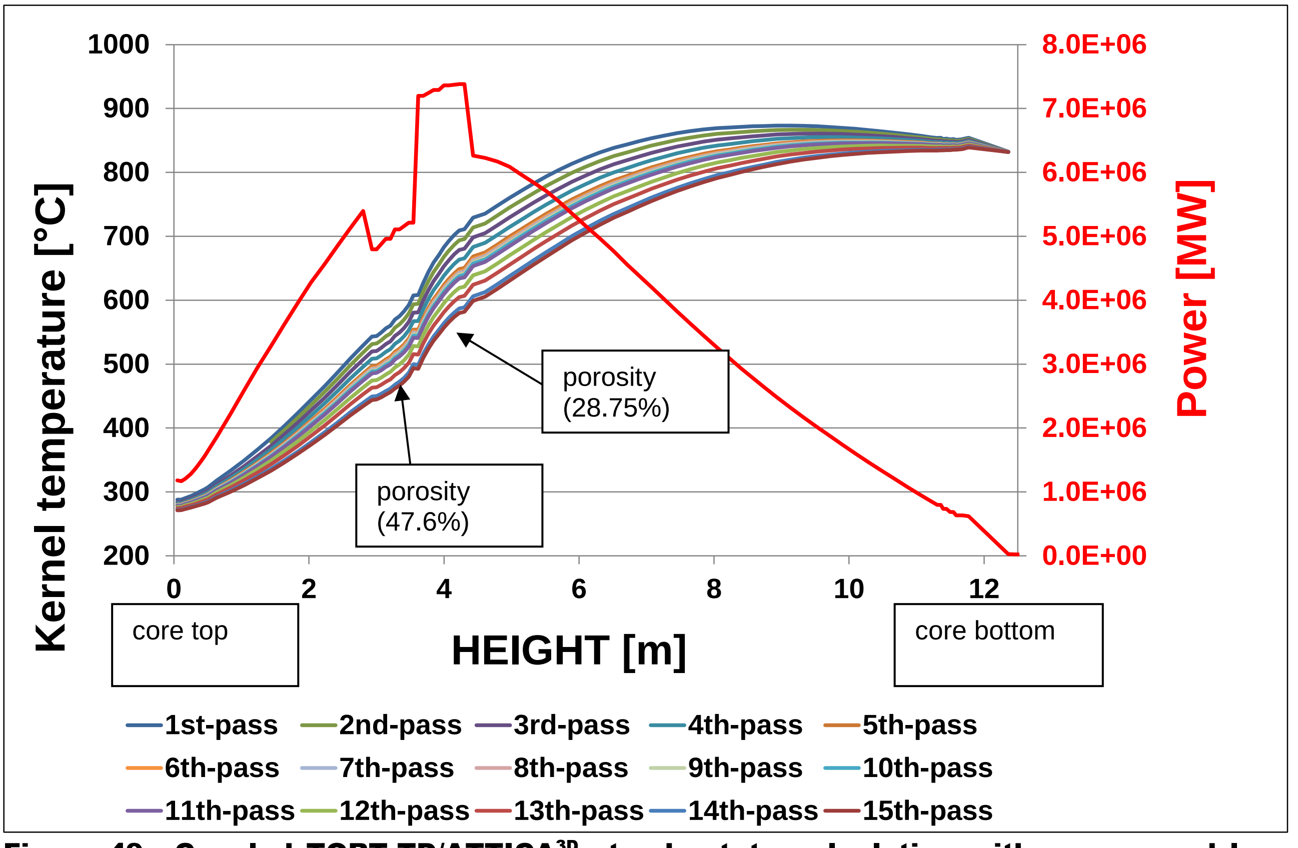

Figure 49 : Coupled TORT-TD/ATTICA^{3D} steady state calculation with a more and less densified cluster of pebbles, left axis : fuel kernel temperatures on the centreline, right axis : power density on the centreline (red)

For the considered worst case scenario of the total control rod ejection case, the power increase remains the same since the mean fuel and moderator temperatures do not differ. However, for the strong reactivity increase (1.3%) caused by the ejected control rods, the maximum fuel temperature results differ significantly. The integral power evolution is the same as shown in Figure 45 reaching a power increase factor around 10, but the maximum fuel kernel temperature increase drastically, see Figure 50. Instead of 1,281 °C in the previous analysis, the case with the fuel pass model reaches **2,241 °C** after 0.9375 seconds. This is much higher than the temperature for the previous cases. But already after less than 10 seconds, the maximum fuel kernel temperature is already below 1600°C, again.

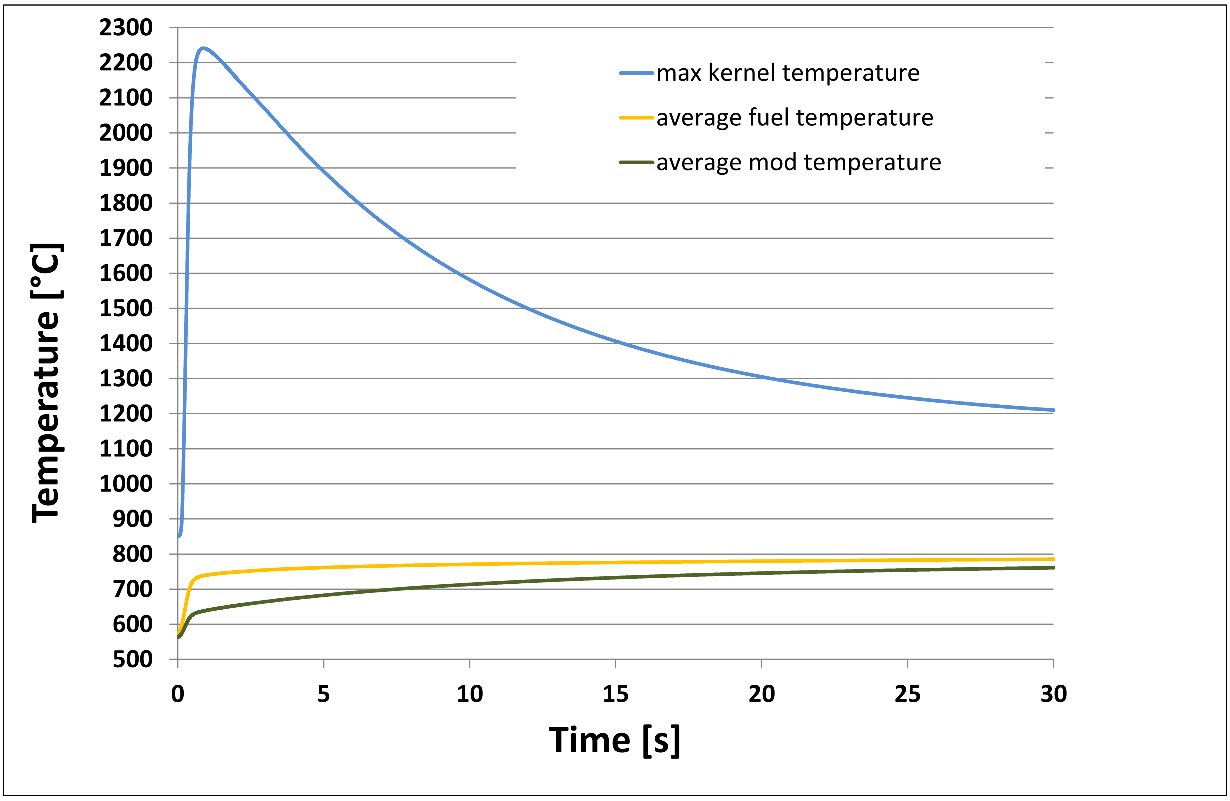

Figure 50 : Maximum kernel temperature and average fuel and moderator temperatures for the total control rod ejection case, power factors assumed.

The fuel temperature model is now analysed at 0.9375 seconds, the time where the maximum temperature is reached, see Figure 51. There, the difference in the maximum fuel kernel temperatures reaches over 1,500 K between the first and the last core-pass with the assumed power factors. For the axial location with the highest temperatures obtained, the temperature distribution over the spherical fuel element is presented for both the graphite and the UO_2-kernels, see Figure 52. Starting from the outermost shell at approximately 500°C the centre of the innermost kernel reaches 2,241°C leading to a temperature difference between the surface and the hottest particle of 1,700 K!

These values for the fresh fuel elements are inadmissibly high and this extreme transient case must be prevented due to appropriate design measures, i.e. limitation of ejection speed or restriction of the maximum number of rods that can be ejected (like in a LWR where the corresponding design basis event is the ejection of the most effective rod). Since the fresh fuel element has no significant amount of fission gases, the inner fission gas pressure might be low enough to stand this transient. This, however, must be evaluated by experiment and fuel performance specialists.

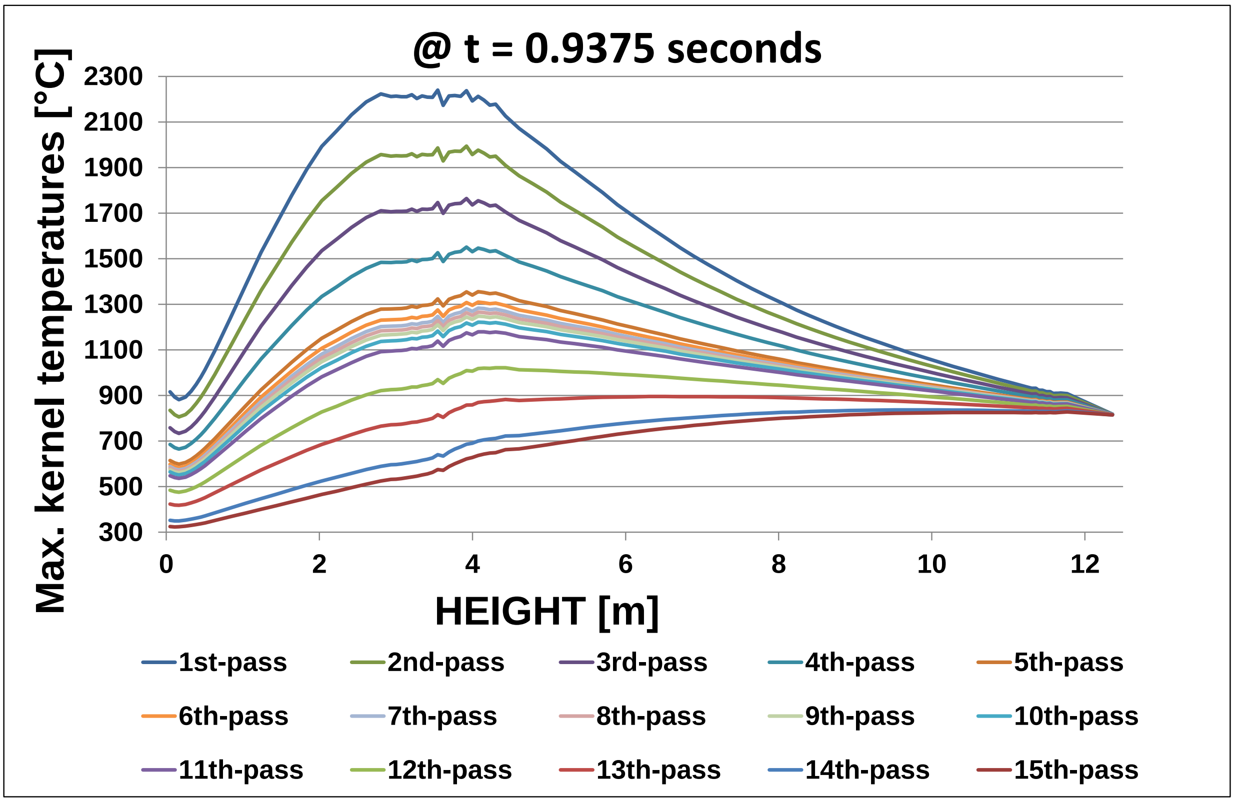

Figure 51 : Distribution of maximum fuel kernel temperatures at the centreline for a total control rod ejection at t = 0.9375 seconds, time of maximum temperature.

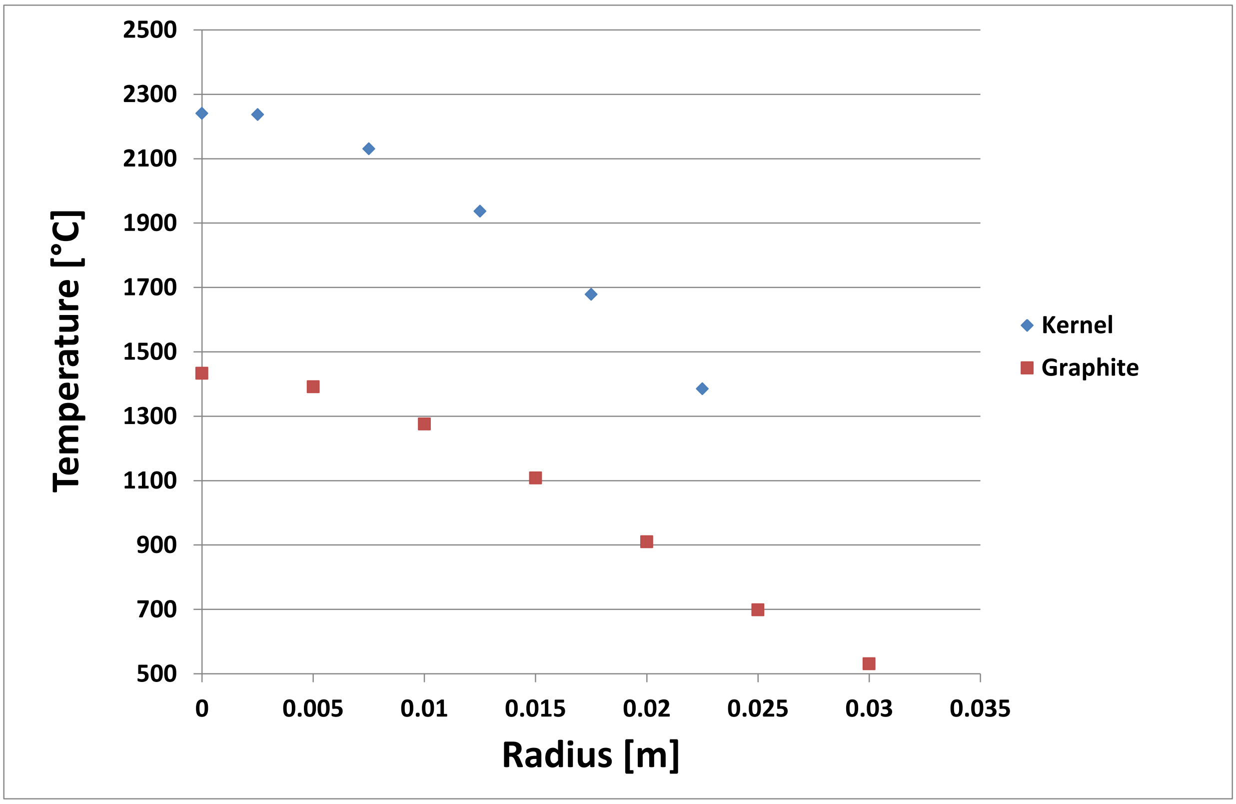

Figure 52 : Temperature distribution of the kernel and shell temperature over the hottest fuel element with assumed power factor of 1.9 times the average pebble power

4.3 Local power factors from neutronic/thermal fluid dynamics steady-state analysis

In this deliverable, the power production factors could be obtained from a steady-state ZIRKUS calculation. Here, the local power factors were determined per burn-up zone (see Figure 10) and core-pass number. The extraction of these power factors from ZIRKUS/THERMIX assumed an ensemble of equally mixed pebbles from each core-pass, assuming the same flux for one burn-up zone. Taking into account the different nuclide densities per burn-up zone the power factors could be derived by a post-processing mechanism..

In the previous chapter, the model improvements in ATTICA3D to account for core-pass numbers were described. From our steady-state analysis system ZIRKUS it was possible to extract the local power production factors per pebble and burn-up zone. It was found that the previously assumed power factors ranging from 1.9 – 0.1 times the average power of a pebble of 1st to 15th core pass are somewhat too high. The power factors determined with ZIRKUS over the whole core region are shown in Figure 53 for pebbles of the 1st core pass and in Figure 54 for pebbles of the 15th core-pass. These power factors do not consider the densification of the pebble bed but there is no reason that the power factors change in a densified region. Apparently the power factors in two figures exhibit a different shape. For fresh fuel they are the highest at the top of the core (z = 1182 cm). In radial direction they are peaked towards the side reflector. For the 15th core pass, the shape is the other way round. Here, the power factors are higher at the bottom of the core, and radially, the highest values of power factors are found in the centre of the pebble bed.

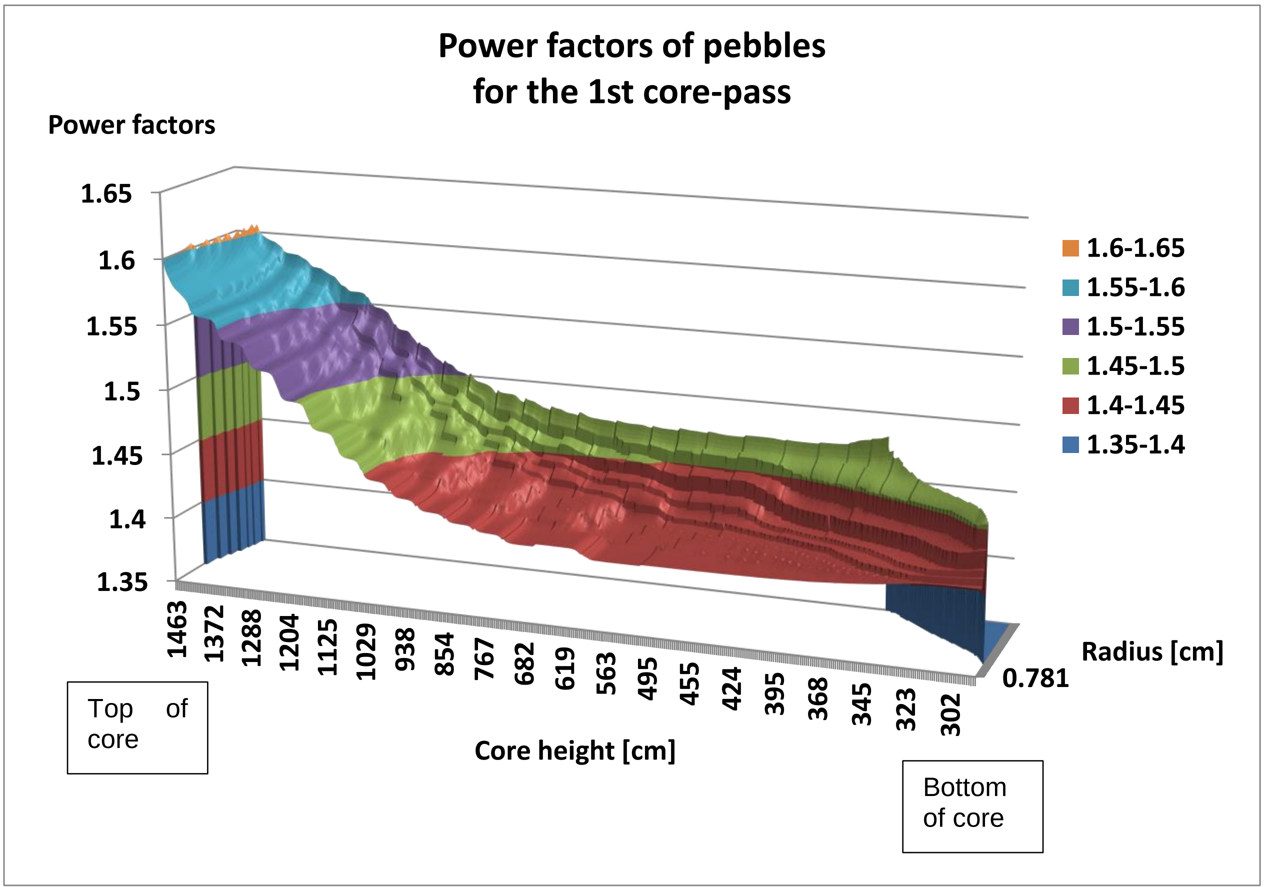

Figure 53: Power factors of pebbles for the 1st core pass

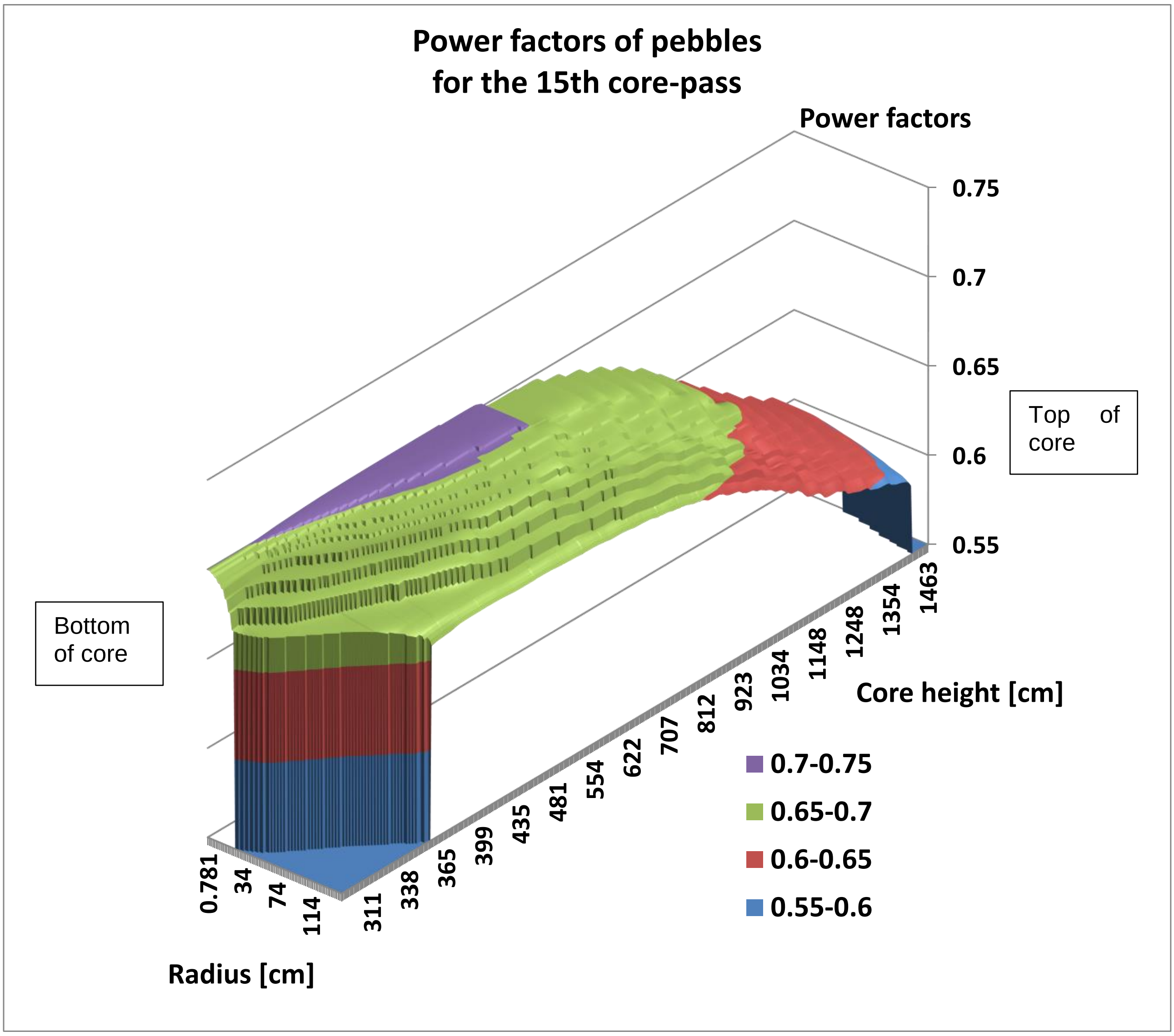

Figure 54: Pebble power factors over the whole core for the 15th core pass with 3 locations of power factors

For our analysis, the clustered pebbles were located at the innermost radial mesh at the location of the power maximum for the rod ejection cases. For the rod withdrawal case the pebble cluster with increased density is again placed at the bottom of the pebble bed. The 3D figures give an overview of the distribution of individual power factors in the core. But for more details the following sections are presented:

3 radial distributions of power factors:

1) @ z = 1463 cm (uppermost region of top cone)
2) @ z = 1110 cm (region of dense cluster)
3) @ z = 357 cm (core bottom above bottom reflector cone)

and

3 axial distributions power factors:

4) @ r = 0 cm also section 7)
5) @ r = 76.1 cm
6) @ r = 149 cm

To clarify the locations, a cross section of the reactor geometry is presented together with the planes to intersect the geometry.

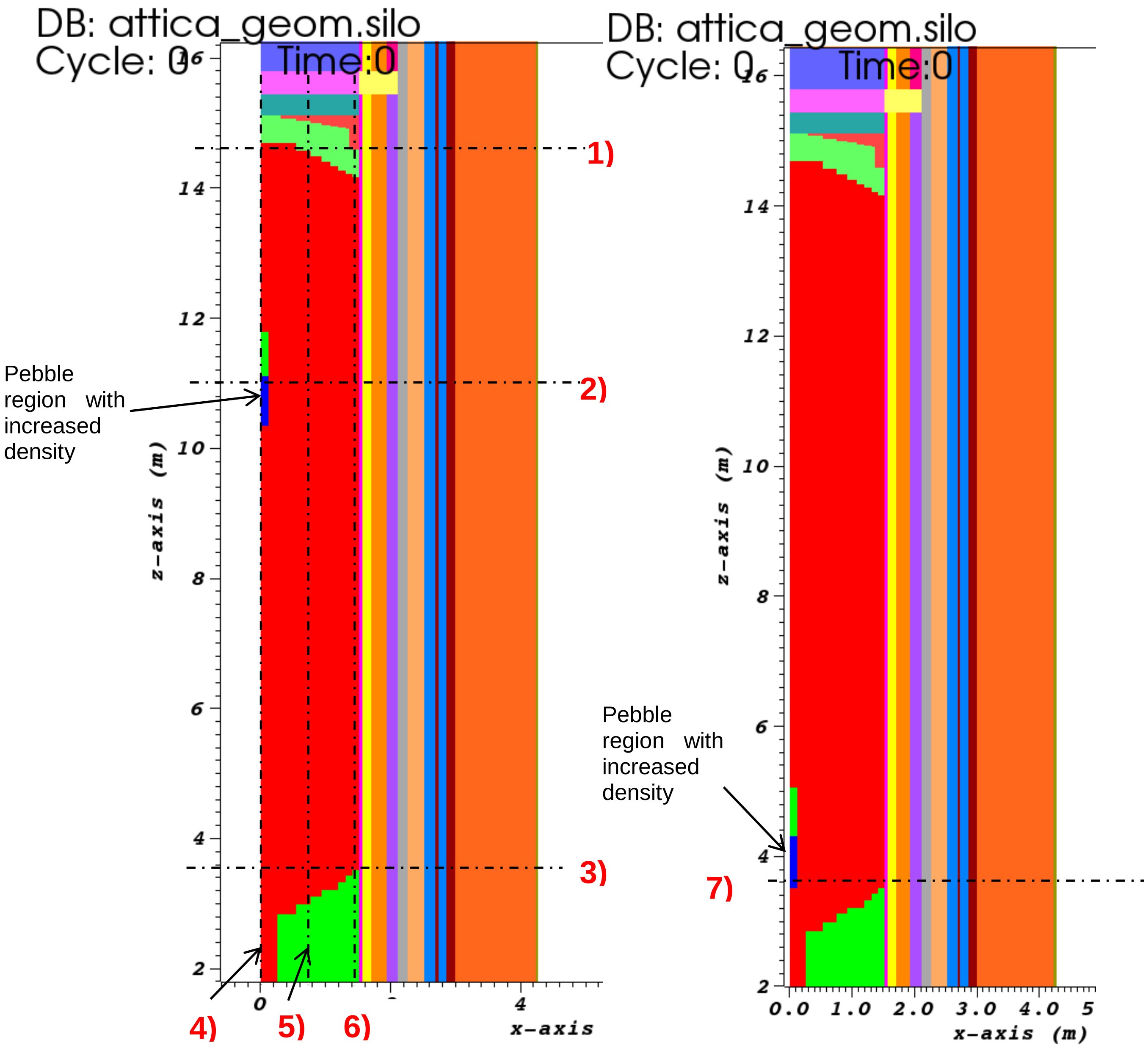

Figure 55: Location of sections for the power factors. Left side: Locations of hotspot and sections of power factors. Right side: Location of pebble cluster with increased densitiy for the second total control rod withdrawal case and the steady-state with reduced mass flow (-20%)

Radial power distributions:

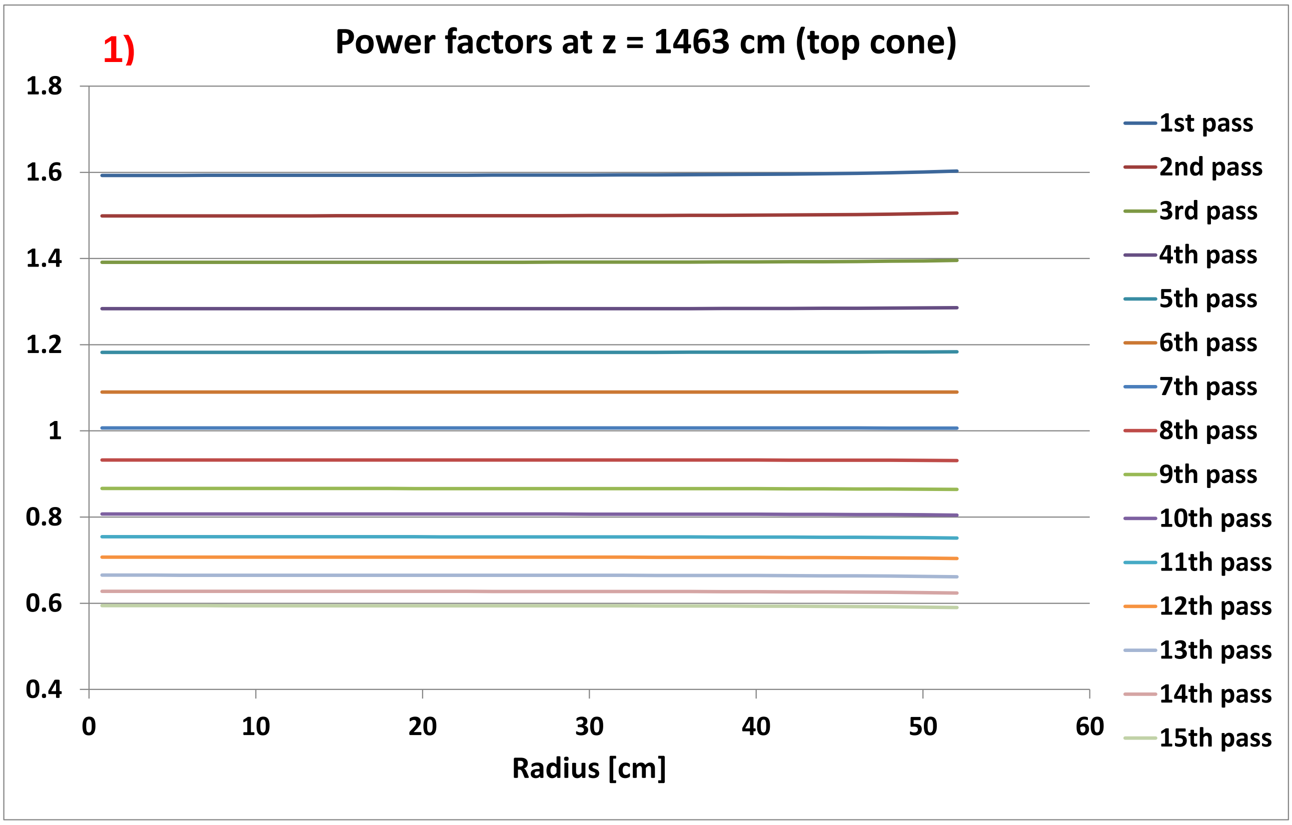

Figure 56: Radial power factors at top of cone, section 1)

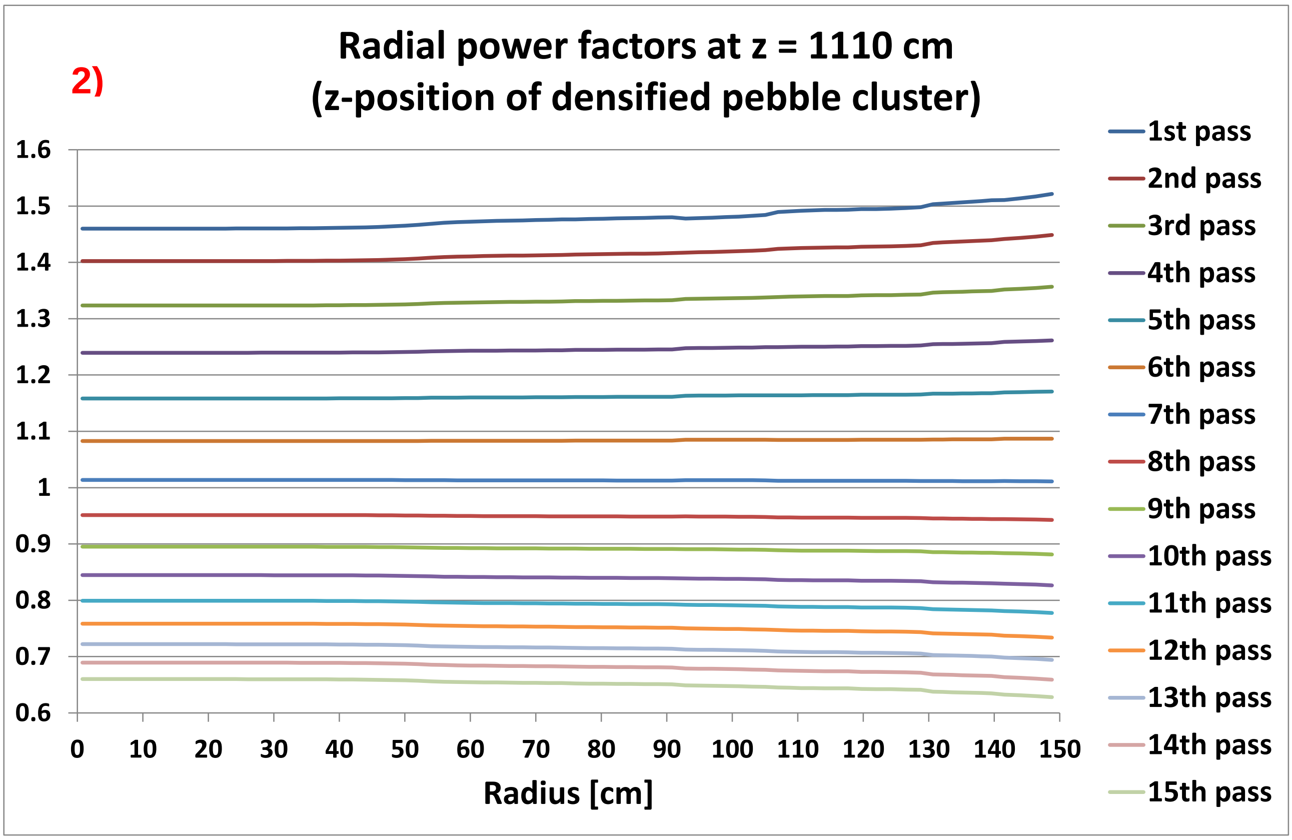

Figure 57: Radial power factors at z = 1110 cm, position of the power maximum, section 2)

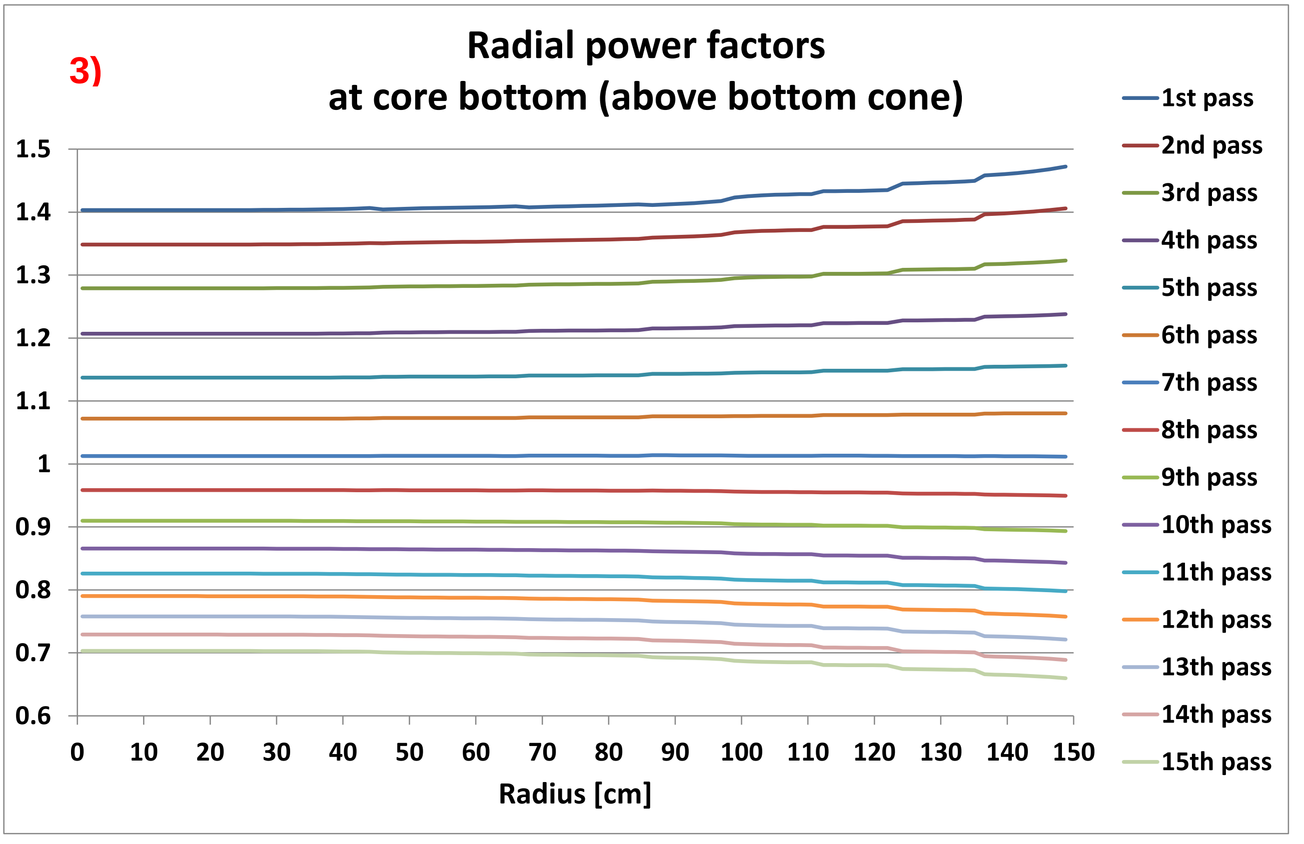

Figure 58: Radial power factors at z = 357 cm, section 3)

The axial power density and power factor distributions at the sections 4), 5) and 6) of Figure 55 are

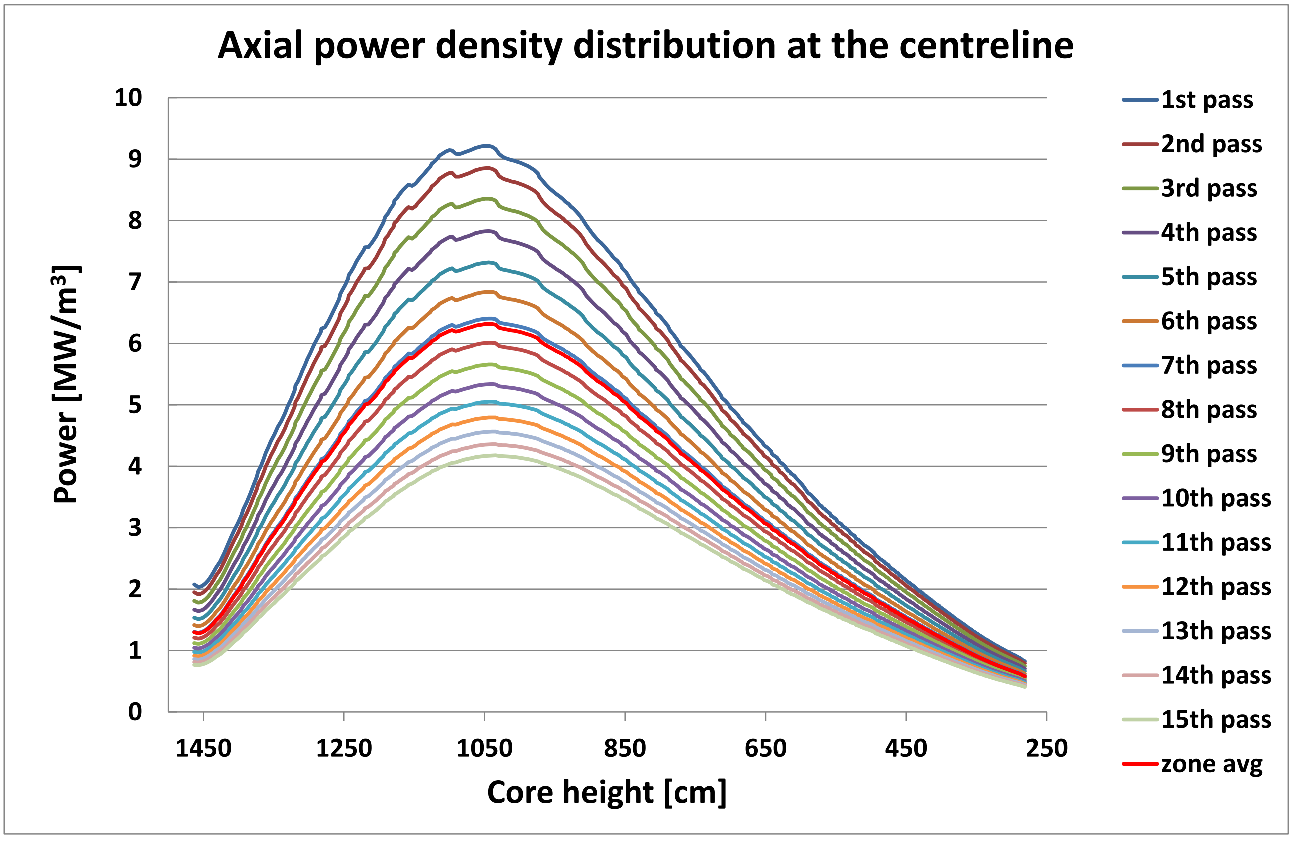

Figure 59: Power density per core-pass number and average value, section 4)

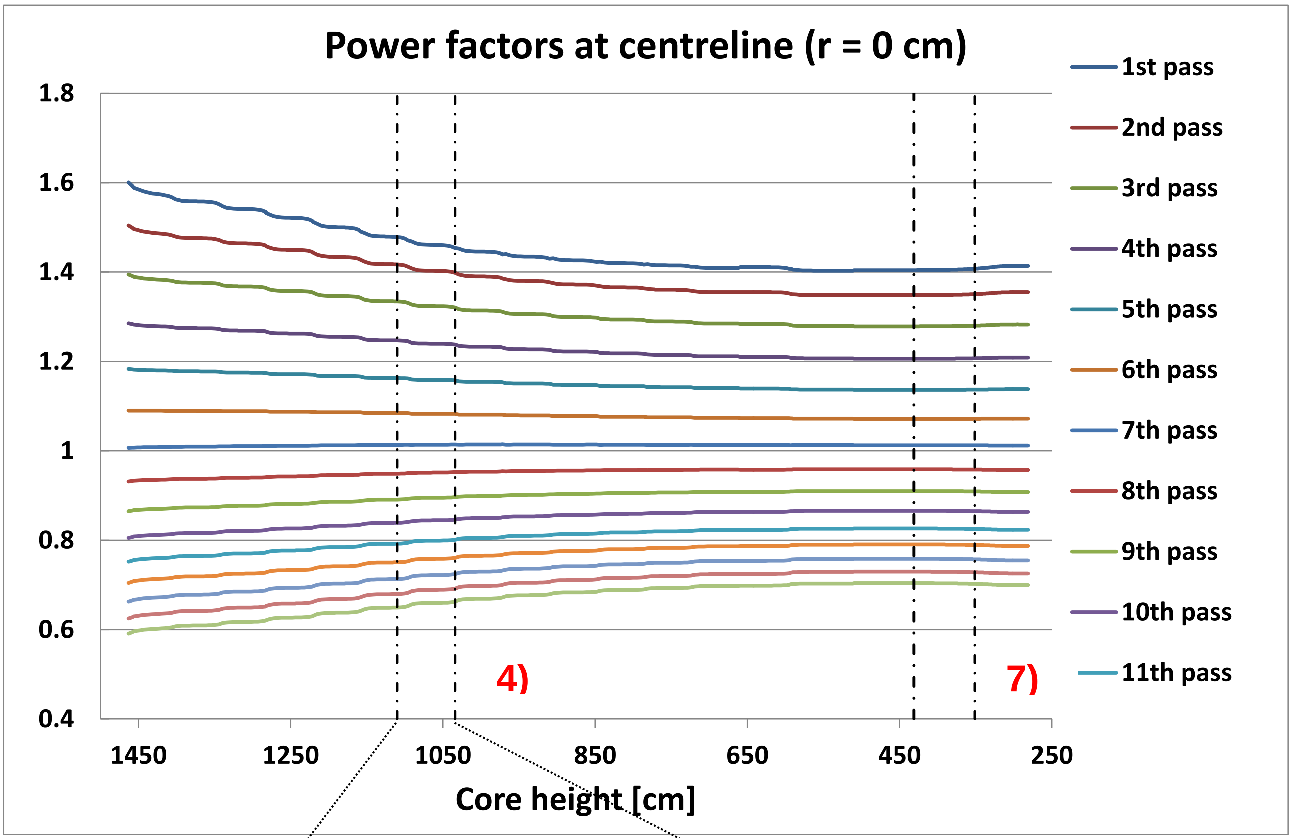

Figure 60 : Axial power factors at centreline

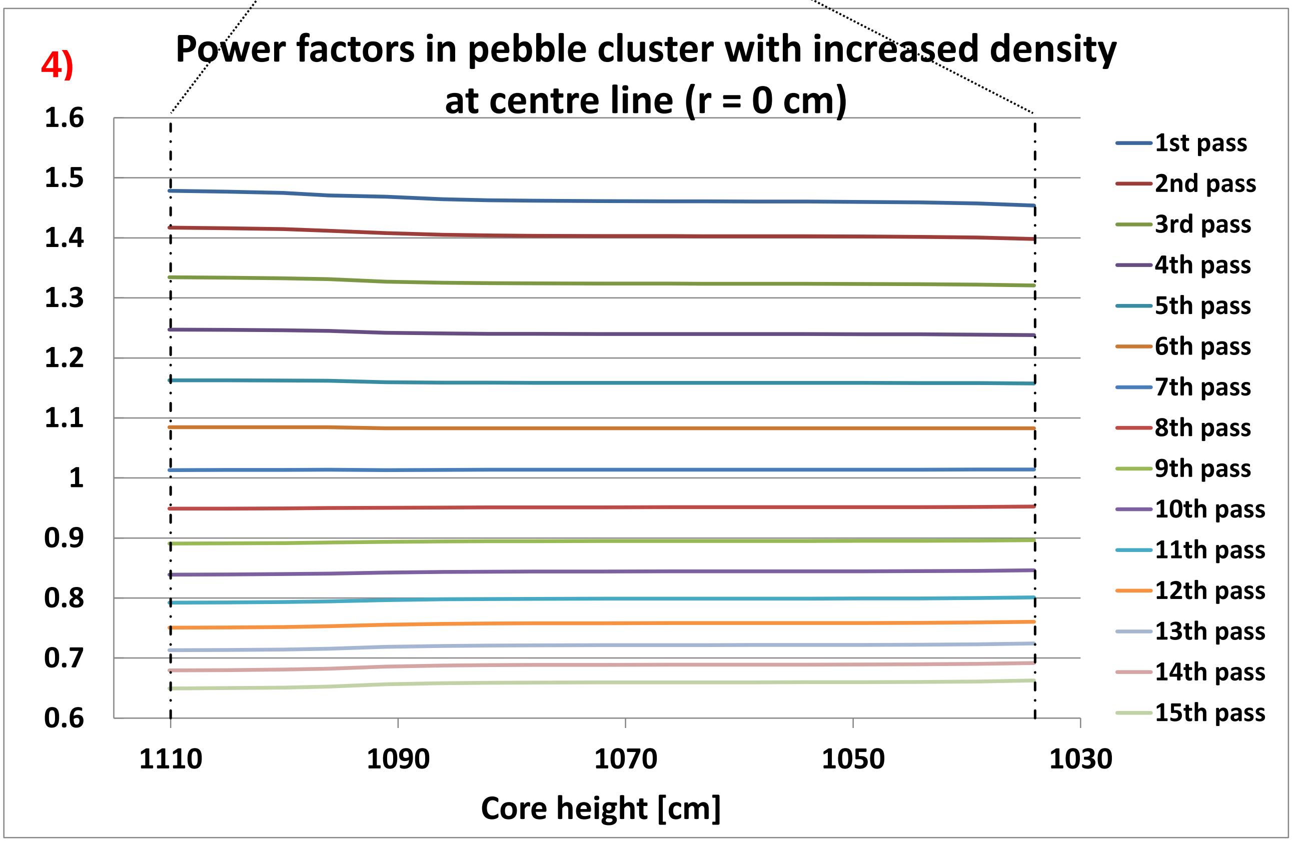

Figure 61: Power factors at the location of the pebble cluster with increased density, the values at 1110 cm are used for the realistic rod ejection/withdrawal scenarios

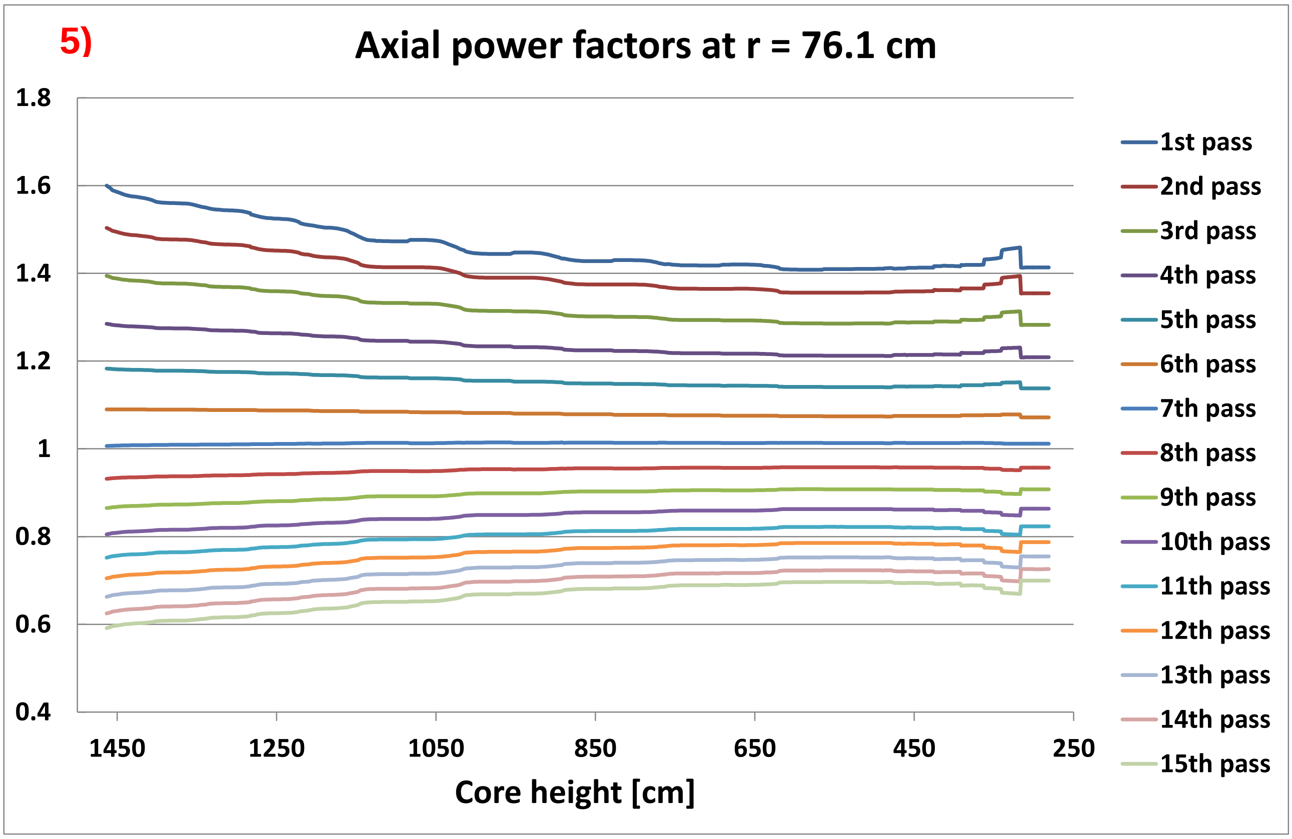

Figure 62: Axial power factors at r = 76.1 cm, section 5)

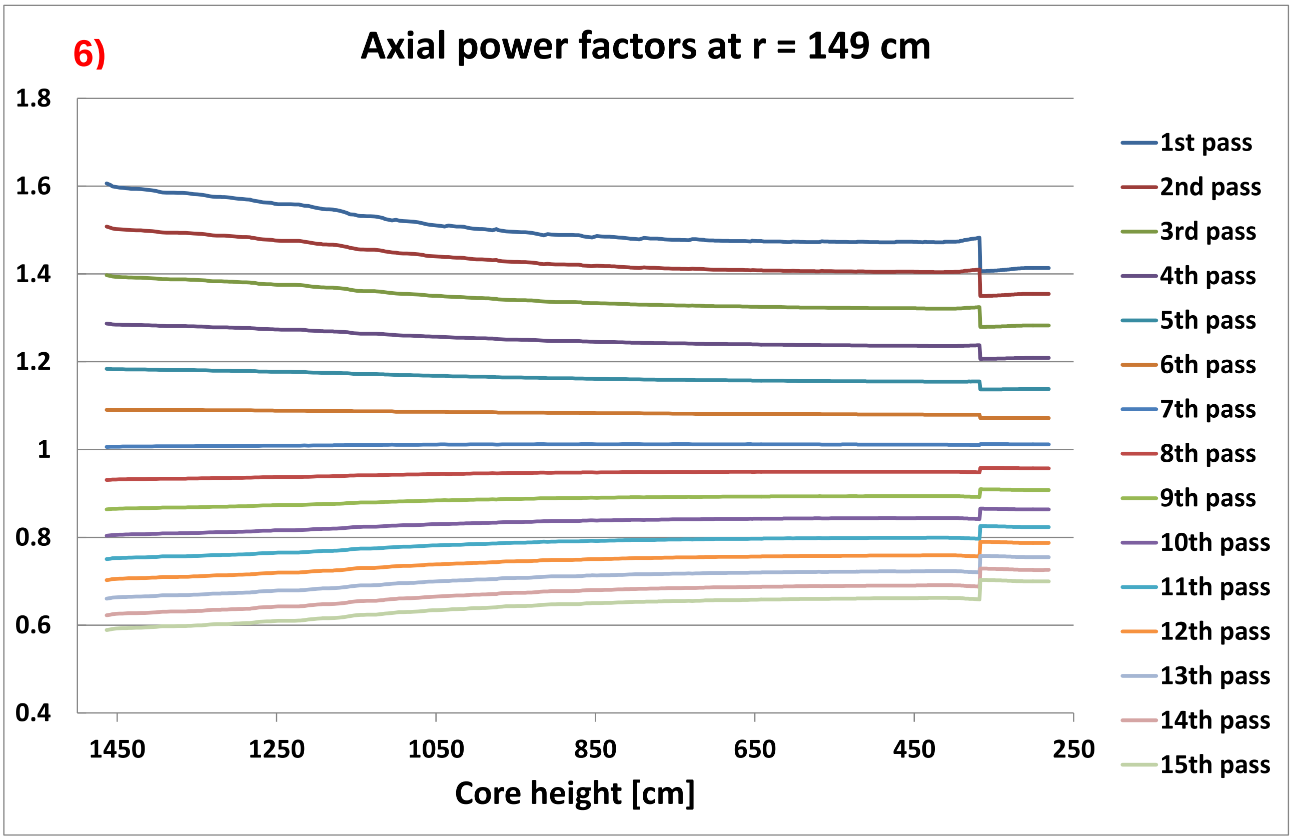

Figure 63: Axial power factors at r = 149 cm, section 6), the values at z = 1463 cm are used for the "conservative" analysis of the next chapter

With the overview of power factors presented in Figure 56 throughout Figure 63, it was decided to analyse a case where the highest power factors are used and, a more realistic case where the power factors of the zone with the pebble cluster of increased density are used. These two scenarios will be referred to as “conservative results” and “more realistic results” and are also compared in the following chapters.

4.4 Results for the total control rod ejection scenario with “realistic” and “conservative” power factors

The new power factors (see Table 5) are introduced into the TORT-TD/ATTICA3D input deck and are used to analyse the changes in temperature for the total rod ejection scenario. The boundary conditions are the same as in the previous analysis, i.e. the ejection of all rods starts at t = 0 seconds and takes 0.1 seconds. The reactor response (without any actuation of safety measures or consequences like de-pressurisation) is simulated for 30 seconds.

The power increase and the average fuel and moderator temperatures remain basically the same like in the case without accounting for core pass number. Differences in parameters for the cases are presented in Table 6, below.

Table 6 : Overview of results for the total control rod ejection scenario

	Initial conditions at t = 0 s			Transient maximum values	
	$T_{mod,avg}$ [°C]	$T_{fuel,avg}$ [°C]	$T_{fuel,max}$ [°C]	Max. total power [MW]	$T_{fuel,max}$ [°C]
Assumed	563.6	573.5	850.7	2376.5 (t = 0.785 s)	2241.3 (t = 0.9375 s)
“Conservative”	563.6	573.5	842.0	2397.6 (t = 0.7875 s)	1896.4 (t = 0.895 s)
“Realistic”	563.6	573.5	838.8	2403.4 (t = 0.7825 s)	1760.3 (t = 0.91 s)

Table 6 reveals that the assumed power factors were obviously estimated too high. Even when taking the most unfavourable power factor configuration (outermost radius at the core top), the power factors are not going beyond 1.6008 which is considerably lower than the value of 1.9 of the previous analysis. This reduction of the power factor leads to a drastic reduction of the maximum temperature (345 K lower), even though still too high for the maximum fuel temperature limit of 1620 °C. In the more realistic scenario, the temperature difference between conservative and realistic power values is still 136.1 K and with 1760.3 °C also above the temperature limit. It remains questionable if this control rod ejection scenario is really the limiting case.

The corresponding temperature distribution over the hottest fuel element and its kernels is shown in Figure 64, below. The temperature of the outer graphite shell is the same for both cases, but the temperature spread over the fuel element for the “conservative” simulation amounts to 1367 K, whereas in the “realistic” scenario the spread amounts to 1231 K which is still very large; even more than twice as large as the heat-up of helium when passing the core!

This has to be evaluated by fuel design experts. Another possibility would be to limit the maximum number of rods to be ejected during licensing. It is common for LWR to allow only the most effective rod to be ejected. A further reduction of the rod efficiency is not possible since the bound reactivity in nominal operation is needed for part load operation in order to override the reactivity bound due to xenon-135.

The timely evolution of the maximum fuel kernel temperature during the total control rod ejection transient is presented in Figure 65.

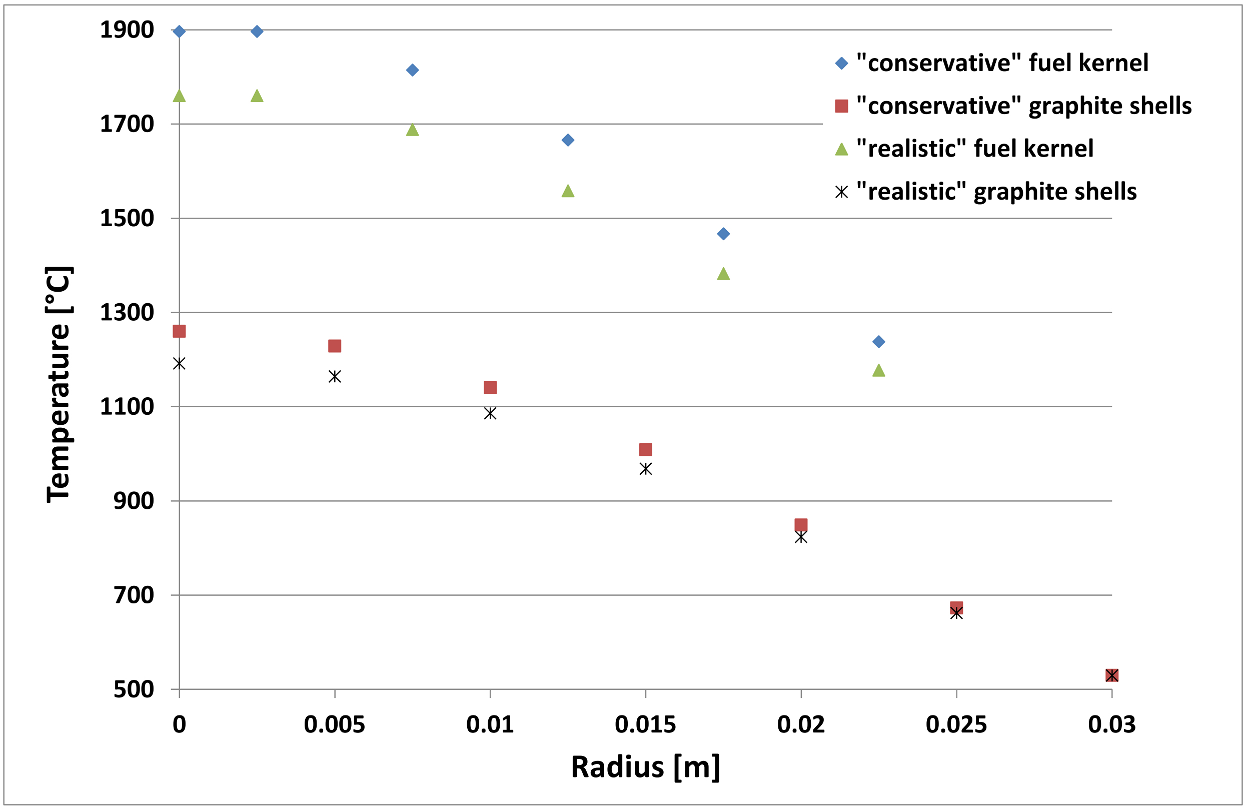

Figure 64 : Temperature distribution over the hottest fuel element in the total control rod ejection scenario with "conservative" and "realistic" values. The time at which the maximum temperature is reached differs slightly (see Table 6)

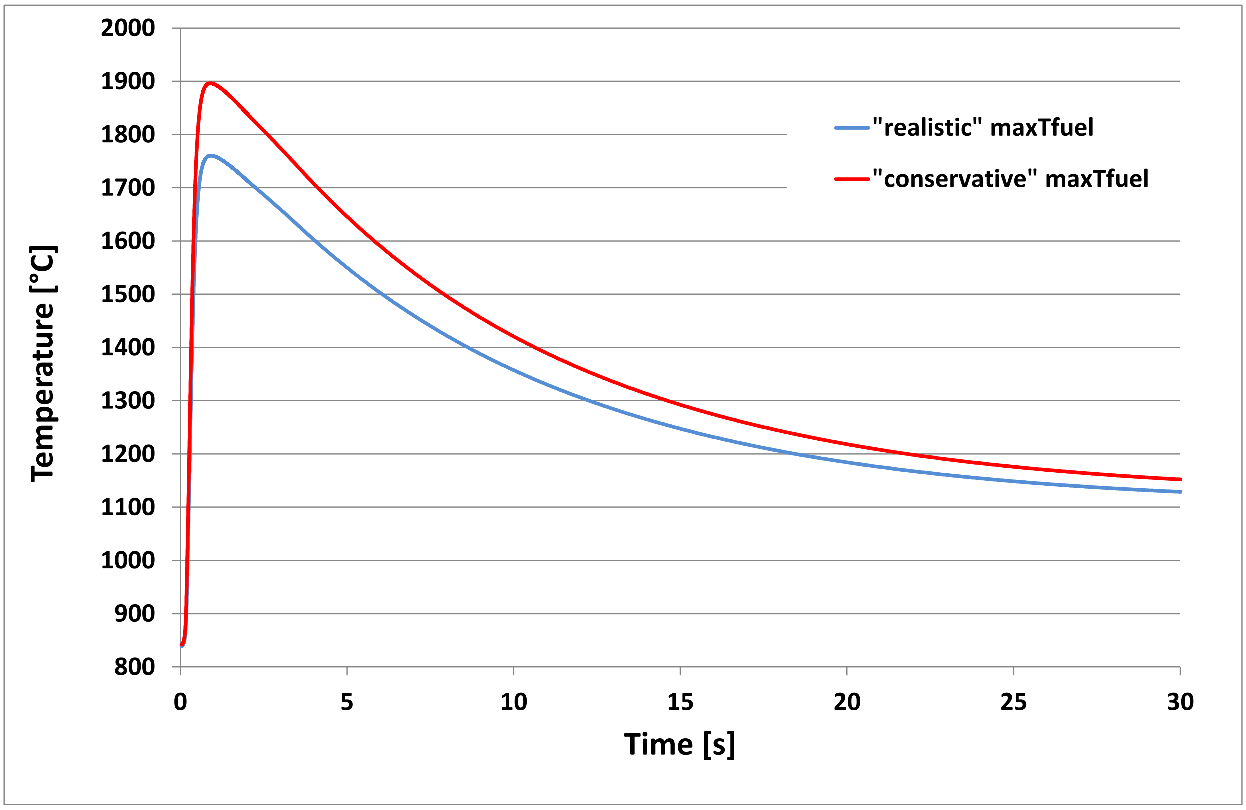

Figure 65: Maximum fuel kernel temperature evolution over the total control rod ejection transient

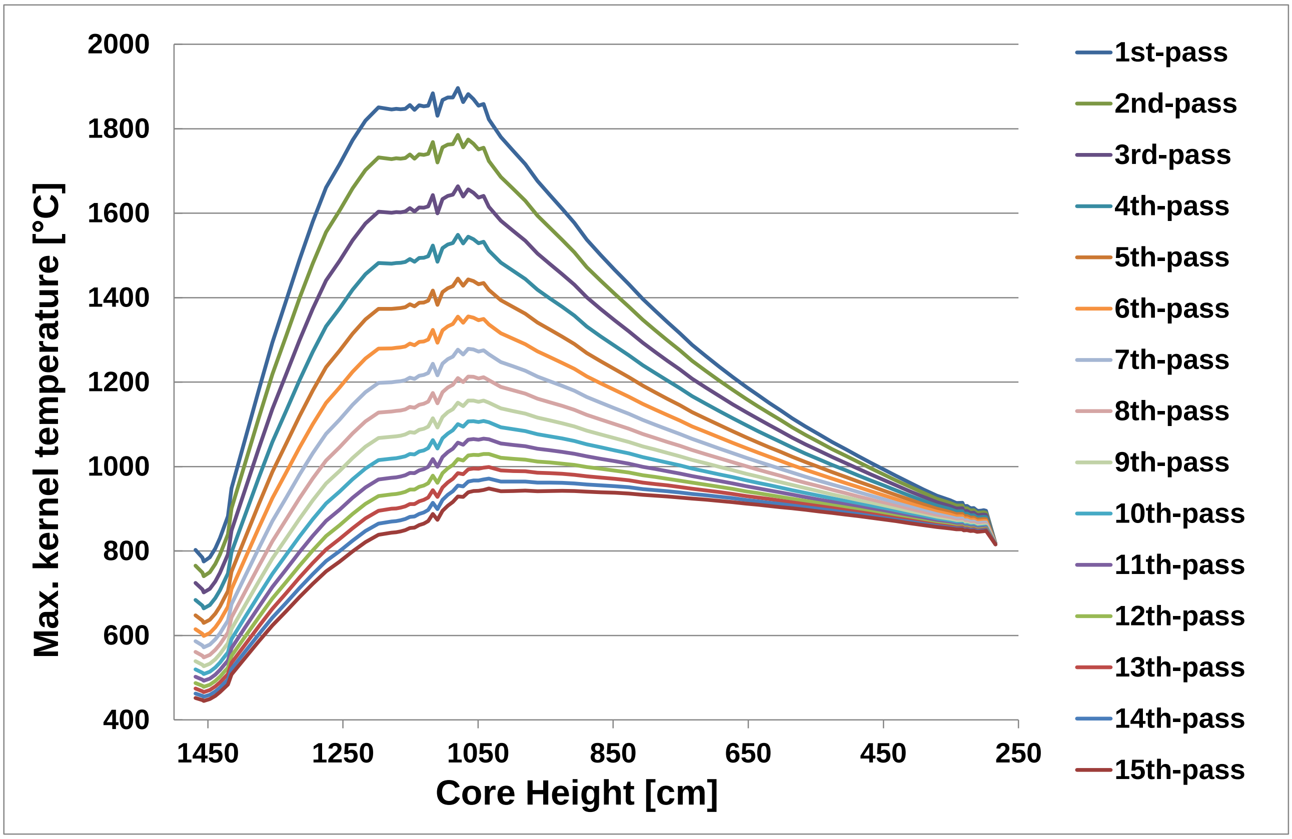

Figure 66: "Conservative" maximum temperatures for the innermost kernel per core-pass number at the centre line at t = 0.875 seconds after start of ejection

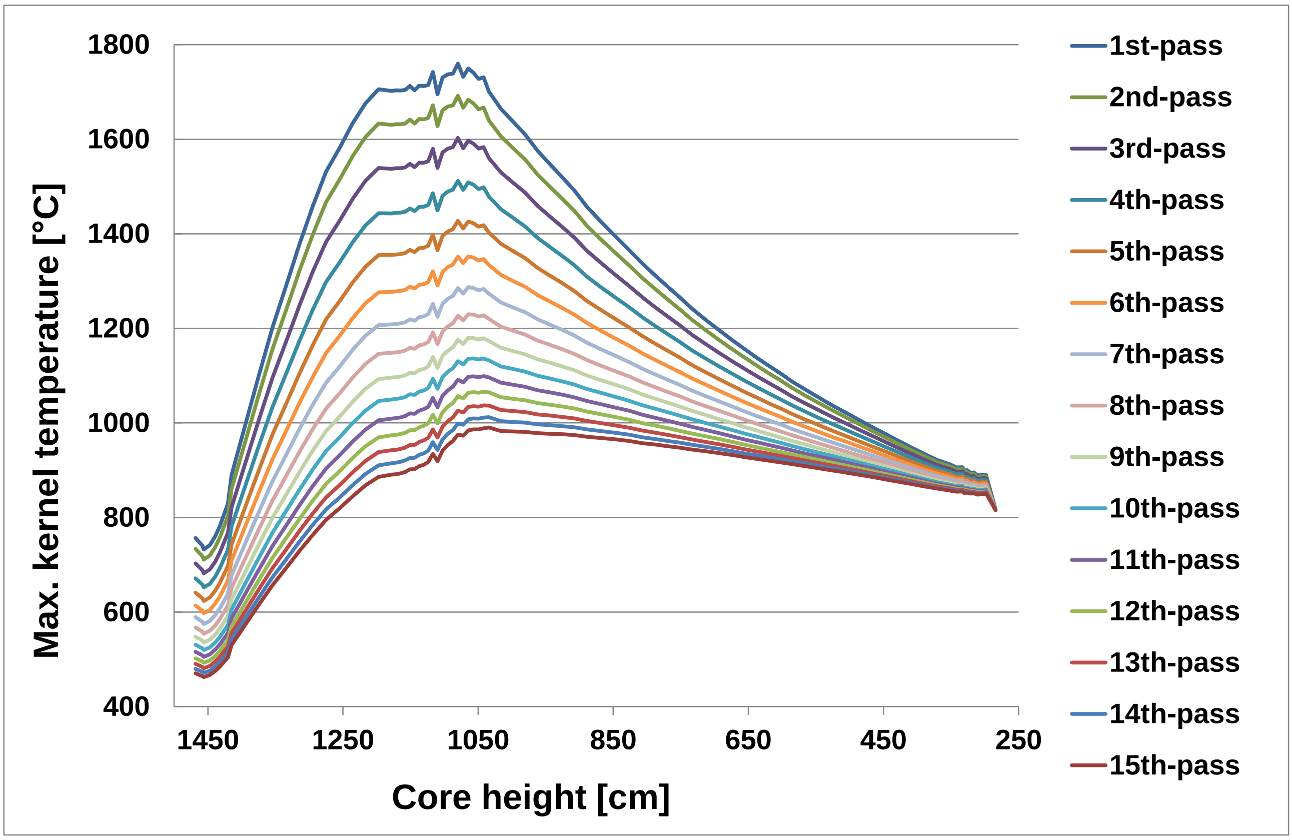

Figure 67: "Realistic" maximum temperatures for the innermost kernel per core-pass number at the centre line at t = 0.91 seconds after start of the ejection

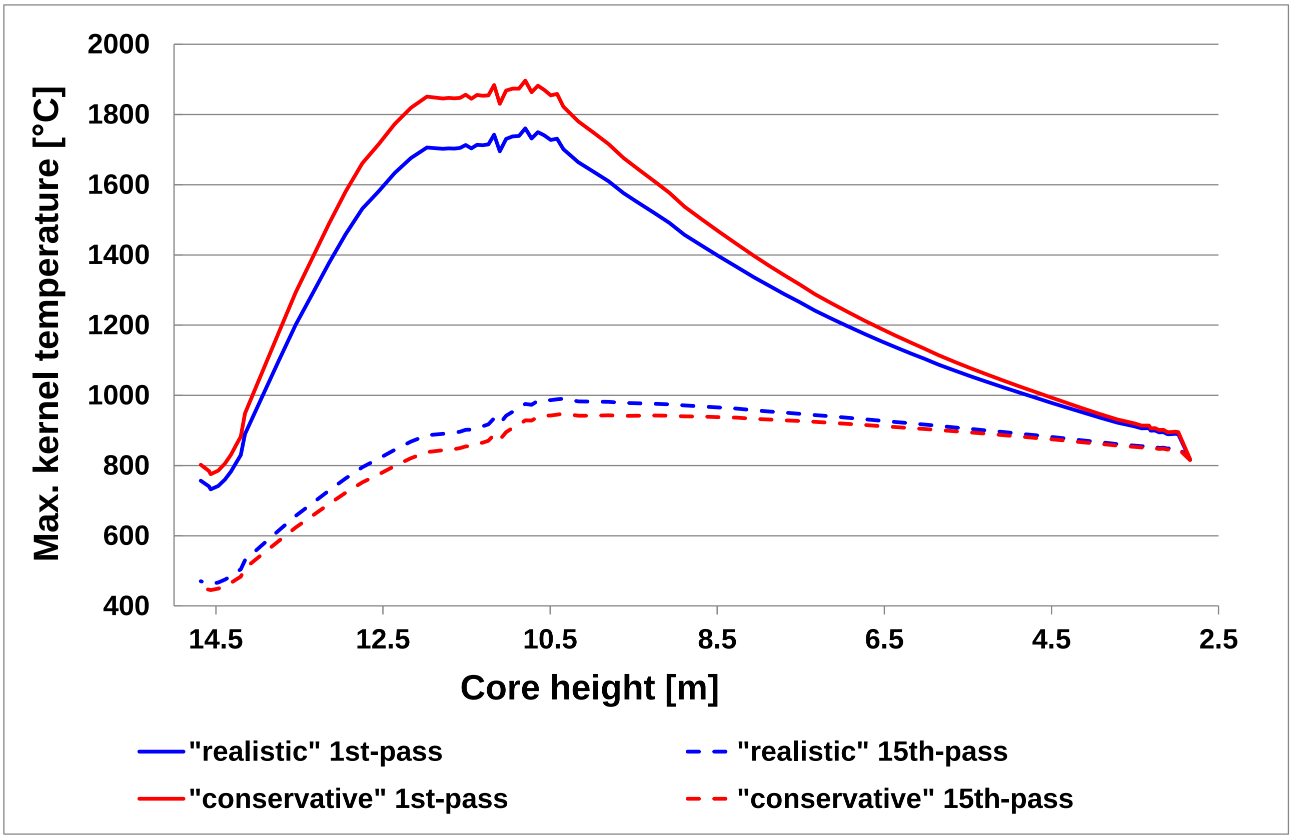

Figure 68: Comparison of maximum kernel temperatures of the "conservative" and the "realistic" approach, the time at which the temperatures are reached differ slightly (see Table 6)

4.5 Results for the total control rod ejection scenario with “realistic” and “conservative” power factors with reduced ejection speed

In the last deliverable D24.22 it was mentioned that also a scenario with reduced ejection speed is analysed. For this analysis, it was assumed that all rods are ejected at a speed of 100 cm/s. This leads to an ejection time of approximately 4.6 seconds which is considerably longer than in the fast ejection case. The reactor response with steady boundary conditions (same mass flow, inlet temperature).

Table 7 gives an overview of the results for the rod ejection with reduced ejection speed. Of course the maximum temperatures are lower since there is the same reactivity increase but over a 46 times longer time. This leads to a maximum relative power of around 8.6 times the nominal power (8.6624 conservative, 8.679 realistic) at ~ 3.4 seconds after the start of the ejection. The maximum temperatures are reached after ~ 3.7 seconds for both transients. For both cases the maximum power and fuel kernel temperatures are reached before the end of the ejection which is at 4.6 seconds. As expected the maximum temperatures are lower than in the fast ejection case of chapter 4.4.

Table 7 : Overview of results for the total control rod ejection scenario with reduced ejection speed

	Initial conditions at t = 0 s			Transient maximum values	
	$T_{mod,avg}$ [°C]	$T_{fuel,avg}$ [°C]	$T_{fuel,max}$ [°C]	Max. total power [MW]	$T_{fuel,max}$ [°C]
"Conservative"	563.6	573.5	842.0	2165.6 (t = 3.410 s)	1803.6 (t = 3.6875 s)
"Realistic"	563.6	573.5	838.8	2169.8 (t = 3.415 s)	1683.0 (t = 3.7025 s)

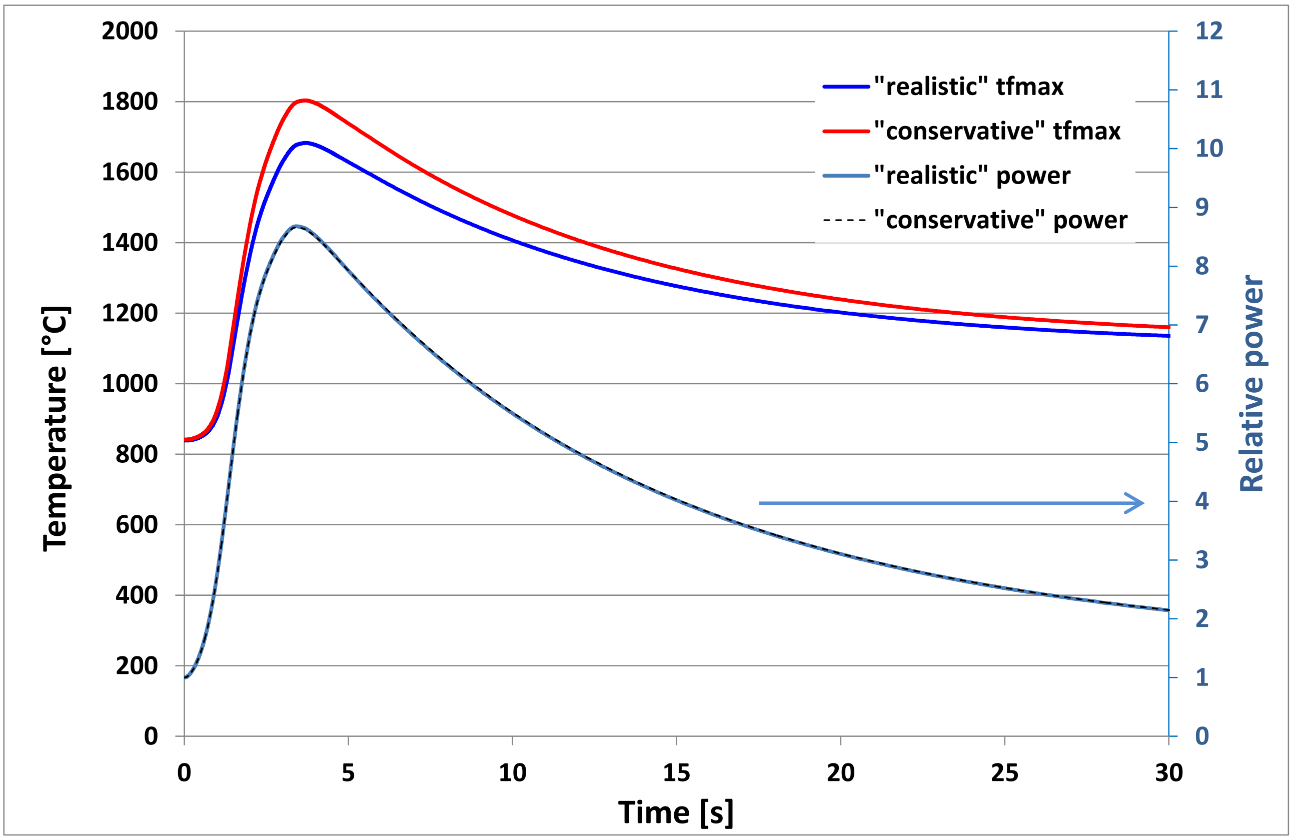

Figure 69 : Left axis : Maximum kernel temperatures in the « conservative » and « realistic » case. Right axis : Power evolution during transient, the power values practically coincide (see Table 7)

4.6 The total control rod withdrawal scenario with "conservative" and "realistic" power factors

The two differing power factors were also used in a total control rod withdrawal scenario for the HTR-PM. In this scenario it is assumed that all rods are pulled from the nominal position during normal operation. The rods are moved at operational speed which is 1 cm/s. The movement goes on for 100 seconds such that in the end the tips of the control rods are 1 metre above the nominal position. After 100 seconds, the reactor remains at this level (same mass flow, same inlet temperature) for 100 seconds.

The reactor response with the hottest temperatures from results with the "conservative" and "realistic" power factor is shown in Figure 70. Here, the temperatures for the hottest fuel kernels are shown with the maximum moderator temperatures (which lie on each other). Also, the power evolutions for the two power factors are shown to exactly coincide. The maximum kernel temperatures differ by less than 15 K at about 100 seconds (at time of biggest difference). The pebble cluster with increased density is at the power maximum (section 2), Figure 55).

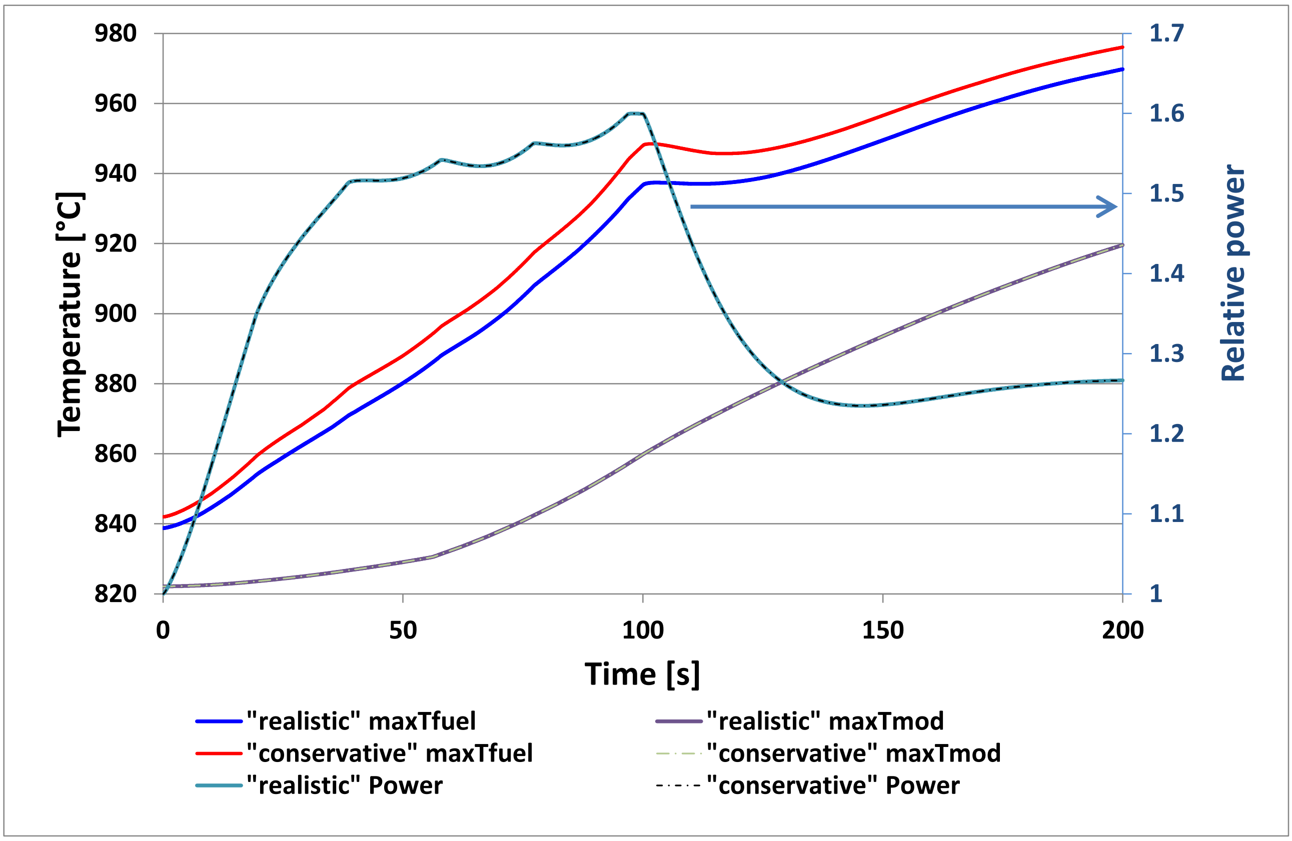

Figure 70: On the left axis : Temperature evolution of the maximum fuel and moderator temperatures with the conservative and realistic values, on the right axis : evolution of power with conservative and realistic power factors.

A second calculation was performed where the pebble cluster of increased density was located at the core bottom (section 7), Figure 55). The results are presented in Figure 70. Here, the temperatures are slightly lower than in the case with the pebble cluster at the power maximum.

In both cases there are no inadmissibly high temperatures. However, the location of the hotspot would have to be placed somewhere between the power maximum and the temperature maximum.

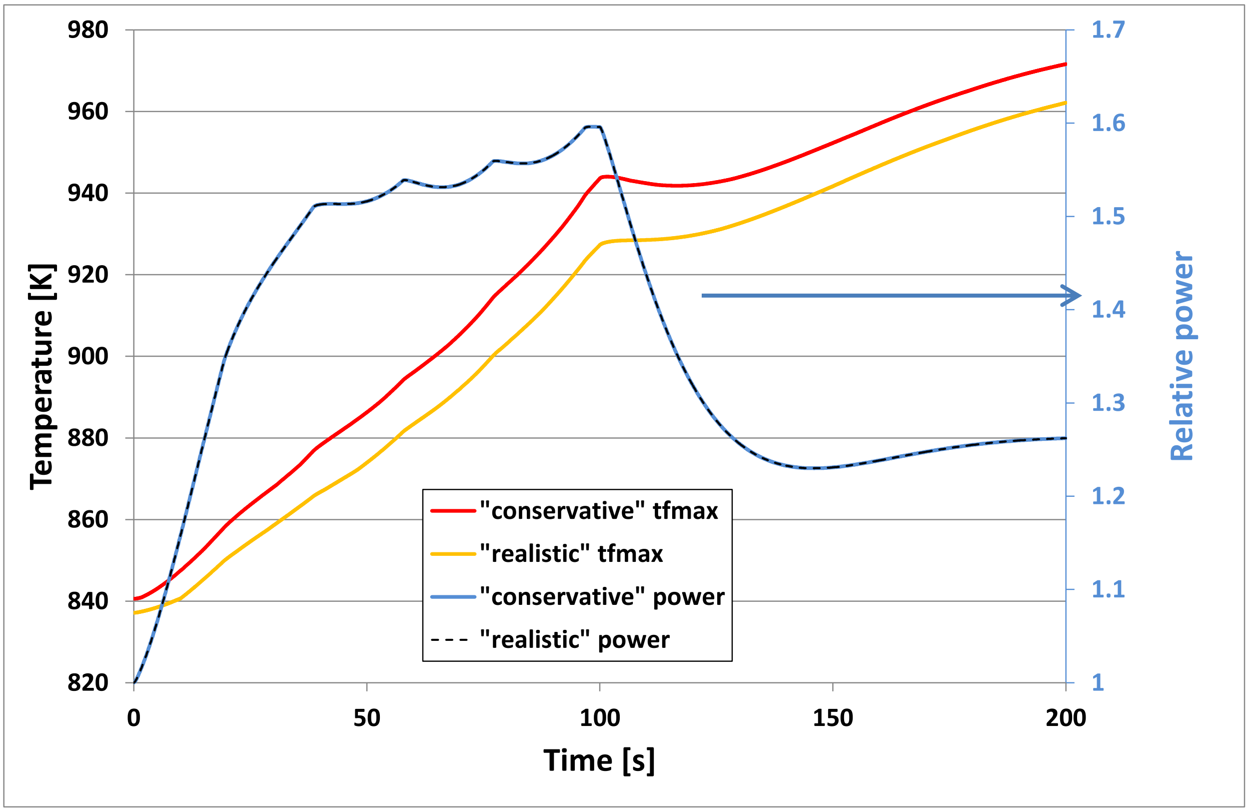

Figure 71: Left axis: Maximum fuel temperature for "conservative" and "realistic" power factors with the pebble cluster of increased density in the central lower part of the core

4.7 Steady-state with only 80 % of the mass flux

In the operation of the AVR, the core by-pass flow was held accountable for the occurring elevated temperatures. Therefore, a coupled steady-state analysis is performed with a reduced mass flow. This reduced mass flow had a flow rate of 76.8 kg/s instead of 96 kg/s as in nominal operation conditions. Due to less cooling gas passing the core the temperature will sooner reach high values. This will shift the power maximum towards the top of the reactor. The corresponding fuel temperatures will have greater resulting values when going towards the bottom.

In Figure 72, the results for the coupled steady-state with the densification at the power maximum location are shown. It is obvious that under these circumstances the fuel temperature is above 900 °C already after 4 metres from the top of the core, i.e. the fuel kernel temperatures increase by 750K within 4 metres. The shape of the kernel temperatures resembles rather a case with very low core-pass number; where the power is peaked at the top and the solid temperatures, after a short distance of heat-up remain at these temperatures.

The coupled steady-state with reduced mass flux was also performed for the pebble cluster of increased density located at the bottom of the reactor. The corresponding maximum kernel temperatures for the first and last fuel pass are plotted with the corresponding power density at the centreline, see Figure 73. Here, the shape of maximum temperature exhibit a more uniform profile compared to Figure 72.

For the steady-state operation this reduced mass flux leads to elevated fuel and also maximum temperatures. The residence time of a fuel element at high temperatures must be limited. Otherwise there can be significant fission product release during normal operation. This outcome has to be evaluated by fuel design experts, but seems to be relatively high for long-term operation.

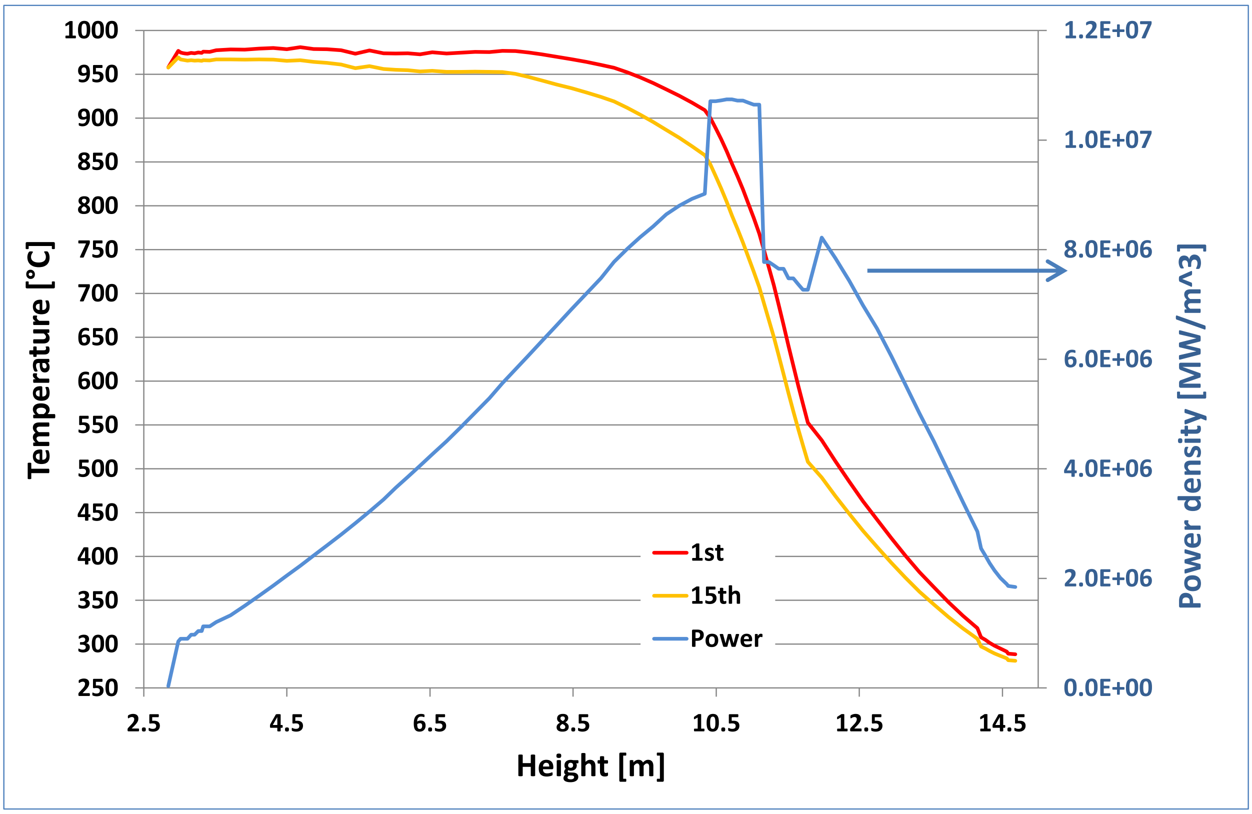

Figure 72: Denisified pebble cluster at the location of power maximum. Left axis: Maximum kernel temperatures with realistic power factors and gas temperature at the centreline. Right axis: corresponding power density

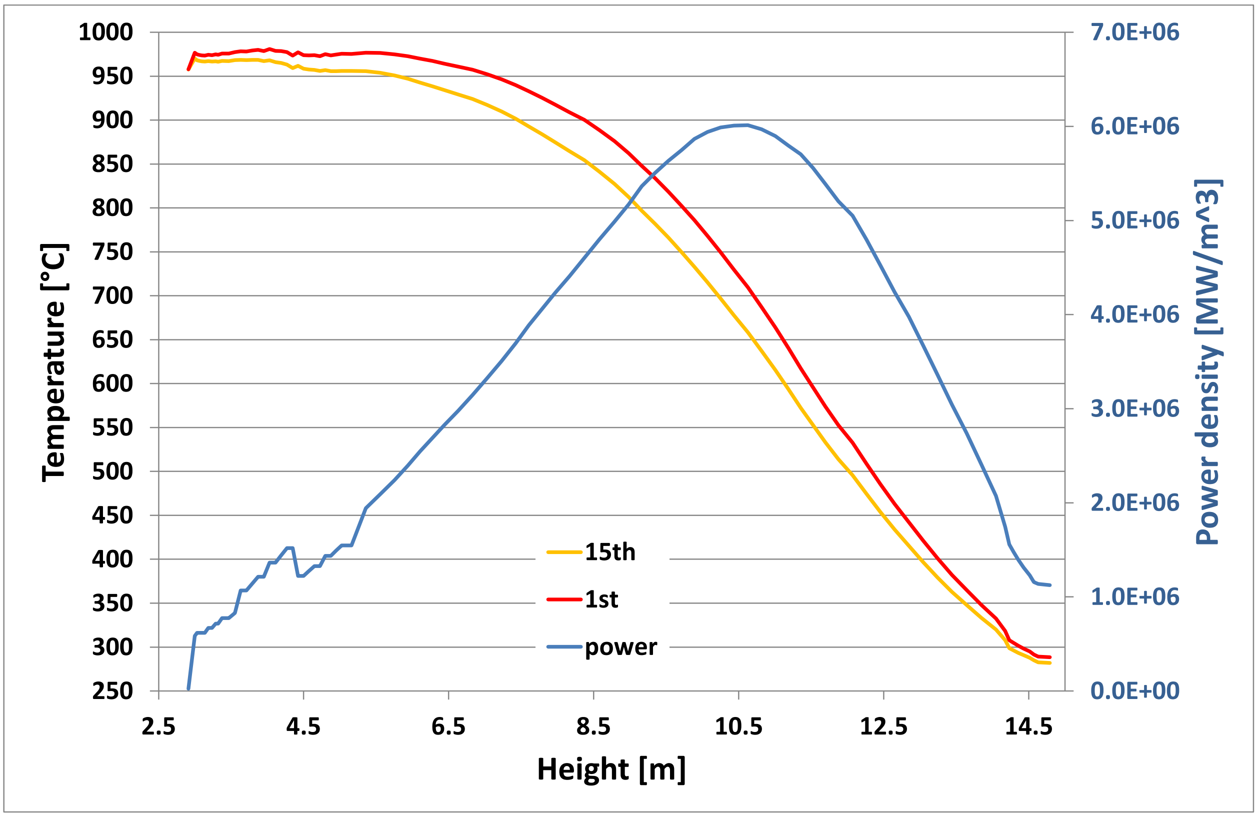

Figure 73: Densified pebble cluster above the lower reflector cone. Left axis: Maximum kernel temperatures for the centreline. Right axis: corresponding power density

5 Summary and Conclusion

In the first chapters 2 and 3 the tools to be used as well as the reference plant (HTR-PM) were specified. In chapter 4 the methodology to simulate densifications within a pebble bed is addressed including the approach used to modify macroscopic cross sections for the pebble clusters with increased density.

Then, the hotspot analysis was performed for the depressurised loss of forced cooling accident as well as several control rod ejection and withdrawal cases with 3 out of 8 control rods ejected. It could be shown that for the cases simulated the densification do not lead to inadmissibly high temperatures. Moreover, if the pebble bed is considered to be a mixture of pebbles without resolution of the respective core-pass number, the results may cover the hottest part by means of averaging.

These analyses have been performed for an ensemble of pebbles, i.e. for a cluster of pebbles with different number of core passes. The HTR-PM concept foresees 15 fuel pebbles core passes, thereby reaching the design burn-up of 90 MWd/kg of HM. Since fuel spheres, at the beginning, have a much higher content of fissile material, the produced power, and hence, the fuel temperatures will also be much higher.

This investigation was performed in the updated version of this deliverable, for the total control rod ejection (all rods out in 0.1 seconds) the maximum fuel kernel temperature was determined to be 2,241°C. This temperature is already way beyond the licensing temperature. However, the assumed power factors proved to be too high when values are compared to values determined by ZIRKUS steady state analysis. A power factor map could be created. This map displayed local variations for core-pass number and location. The hotspot analysis was thus repeated taking the most conservative power factors which lead to the highest temperatures and most realistic ones from the location of the pebble cluster with increased density. These power factors lead to maximum temperatures of **1,896°C** for the “conservative” power factors and to **1,760°C** when using the “realistic” values.

Also, a scenario with reduced ejection speed was analysed. Instead of 0.1 seconds, the rods take 4.6 seconds. Of course with this reduced ejection speed there is less reactivity inserted per time and hence, the resulting temperatures are lower (while the power evolutions are alike). The maximum temperatures for this case were **1,803°C** for the “conservative” case, **1,683°C** for the “realistic” one.

In both cases the fast and the slow rod ejection the temperatures exceeded maximum allowable temperatures, but only for less than 10 seconds. However the temperature gradient over the fuel elements could be hard to bear from a thermal point of view.

Two cases of total control rod withdrawals were also analysed with realistic and conservative factors. In this transient the rods were pulled from the nominal operation position for 100 seconds. After 100 seconds, all boundary conditions were the same, especially the inlet temperature and the mass flow rate. For this analysis the location of the densification was first located at the power maximum and then at the temperature maximum at the bottom of the core. Both cases did not yield any temperatures too high. When comparing the temperatures with a pebble cluster of higher density at different times (0, 50, 100, 150 and 200 seconds), it becomes obvious that even with accounting for core pass numbers the temperatures stayed well below any limits.

As for the rod ejection case, temperatures where exceeded for a short time, a steady-state analysis was done for the location of the pebble cluster with increased density at the power maximum and at the core bottom accounting for core pass number. The mass flow was also reduced by 20% (which was presumably the percentage of core by-pass flow in the AVR). For the case with densification at the power maximum the maximum kernel temperatures increase by 750 K within the first 4 metres of the core. They then remain at elevated temperatures. The case with the densification at the temperature maximum did not display unfavourable conditions. Only the high outlet temperatures which are a direct consequence of the gas flow reduction might be of concern.

To summarise the whole analyses presented here, it can be said that without consideration of the core-pass number there are no temperatures beyond the maximum temperature limit of 1620°C. However, if the core-pass number is accounted for, the control rod ejection scenarios lead to temperatures above that limit. But only for less than 10 seconds (depending on the absolute value of power factors) until the heat is transported out of the coated particles and into the graphite moderator. For the control rod withdrawal, no too high temperatures could be detected. For the steady-state operation with a 20 % reduction of mass flow the temperatures might be too high for a too long time relative to their total time of residence in the core; such that fission product release during operation might occur.

Of course, with reduced mass flow, all the described transient cases would increase the maximum fuel kernel temperatures even further. It thus should be ensured that the core by-pass or the core is as low as possible. This initial by-pass might increase during long-term operation since the graphite is shrinking with the fast neutron dose until a certain dosage when it starts growing again.

6 Annexes

Annex 1 – Document approval by beneficiaries' internal QA

6.1 Annex 1: Document approval by beneficiaries' internal QA

Fill involved beneficiaries as appropriate (mandatory for Milestones and Deliverables, but optional for other document type)

#	Name of beneficiary	Approved by	Function	Date
1				
2				
3				
4				
6				
7				
8				
9				
10				
11				
12				
13				
14				
15				
16				
17				
18				
19				
20				
21				
22				

6.2 References

[1] W. Bernnat, W. Feltes, **Models for reactor physics calculations for HTR pebble bed modular reactors**, Nuclear Engineering and Design 222 (2003) 331–347

[2] D. Mathews, **An Improved Version of the Microx-2 Code**, Paul Scherer Institut, PSI Bericht Nr. 97-11, November 1997.

[3] X-5 Monte Carlo Team, **MCNP – A General Monte Carlo N-Particle Transport Code, Version 5, Los Alamos National Laboratory**, LA-UR-03-1987, revised 10/3/05.

[4] Rhoades, W. A., Simpson, D. B. (1991). **The TORT Three dimensional Discrete Ordinates Neutron/Photon Transport Code (TORT Version 3)**, ORNL/TM-13221.

[5] A. Seubert, K. Velkov and S. Langenbuch, **The Time-Dependent 3-D Discrete Ordinates Code TORT-TD with Thermal-Hydraulic Feedback by ATHLET Models**, Physor 2008, Interlaken, Switzerland, September 14-19, 2008.

[6] Seubert, A. Sureda, J. Bader, J. Lapins, M. Buck, E. Laurien, **The 3-D time-dependent transportcode TORT-TD and its coupling with the 3D thermal-hydraulic code ATTICA^{3D} for HTGR applications**, Nucl. Eng. and Design 2011, in press.

[7] The Nuclear Safety Standards Commission (Kerntechnischer Ausschuss - KTA), **Reactor Core Design for High-Temperature Gas-Cooled Reactor**, KTA 3102, 1983.

[8] H. Reutler and G.H. Lohnert, **ADVANTAGES OF GOING MODULAR IN HTRs**, Nuclear Engineering and Design 78 (1984) 129-136.

[9] Zuoyi Zhang, Zongxin Wu, Dazhong Wang, Yuanhui Xu, Yuliang Sun, Fu Li , Yujie Dong, **Current status and technical description of Chinese 2×250MWth HTR-PMdemonstration plant**, Nuclear Engineering and Design 239 (2009) 1212–1219.

[10] Yanhua Zheng, Lei Shi, Yujie Dong, **Thermohydraulic transient studies of the Chinese 200 MWe HTR-PM for loss of forced cooling accidents,** Annals of Nuclear Energy 36, pp 742–751, 2009.

[11] Rainer Moormann, **A safety re-evaluation of the AVR pebble bed reactor operation and its consequences for future HTR concepts,** Forschungszentrum Jülich Jül-4275, Juni 2008.

[12] Association of German Engineers (VDI) - Society for Energy Technologies (Publ.), **AVR-Experimental High-Temperature reactor; 21 years of successful operation for a future energy technology**, page 154ff, VDI-Verlag GmbH, Düsseldorf 1990.

[13] G.J. Auwerda, J.L. Kloosterman, D. Lathouwers, T.H.J.J. van der Hagen: **Macroscopic and Microscopic Packing Properties of Experimental and Computational Pebble Beds**, Nuclear Technology (2013). Submitted

[14] DIN 25485**: Berechnung der Nachzerfallsleistung der Kernbrennstoffe von Hochtemperaturreaktoren mit kugelförmigen Brennelementen (English: German Industrial**

Standard, Calculation of decay heat for fissile material of high temperature reactors with spherical fuel elements), Mai 1990.

[15] F. Reitsma, K. Ivanov, T. Downar, H. de Haas, H. D. Gougar: **The OECD/NEA/NSC PBMR Coupled Neutronics/Thermal Hydraulics Transient Benchmark: The PBMR-400 Core Design**, Proceedings of PHYSOR 2006, Canadian Nuclear Society, (14.-16. September 2006)